

# A DIGITAL MICROFLUIDIC LAB-ON-A-CHIP FOR CLINICAL DIAGNOSTIC APPLICATIONS

by

Vijay Srinivasan

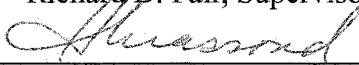
Department of Electrical and Computer Engineering  
Duke University

Date: 4/25/05

Approved:



Richard B. Fair, Supervisor



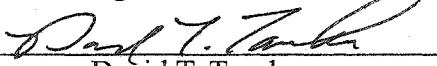
Hisham Z. Massoud



Krishnendu Chakrabarty



Hugh C. Crenshaw



David T. Tanaka

Dissertation submitted in partial fulfillment of the  
requirements for the degree of Doctor of Philosophy  
in the Department of Electrical and Computer Engineering  
in the Graduate School of  
Duke University

2005

UMI Number: 3181507

Copyright 2005 by  
Srinivasan, Vijay

All rights reserved.

#### INFORMATION TO USERS

The quality of this reproduction is dependent upon the quality of the copy submitted. Broken or indistinct print, colored or poor quality illustrations and photographs, print bleed-through, substandard margins, and improper alignment can adversely affect reproduction.

In the unlikely event that the author did not send a complete manuscript and there are missing pages, these will be noted. Also, if unauthorized copyright material had to be removed, a note will indicate the deletion.



---

UMI Microform 3181507

Copyright 2005 by ProQuest Information and Learning Company.  
All rights reserved. This microform edition is protected against  
unauthorized copying under Title 17, United States Code.

ProQuest Information and Learning Company  
300 North Zeeb Road  
P.O. Box 1346  
Ann Arbor, MI 48106-1346

Copyright © 2005 by Vijay Srinivasan  
All rights reserved

## ABSTRACT

# A DIGITAL MICROFLUIDIC LAB-ON-A-CHIP FOR CLINICAL DIAGNOSTIC APPLICATIONS

by

Vijay Srinivasan

Department of Electrical and Computer Engineering  
Duke University

Date:

4/25/05

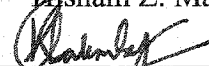
Approved:



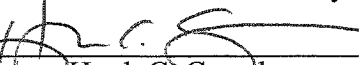
Richard B. Fair, Supervisor



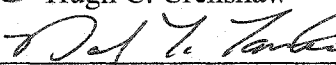
Hisham Z. Massoud



Krishnaendu Chakrabarty



Hugh C. Greshaw



David T. Tanaka

An abstract of a dissertation submitted in partial fulfillment of the  
requirements for the degree of Doctor of Philosophy  
in the Department of Electrical and Computer Engineering  
in the Graduate School of  
Duke University

2005

## Abstract

The emerging paradigm of the lab-on-a-chip powered by microfluidics is expected to revolutionize miniaturization, automation and integration in the life science laboratory. However, the state-of-the-art microfluidic technologies, which are based on continuous-flow in etched microchannel, have not been able to fully deliver the promised benefits of microfluidics. This is primarily due to their incompatibility with common sample matrices and architectural inflexibility. In this thesis a nanoliter droplet-based microfluidic lab-on-a-chip, based on electrowetting actuation, is developed as an alternative to continuous-flow systems. The lab-on-a-chip is designed to perform fully integrated and automated assays on a human physiological sample. Individual components of the lab-on-a-chip are first designed and then integrated on the same monolithic chip for fully automated analysis of multiple samples. Biocompatibility of the electrowetting system is established by demonstrating repeatable and rapid transport of human physiological fluids such as whole blood, serum, plasma and saliva, and proteins such as bovine serum albumin. Automated droplet formation from an on-chip reservoir is also shown for serum samples and enzymatic reagents. A colorimetric enzyme-kinetic assay (based on the Trinder's reaction) for glucose is developed and used as the model system to evaluate the applicability of the lab-on-a-chip for clinical assays. Glucose assays performed using standard solutions on the electrowetting chip compared well with results obtained using a reference method on a spectrophotometer. There is also no significant change in the activity of the enzymes under electrowetting conditions. In order to demonstrate the multiplexed operation of the lab-on-a-chip three assays were each done on 40, 80 and 120 mg/dL glucose standards in fully integrated and automated fashion. The results were used to generate a calibration curve and also study the repeatability of the assays, which is a measure of droplet volume variability and cross contamination. Excellent reproducibility ( $CV < 3\%$ ) was seen in the assays indicating neg-

ligible cross contamination and excellent volume reproducibility. Glucose assays done on serum however did not compare well with reference methods and this is attributed to interferences which assume more significance while using lower sample to reagent mixing ratios. This work represents the first demonstration of fully integrated and automated operation of a digital microfluidic lab-on-a-chip in the nanoliter scale for biological assays on clinically relevant sample matrices. Future work involves implementing dilution strategies on-chip, developing more sensitive detection methodologies, and system integration issues such as assembly, packaging, and temperature control.

## Acknowledgements

I would like to acknowledge the contributions of several people who made this work possible. First, I would like to express my gratitude to my advisor, Dr. Richard Fair for his guidance and vision throughout this project. I would also like to thank the other members of my committee, Dr. Hisham Massoud, Dr. Krishnendu Chakrabarty, Dr. David Tanaka and, Dr. Hugh Crenshaw for their constant support and encouragement. Special appreciation is owed to Dr. Vamsee Pamula and Dr. Michael Pollack for their guidance in this project. I would also like acknowledge the contribution of my colleague Philip Paik to this project. Blood samples were provided by Barbara Fouse and Susan Neblett from the DUMC and special thanks to them. I would also like to acknowledge the participation of Stefan Ufer and the Biomedical Microsensors Laboratory at North Carolina State University in fabricating the devices used in this project, and Don Pearce at the Medical Center Instrumentation shop for mechanical system design. I would also like to thank Hong Ren, Harinath Chakrapani, Divakar Kompalli, and Prasant Potuluri all of whom have contributed to aspects of this research. Finally, but not least, I would like to thank my family and friends for their patience and encouragement throughout this process.

# Contents

<b>Abstract</b>	iv
<b>Acknowledgements</b>	vi
<b>List of Tables</b>	xiii
<b>List of Figures</b>	xiv
<b>1 Background and Motivation</b>	1
1.1 Introduction . . . . .	1
1.2 The Microfluidic Lab-on-a-chip . . . . .	2
1.2.1 Applications of a Lab-on-a-chip . . . . .	3
1.3 Clinical Diagnostics . . . . .	3
1.3.1 Conventional clinical diagnostics . . . . .	3
1.3.2 Microfluidic technologies in clinical diagnostics . . . . .	4
1.3.3 Commercial Microfluidic Devices . . . . .	5
1.4 Droplet-based Discrete Microfluidics . . . . .	7
1.4.1 Electrowetting-based droplet actuation . . . . .	7
1.5 Electrowetting-based lab-on-a-chip for Clinical Diagnostics . . . . .	9
1.5.1 Related research . . . . .	11
<b>2 Nanoliter Lab-on-a-chip Design and Fabrication</b>	12
2.1 Lab-on-a-chip specifications . . . . .	12
2.1.1 Fluidic input port . . . . .	12
2.1.2 Liquid reservoirs . . . . .	13
2.1.3 Droplet pathways . . . . .	13

2.2	Lab-on-a-chip Design . . . . .	14
2.2.1	Fluidic Input Port . . . . .	14
2.2.2	Fluid Reservoirs . . . . .	16
2.2.3	Fluidic Droplet Pathways . . . . .	17
2.3	Fabrication of Lab-on-a-chip and System Assembly . . . . .	20
2.3.1	Design specifications . . . . .	20
2.3.2	Chip fabrication . . . . .	21
2.3.3	Top plate fabrication . . . . .	22
2.3.4	Detection Instrumentation . . . . .	24
2.3.5	System assembly . . . . .	26
2.4	Testing of fabricated lab-on-a-chips . . . . .	26
2.4.1	Material defects . . . . .	26
2.4.2	Chip loading . . . . .	28
2.4.3	Droplet dispensing . . . . .	28
2.4.4	Droplet pathways . . . . .	29
2.5	Chapter summary . . . . .	30
<b>3</b>	<b>Biocompatibility of the Electrowetting System</b>	<b>31</b>
3.1	Transport of Biological Fluids . . . . .	31
3.1.1	Measure of droplet transportability . . . . .	32
3.1.2	Transport of Pure Protein Solution . . . . .	33
3.1.3	Transport of Physiological Fluids . . . . .	35
3.2	Droplet generation from on-chip reservoir . . . . .	36
3.2.1	Droplet formation for pure proteins . . . . .	37
3.2.2	Droplet formation for physiological fluids . . . . .	38

3.3	Chapter summary . . . . .	38
<b>4</b>	<b>Clinical Assay on the Electrowetting Platform</b>	<b>39</b>
4.1	On-chip biological assay . . . . .	39
4.1.1	Microfluidic glucose analyzers . . . . .	39
4.2	Glucose Assay Development . . . . .	40
4.2.1	Rate-Kinetic Assay . . . . .	41
4.2.2	Analytical Range . . . . .	42
4.2.3	Analytical Sensitivity . . . . .	42
4.2.4	Lineweaver-Burke Plot . . . . .	43
4.3	Experimental setup . . . . .	43
4.3.1	Chemicals . . . . .	43
4.3.2	Optical detection . . . . .	44
4.4	On-chip Glucose Assay . . . . .	44
4.4.1	Dilution factor of 2 (DF=2) . . . . .	46
4.4.2	Dilution factor of 3 (DF=3) . . . . .	46
4.4.3	Analytical range . . . . .	52
4.5	Assays for Lactate and Creatinine . . . . .	53
4.5.1	Lactate Assay . . . . .	53
4.5.2	Creatinine Assay . . . . .	54
4.6	Chapter summary . . . . .	56
<b>5</b>	<b>Automated and Integrated Assays on a Lab-on-a-chip</b>	<b>58</b>
5.1	Microfluidic automation . . . . .	58
5.1.1	Pipelined Glucose Assays . . . . .	58
5.2	Assay Repeatability . . . . .	60

5.3	Serial Assays on Multiple Glucose Samples . . . . .	61
5.3.1	Within-run variation . . . . .	61
5.3.2	Comparison with off-chip results . . . . .	64
5.4	Serial Assays on Same Glucose Sample . . . . .	64
5.5	Glucose assay on serum . . . . .	69
5.6	Lactate assay on-chip . . . . .	72
5.7	Chapter summary . . . . .	72
<b>6</b>	<b>Conclusions and Future Work</b> . . . . .	<b>73</b>
6.1	Conclusions . . . . .	73
6.1.1	Lab-on-a-chip Architecture . . . . .	73
6.1.2	Biocompatibility . . . . .	74
6.1.3	Biological assays . . . . .	75
6.1.4	Integrated and automated lab-on-a-chip . . . . .	76
6.2	Future Work . . . . .	77
6.2.1	Dilution factor . . . . .	78
6.2.2	Detection methodologies . . . . .	79
6.2.3	System integration . . . . .	79
<b>A</b>	<b>Protein Stamping for MALDI Mass Spectrometry using an Electrowetting-based Microfluidic Platform</b> . . . . .	<b>81</b>
A.1	Abstract . . . . .	81
A.2	Introduction . . . . .	82
A.3	Materials and Methods . . . . .	84
A.3.1	Chip fabrication . . . . .	84
A.3.2	Chemicals . . . . .	84

A.4	Manipulation of Protein Samples by Electrowetting . . . . .	85
A.4.1	Protein Droplet Transport . . . . .	86
A.4.2	Protein Droplet Formation . . . . .	87
A.5	Passive Protein Stamping . . . . .	87
A.6	Results and Discussion . . . . .	88
A.6.1	Transport of BSA droplets . . . . .	88
A.6.2	BSA Droplet Formation . . . . .	89
A.6.3	Protein Stamping . . . . .	90
A.6.4	MALDI-MS on protein calibration solution . . . . .	91
A.7	Conclusions . . . . .	92
A.8	Acknowledgements . . . . .	94
<b>B</b>	<b>A Droplet-based Lab-on-a-chip for Colorimetric Detection of Nitroaromatic Explosives</b>	<b>95</b>
B.1	Abstract . . . . .	95
B.2	Introduction . . . . .	95
B.3	Materials and Methods . . . . .	97
B.3.1	Chemicals . . . . .	97
B.3.2	Electrowetting setup and Chip Fabrication . . . . .	98
B.3.3	Colorimetric method for the detection of TNT . . . . .	98
B.3.4	Optical Detection . . . . .	99
B.3.5	System Operation Protocol . . . . .	99
B.4	Results and Discussion . . . . .	100
B.4.1	Absorbance spectra of colored product . . . . .	100
B.4.2	TNT reaction on a spectrophotometer . . . . .	100

B.4.3	Detection of TNT on-chip . . . . .	101
B.4.4	Detection of TNT in a mixture of TNT and DNT . . . . .	102
B.5	Conclusions . . . . .	104
B.6	Acknowledgements . . . . .	105
<b>C</b>	<b>3-D Imaging of Moving Droplets for Microfluidics Using Optical Coherence Tomography</b>	<b>106</b>
C.1	Abstract . . . . .	106
C.2	Introduction . . . . .	106
C.3	Experimental Setup . . . . .	107
C.4	Results and Discussion . . . . .	108
C.4.1	Static Contact Angle . . . . .	108
C.4.2	Dynamic Contact Angle . . . . .	109
C.4.3	Flow Patterns during Transport . . . . .	109
C.4.4	Quantitative Contact Angle Data . . . . .	111
C.5	Conclusions and Future Work . . . . .	111
C.6	Acknowledgement . . . . .	111
<b>Bibliography</b>		<b>112</b>
<b>Biography</b>		<b>118</b>

## List of Tables

1.1	Commonly measured analytes in a clinical chemistry analyzer . . . . .	4
5.1	Coefficient of variation for the three different glucose concentrations . . .	61
5.2	Comparison of serum glucose values obtained using dilution factors of 2 and 100 . . . . .	71

## List of Figures

1.1	Cross-section and top view of the most basic electrowetting setup . . . . .	8
2.1	Design of the loading port on-chip . . . . .	15
2.2	Droplet formation from an on-chip reservoir . . . . .	18
2.3	Figure showing the synchronized motion of two droplets on a three-phase bus . . . . .	19
2.4	High-level architecture for clinical LoC showing the microfluidic elements	20
2.5	Two-layer metal process for fabrication a 2D lab-on-a-chip . . . . .	22
2.6	Top view image of the fabricated prototype lab-on-a-chip . . . . .	23
2.7	Optical absorbance measurement instrumentation used to monitor color change . . . . .	25
2.8	Electrolysis due to insulator breakdown in the reservoirs . . . . .	27
2.9	Sample injection into an on-chip reservoir . . . . .	28
2.10	Bus contention causing a droplet to split while moving on the 3-phase bus	30
3.1	Switching frequency of different concentrations of BSA droplets as a function of the applied voltage . . . . .	34
3.2	Switching frequency of droplets of various physiological fluids as a function of voltage applied . . . . .	36
3.3	Transport of $1.5\mu L$ whole blood droplet across 5 electrodes at 10Hz and 52V. The electrode material is transparent indium tin oxide . . . . .	37
4.1	Snapshots of a colorimetric glucose assay on an electrowetting chip . . . . .	45
4.2	Absorbance versus time for Glucose concentrations from 25mg/dL to 300mg/dL, for a sample dilution factor of 2. . . . .	47

4.3	Rate of reaction as a function of glucose concentrations from 25mg/dl to 800mg/dl, for a sample dilution factor of 2. . . . .	47
4.4	Rate of reaction as a function of glucose concentration in the linear range, for a sample dilution factor of 2. . . . .	48
4.5	Rate of reaction as a function of glucose concentrations from 100mg/dL to 800mg/dL, for a sample dilution factor of 3. . . . .	49
4.6	Rate of reaction as a function of glucose concentrations in the linear range, for a sample dilution factor of 3. . . . .	49
4.7	Comparison of results from a spectrophotometer and our electrowetting-based LoC, for a dilution factor of 3. . . . .	50
4.8	Comparison of results from a spectrophotometer and our electrowetting-based LoC, in the linear range, for a dilution factor of 3. . . . .	51
4.9	Lineweaver-Burke plot for Glucose Assay . . . . .	52
4.10	Calibration curve for a lactate assay done on a spectrophotometer . . . . .	55
4.11	Kinetics of a enzymatic creatinine assay on a spectrophotometer . . . . .	56
4.12	Calibration curve for the creatinine assay done on a spectrophotometer . . . . .	57
5.1	A flowchart describing the pipelined operation of two glucose assays . . . . .	59
5.2	A snapshot during the course of a pipelined glucose assay on a digital microfluidic lab-on-a-chip . . . . .	60
5.3	The absorbance measured as a function of time for nine serial glucose assays - three different glucose concentrations assayed three times each . . . . .	62
5.4	On-chip calibration curve for multiple glucose assays . . . . .	63
5.5	Michaelis-Menten Curve (on-chip assays) . . . . .	65
5.6	Michaelis-Menten Curve (off-chip spectrophotometric assay) . . . . .	66

5.7	Absorbance as a function of time for multiple glucose assays on the same 120mg/dL sample . . . . .	67
5.8	Reaction rate versus the run number for multiple glucose assays on the same 120mg/dL sample . . . . .	68
5.9	Absorbance as a function of time for multiple glucose assays on the same 40mg/dL sample . . . . .	69
5.10	Reaction rate versus the run number for multiple glucose assays on the same 40mg/dL sample . . . . .	70
A.1	Top and side views of a typical electrowetting setup . . . . .	85
A.2	High level schematic of the droplet stamping setup . . . . .	89
A.3	Maximum switching frequency of a BSA droplet as a function of the voltage for various concentration of BSA . . . . .	90
A.4	Time lapsed images of a protein stamping experiment . . . . .	91
A.5	Mass spectra of the ABI4700 MALDI calibration solution . . . . .	93
B.1	Schematic of the electrowetting lab-on-a-chip integrated with optical detection	97
B.2	Absorbance spectra of colored complexes formed in the reaction between TNT/DNT and KOH using DMSO as the solvent . . . . .	100
B.3	Absorbance of the colored complex for various concentrations of TNT as a function of time on the spectrophotometer . . . . .	101
B.4	Calibration curve of absorbance with respect to the concentration of TNT demonstrating a linear relation on the spectrophotometer . . . . .	102
B.5	Absorbance of the colored complex for various concentrations of TNT as a function of time on the electrowetting chip . . . . .	103
B.6	Calibration curve of absorbance with respect to the concentration of TNT demonstrating a linear relation on the electrowetting chip . . . . .	103

B.7	Absorbance of TNT at 505 nm with varying amounts of TNT+DNT demonstrating the noninterference of DNT with the TNT reaction. At 0% TNT in the mixture, DNT is 100%	104
C.1	Images showing the change in static contact angle of a droplet containing beads as a the voltage is changed	108
C.2	Images showing the change in dynamic contact angle of a milk droplet as it moves from one electrode to another	109
C.3	Flow profiles inside a moving droplet illustrating complete reversibility of flow	110

# **Chapter 1**

## **Background and Motivation**

### **1.1 Introduction**

Producing results in a shorter time, with higher confidence and at a lower cost is one of the constant priorities in any life-science laboratory. The key technology trends that are currently driving these factors in a laboratory setting are automation, integration and miniaturization [1]. Automation and integration minimizes human intervention in an experiment enabling more samples to be processed per unit time. Minimal human intervention also saves labor costs and valuable researcher time which could be channeled into more innovative tasks. High levels of parallelism and its associated throughput benefits are also enabled by automation and integration. Miniaturization lowers the volume of samples which minimizes invasiveness of sample collection procedures and iatrogenic losses. Small sample volumes are also critical for pediatric patients, especially neonatal babies. The consumption of reagents is also drastically reduced, lowering the cost per test and also minimizing waste and its associated disposal costs. Physical processes such as separation and diffusion are also expedited significantly in microscales. Miniaturization, automation and integration also enable instruments to be used at the point of care or sample collection [2].

Automation and integration in the laboratory began with the introduction of mechanized robotic systems for fluid handling in the highly parallel microtiter (or well plate) formats [3]. These systems were initially designed to do simple and highly repetitive tasks such as pipetting, and have now evolved to become sufficiently flexible and reprogrammable to meet the constantly changing needs in a laboratory. State-of-the-art robotic systems can handle microliters of liquids routinely with a few systems extending into the

10s of nanoliter ranges too [4, 5]. However the volume reproducibility suffers as the volumes scale down to nanoliters (6% at 100nL for Caliper's Sciclone ALH3000 as compared to 2% at 1 $\mu$ L). Robotic systems that can handle nanoliters of samples are also prohibitively expensive, affordable only by large labs for high throughput applications.

## 1.2 The Microfluidic Lab-on-a-chip

The early 90s saw the emergence of microfluidic technologies which could precisely handle liquids in nanoliter and sub-nanoliter quantities. Powered by microfluidics a new paradigm for miniaturized integrated analysis systems has emerged since and is popularly referred to as the lab-on-a-chip (LoC) or Micro Total Analysis System (MicroTAS) [6]. A lab-on-a-chip, as the name suggests, is a device which integrates various components of a bench-scale wet laboratory on the same miniaturized device. The functional operation of a typical lab-on-a-chip includes steps such as sample preparation, sample analysis (including mixing and reactions), separation and detection. [7] These steps are analogous to manual tasks currently performed in a conventional laboratory, except that in a lab-on-a-chip these occur in microscopic fluidic pathways and in an integrated fashion.

Microfluidic lab-on-a-chips can easily handle liquid volumes in the sub-nanoliter range without the associated loss in reproducibility. This is because microfluidic devices are typically fabricated using lithography processes which can have resolutions in the nanometer range. The small size of microfluidic devices also uniquely enables them to be used at the point of sample collection. Since microfluidic devices are designed to be mass-manufacturable they are considerably cheaper than robotic systems. Microfluidic systems can also provide higher levels of automation and integration than robotic systems due to their small form factor. It must be pointed out that robotics and microfluidics are not necessarily competing technologies and are in fact complementary in many applications. Real world samples are still collected in microliter volumes and robotic systems can provide

a good interface between the microscopic lab-on-a-chip and the macroscopic real world especially in high-throughput systems.

### **1.2.1 Applications of a Lab-on-a-chip**

Most current applications for a lab-on-a-chip are analytical in nature, and these include clinical diagnostics [8], drug discovery and protein analysis [9], molecular diagnostics, immunoassays [10], and cell culture and handling [11].

## **1.3 Clinical Diagnostics**

Clinical diagnostics is one of the most promising applications for microfluidic lab-on-chip systems, especially in a point-of-care or near-patient setting [12]. Clinical diagnostics refers to the measurement of clinically significant analytes in physiological fluids for either the prevention or treatment of disease. All the benefits of miniaturization such as reduced reagent consumption, reduced sample requirement, decreased analysis time and higher levels of throughput and automation, are realized in this application. Smaller patient sample volumes minimize the invasiveness of sample drawing procedures and reduces iatrogenic blood losses particularly in geriatric and pediatric patients (especially neonatal babies). Reduced reagent consumption significantly lowers cost, which is a major concern in clinical laboratories. Analysis times may also be effectively shortened due to the high levels of parallelism possible in microfluidic systems.

### **1.3.1 Conventional clinical diagnostics**

Clinical diagnostics in humans is commonly performed on physiological body fluids such as whole blood, serum, plasma and urine. Other fluids such as saliva [13], sweat [14], cerebral spinal fluid (CSF) and tears have also been used to assay specific analytes.

The number of analytes that are measured in a commercial high-throughput clinical chemistry analyzer ranges from 60 to 130 [15]. These analytes can be categorized according to their biological function into amino acids, proteins, cytokines, enzymes, carbohydrates, lipids, vitamins, electrolytes, blood gases, trace elements, drugs, tumor markers and nucleic acids [16]. Some of these analytes are measured more commonly than others. Table 1.1 shows a list of the most frequently measured analytes in clinical practice [12]. For a more comprehensive list the reader is referred to [16]. Traditionally photometric techniques have been used for measurement in clinical analyzers, though other methods such as electrochemical detection and fluorescence are also common now.

**Table 1.1:** Commonly measured analytes in a clinical chemistry analyzer

Glucose	Creatinine	Iron
Lactate	Bilirubin	Albumin
pCO <sub>2</sub>	Urea	Cholesterol
pO <sub>2</sub>	Sodium	Globulin
pH	Chloride	Neurotransmitters
Potassium	Cortisol	Triglyceride

### 1.3.2 Microfluidic technologies in clinical diagnostics

The use of microfluidic lab-on-chip technology for clinical applications has been reviewed extensively in [12, 17]. Currently almost all microfluidic devices are based on continuous fluid flow in permanent microchannels etched in glass, plastic or other polymers. Electrokinetic phenomena using electroosmosis for pumping and electrophoresis for separation are the most commonly used fluid actuation methods used. Electrokinetic methods are very popular because they scale favorably with miniaturization and do not require any mechanical pumps or valves for fluidic control. Electrophoresis has been used widely in clinical analysis for separation of a large class of analytes, including amino acids, DNA fragments, carbohydrates, proteins, drugs and vitamins [16, 18]. A general review of electrokinetically

driven microfluidic chips for fluidic manipulations and their applications can be found in [19].

The main drawback of electrokinetic methods is their incompatibility with several common samples [17]. This is due to their high sensitivity to liquid properties such as pH and ionic strength. For example physiological fluids with high ionic strength such as whole blood and urine cannot be pumped using electroosmotic flow due to excessive Joule heating [20]. Alternative actuation strategies which are fluid property independent are required in such cases.

Positive displacement methods using syringe pumps are the second most common actuation method used due to their ease of use and compatibility with a wide variety of samples [21, 22, 23, 24]. This technique has been combined with *in-vivo* microdialysis sampling for continuous on-line monitoring of small molecules such as glucose, lactate and Cl<sup>-</sup> [25, 26]. However if a high degree of fluidic control is desired some valving scheme is required which increases fabrication complexity. For this reason most microfluidic systems using syringe pumps are very simple and have only a couple of channels. Another novel micropumping method which is again fluid property independent is based on using inertial centrifugal forces to actuate liquids in a compact disc format [20, 27].

### 1.3.3 Commercial Microfluidic Devices

Despite the extensive research in microfluidic technology for more than a decade there are only a handful of successful commercial devices available in the market. Most of these devices, though they have microfluidic elements on them, do not actually have enough functionality or flexibility to be called a lab-on-a-chip.

Despite its ubiquity in academia there are no commercial devices that use electroosmosis for actuation, and only one product (Caliper Labchip) which uses electrophoresis for separation. Passive schemes using capillary forces and external pressure driven devices are

more common due to their compatibility with a wider range of samples. A brief review of the actuation mechanisms in commercial microfluidic devices for clinical applications is presented in the following paragraphs.

Caliper Technologies' LabChip device uses electrokinetic actuation to perform fluorogenic enzyme assays, separation-based kinase assays, and cell-based assays [5]. The Gyrolab microlaboratory from Gyros [28] and LabCD integrated microfluidic system from Tecan [29] are based on the compact disc format and use centrifugal and capillary actuation for microfluidic protein assays.

Micronics' ORCA Microfluidics [30] platform combines various pressure driven microfluidic elements, such as the diffusion based H-Filter and T-Sensor platforms, in a disposable microchip for point-of-care immunoassays on whole blood. The Biosite Triage Cardiac system [31] measures cardiac markers in whole blood in a microcapillary based device for point-of-care testing. Another popular microfluidic instrument for point-of-care testing is the handheld I-Stat [32] analyzer which can measure blood chemistry (glucose, blood gases, electrolytes, urea and more) in whole blood. The I-stat analyzer uses a combination of capillary action and external pressure for fluid actuation.

One can easily observe that all the microfluidic devices discussed above are very simple in function and operation, and cannot deliver the complexity required and promised by the lab-on-a-chip. The main reason for this is due to the use of continuous fluid flow in microchannels. Continuous-flow based microfluidic devices are extremely rigid in their architecture and function, and offer very little flexibility, scalability (in dimension and function) and reconfigurability. The microchannel configurations are usually tied to the specific application they have been designed for. Even minor variations in protocols are not possible and would require a complete redesign of the devices.

## 1.4 Droplet-based Discrete Microfluidics

An alternative to continuous-flow microfluidic systems is to manipulate the liquid as discrete microdroplets without any fixed microchannels. This approach has several advantages over continuous-flow systems the most important being reconfigurability and scalability of architecture [33]. Droplet-based protocols are functionally equivalent to bench-scale wet chemistry, thus established assays and chemistry protocols can simply be scaled down.

Electrowetting and dielectrophoresis have been the two most commonly used phenomena to actuate droplets. Though both of these phenomena have an electrostatic origin electrowetting, is fundamentally a contact line effect whereas dielectrophoresis is a body effect. Dielectrophoresis typically uses high frequency AC voltage ( $>50\text{Hz}$ ) which can cause significant Joule heating in samples even at moderate ionic strengths [34]. There is negligible Joule heating in electrowetting since it can use DC or low frequency AC. Electrowetting therefore appears to be applicable for a wider matrix of samples as compared to dielectrophoresis.

### 1.4.1 Electrowetting-based droplet actuation

Electrowetting refers to the modulation of the interfacial tension between a polar liquid phase and a solid electrode by the application of an electric potential between the two. To prevent electrolysis of the liquid phase the solid electrode is insulated. In the simplest implementation of an electrowetting system, the microdroplet is sandwiched between two surfaces, a patterned electrode array and a continuous ground plane [35] and is completely surrounded by an immiscible filler fluid. The two planes are separated by a spacer which defines the height of the droplet. The electrode array is insulated from the droplet and all surfaces are hydrophobized. The droplet size is typically just large enough to completely cover a single electrode and slightly overlap the adjacent electrodes. By switching the

voltage applied across adjacent electrodes interfacial tension gradients can be created to move the droplet to the charged electrode.

Figure 1.1 shows the side cross-section and a top view of the most basic electrowetting setup. The metal electrodes are typically defined in chrome or indium tin-oxide. The insulator is a  $1\mu m$  film of Parylene C which is eventually hydrophobized by a 50nm film of the amorphous fluoropolymer Teflon AF. A low viscosity silicone oil (1cSt) is used as the immiscible filler fluid.

The motion of a droplet in an electrowetting system is discrete in space (on the patterned array electrodes) and in time since it is typically operated by a single system clock. Fundamental fluidic operations such as transport, merging and splitting can be thought of as single-instruction operations which happen in one switching/ clock cycle. Other fluidic operations such as droplet formation and mixing can be programmed as a sequence of these single-clock cycle instructions. Due to its similarity to the functioning of a digital microprocessor this approach is referred to as “digital” microfluidics. It is important to note that all droplet-based microfluidic systems are not necessarily discrete in space and time and therefore not digital.

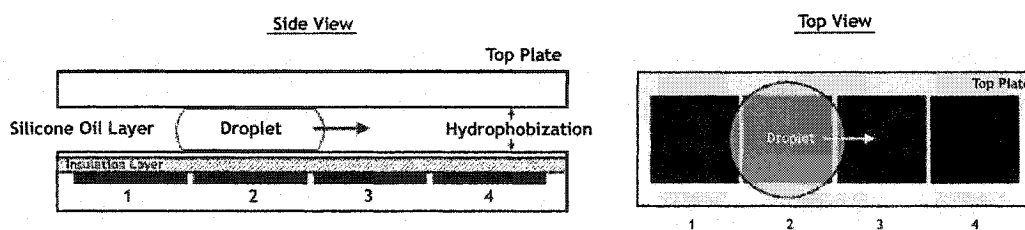


**Figure 1.1:** Cross-section and top view of the most basic electrowetting setup

## 1.5 Electrowetting-based lab-on-a-chip for Clinical Diagnostics

Several functional components of an electrowetting-based lab-on-a-chip have been demonstrated previously by other researchers.

1. *Sample injection/dispensing* - Dispensing of unit-sized 700nL droplets of 0.1M potassium chloride (KCl) solution from a larger initial droplet was demonstrated by Pollock [35]. The droplets were formed by extending a finger of liquid away from the reservoir till droplet break off. Droplets were also dispensed from an external source using a pipette to inject liquid onto an energized electrode and retract the liquid to form a droplet on the energized electrode [35]. Dispensing of microliter droplets using external pressure from an off-chip reservoir by capacitance metering was demonstrated by Hong [36]. The volume variation measured by capturing images of the dispensed droplets was found to be less than 2%.
2. *Sample manipulation* - Transport of nanoliter droplets of an electrolyte (0.1M KCl) at a maximum average speed of 10cm/sec using voltages less than 60V, was shown in [33]. Droplets were manipulated both in air and other immiscible filler fluids such as silicone oil. The motion of the droplets was independent of the molar concentration and the viscosity of the liquid. However, the motion of the droplets was significantly inhibited with increasing viscosity of the filler fluid [35]. Other essential droplet operations such as splitting and merging were demonstrated in [33].
3. *Sample preparation* - An on-chip serial dilution scheme was presented in [37]. The dilution scheme used a serial dilution architecture with the mixing and splitting of two droplets of different concentration to result in an intermediate concentration as the fundamental operation. A range of dilution factors can be obtained by repeating the basic dilution step. The dilution architecture was tested for dilution factors of 2,

4 and 8 using a dye droplet as the sample and 0.1M KCl as the buffer. The errors in the dilution were  $\approx$ 15% for a dilution factor of 4 and  $\approx$ 25% for a dilution factor of 8. The errors increased exponentially with each dilution step and the total error after the Nth dilution can be modeled by the equation  $E_N = 1 - (1 - E_0)^N$ .  $E_N$  is the error after N dilution steps (dilution of  $2^N$ ) and  $E_0$  is the error in the basic two-fold dilution step. This suggests that the serial dilution protocol may not be suitable for large dilutions.

4. *Mixers* - Due to the highly laminar flow conditions and flow reversibility, mixing on any microfluidic system is a challenge. Droplet mixing on the electrowetting system has been extensively studied by Paik [38]. Purely diffusive mixing took about 90 seconds for two  $1\mu\text{L}$  droplets and was significantly accelerated by just moving the coalesced droplet around. The fastest time for mixing two  $1.3\mu\text{L}$  droplets in a linear oscillation on 4 electrodes was observed to be 4.6 seconds [39]. Mixing times were further reduced at this ratio to less than 3 seconds using a two-dimensional array mixer, which mitigated the effects of flow reversibility to an extent. A split-and-merge mixer which used repeated splitting and merging resulted in an even shorter mixing time of less than two seconds [40].

All the experiments described above were done using non-biological aqueous salt solutions and using manually dispensed droplets (with the exception of the automated dispensing experiments) which were usually  $1\mu\text{L}$  in volume.

The overall objective of this thesis is to design and build a nanoliter lab-on-a-chip platform for integrated and automated analysis of clinical samples. In chapter 2 the requirements of the lab-on-a-chip are outlined and the individual functional components are designed. The fabrication and testing of both the individual components and the integrated lab-on-a-chip is also discussed in 2. In chapter 3 the compatibility of the electrowetting system with clinically relevant biological samples and reagents is evaluated using droplet

transport and droplet formation as performance metrics. An enzymatic glucose assay is developed in chapter 4 and the feasibility of performing biological assays on the electrowetting platform is demonstrated. Chapter 5 describes the testing and validation of the integrated lab-on-a-chip by performing fully automated assays on multiple samples, all the way from sample injection to detection. Conclusions and future extensions of this work are presented in 6.

### **1.5.1 Related research**

The electrowetting lab-on-a-chip has also been used for proteomic applications [41] (Appendix A) to reformat protein samples from a microtiter well-plate and stamp them onto a MALDI plate. The electrowetting system has also been used in environmental applications to detect TNT using a colorimetric assay [42](Appendix B). Fundamental studies on the electrowetting phenomena have also been done using Optical Coherence Tomography to image cross-sections of the droplets at high resolutions as they are moving [43] (Appendix C).

# **Chapter 2**

## **Nanoliter Lab-on-a-chip Design and Fabrication**

In this chapter a generic architecture is developed for a fully automatable and programmable droplet-based lab-on-a-chip for analysis of clinical samples. The lab-on-a-chip along with the detection instrumentation is designed to be a sample-in-result-out system, with all the intermediate steps being integrated and automated on-chip. Individual components of the lab-on-a-chip such as fluidic input ports, droplet formation units and pathways are first designed, tested, and integrated on the same monolithic device. The fabrication and testing of a prototype lab-on-a-chip and system assembly, including detection instrumentation, is also discussed in this chapter.

### **2.1 Lab-on-a-chip specifications**

The individual components of the lab-on-a-chip and their design requirements are outlined in this section. The functional components of the lab-on-a-chip are the fluidic input ports, droplet generation units and droplet pathways for transport, mixing and incubation.

#### **2.1.1 Fluidic input port**

The fluidic input port is the interface between the external world and the lab-on-a-chip. The design of the fluidic input port is challenging due to the huge discrepancy in the scales of real world samples (microliters) and the lab-on-a-chip (nanoliters). The electrowetting system also poses a slightly different problem due to the presence of the filler fluid (silicone oil) which always creates the possibility of development of air bubbles during liquid injection.

The main requirement of the fluidic input port is that the liquid should be stable in the reservoirs and not spontaneously flow back to the loading port after loading. The entrapment of air as bubbles in the filler fluid should be completely avoided or minimized during the loading process.

### **2.1.2 Liquid reservoirs**

The injected liquids are stored in reservoirs from which unit-sized droplets can be generated or dispensed. Once the reservoirs are loaded the lab-on-a-chip must be able to automatically dispense unit-droplets by software programming. Droplet generation should use only electrowetting forces without requiring additional external pressure sources which adds to design complexity and nullifies the advantages of the lab-on-a-chip being operable using only electrical control. The lab-on-a-chip should at least have three reservoirs - one each for the sample, reagent and calibrant, and one waste area to dispose the droplets after analysis. Each reservoir should be independently controllable to generate droplets on demand. The capacity of each reservoir should be at least 500nL which is the smallest volume that can be routinely handled using a manually operated pipette. The reservoirs should be able to dispense a large number of droplets ( $> 10$ ) to ensure the significance of any statistical studies. The droplets should be optimal in size (and volume) - just large enough to ensure reliable transport and maximum liquid utilization. The volume variation between droplets should also be as small as possible and not more than 5%.

### **2.1.3 Droplet pathways**

Droplet pathways consist of contiguous electrodes, which connect different areas of the chip. These electrodes can be used either simply for transport or for other more complex operations such as mixing and splitting. All the materials including the electrodes should be clear in areas which are to be used for optical interrogation. The number of

electrical input pads controlling the droplet pathways (and the dispensing unit) should be minimized to simplify the controller design and interconnect routing. The signals should be programmable and controllable in real-time by software.

## 2.2 Lab-on-a-chip Design

In this section the design of the various individual lab-on-a-chip components is presented for the requirements outlined before.

### 2.2.1 Fluidic Input Port

In the proposed architecture the fluidic input port is designed for manual loading of the reservoirs using a pipette. The sample (or reagent) is injected into the reservoir through a loading hole in the top plate, designed to fit a small volume ( $<2\mu\text{L}$ ) pipette tip. The loading hole is connected to the reservoir by a narrow channel of width  $w$ , patterned in the spacer material as shown in Figure 2.1. From the Laplace equation the liquid pressure in the reservoir can be calculated to be on the order of  $\gamma(1/R + 1/h)$  where  $R$  is the radius of the reservoir,  $h$  is the height of the reservoir and  $\gamma$  is the interfacial tension of the liquid with the surrounding media. Since  $R$  is typically much greater than  $h$  the pressure can be approximated as  $\gamma/h$ . The pressure in the channel connecting the loading port and the reservoir is  $\gamma(1/w + 1/h)$ . If  $w$  is on the order of  $h$  then the pressure in the channel is  $2\gamma/h$  which is twice the pressure in the reservoir. Therefore by choosing  $w$  to be close to  $h$  the liquid can be forced to remain in the reservoir and not spontaneously flow back into the loading hole. This pressure difference is initially overcome by the positive displacement pipetting action to fill the reservoir with the liquid.

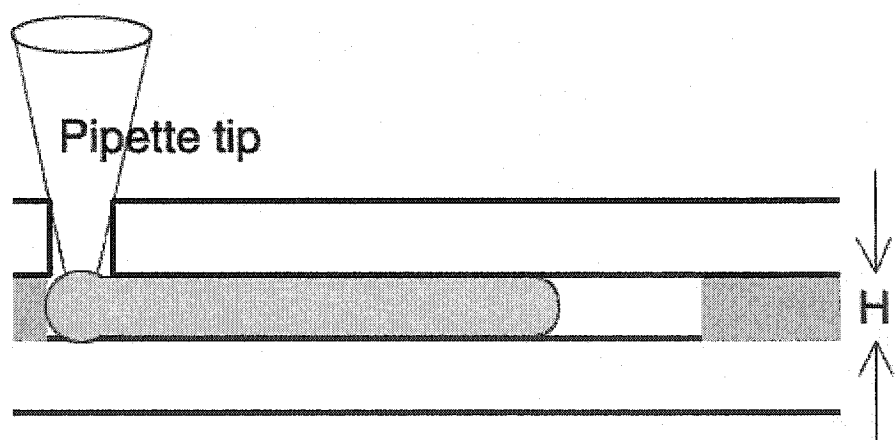
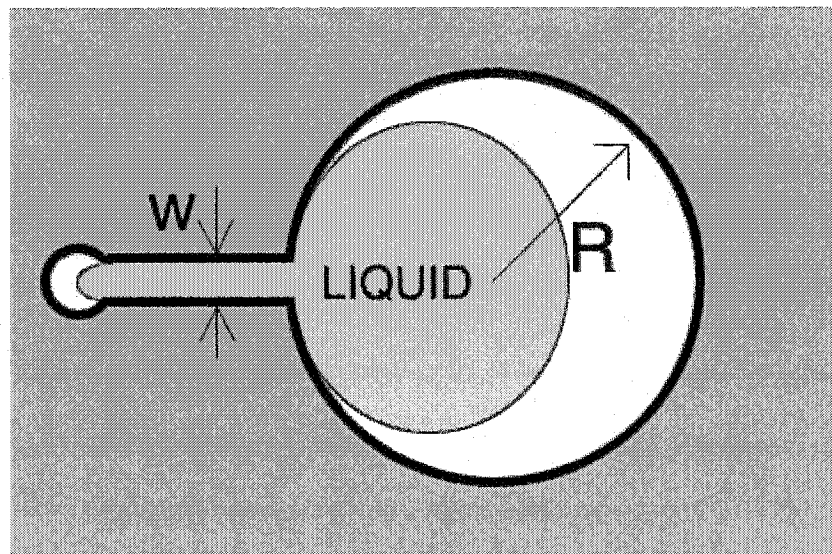


**Figure 2.1:** Design of the loading port on-chip

### **2.2.2 Fluid Reservoirs**

In the proposed lab-on-a-chip architecture, the droplets are formed from an on-chip reservoir which is physically defined by the spacer material. Droplet dispensing from an on-chip reservoir occurs in the following three steps [37].

1. A liquid column is extruded from the reservoir by activating a series of electrodes adjacent to it.
2. Once the column overlaps the electrode on which the droplet is to be formed, all the remaining electrodes are deactivated to form a neck in the column.
3. The electrode in the reservoir is then activated to pull the liquid back causing the neck to break completely and form a droplet.

Though simple in principle, the reliability and repeatability of the dispensing process is affected by several design and experimental parameters. The design parameters include the reservoir shape and size, shape and size of the pull-back electrode, size of the unit electrode (and correspondingly the unit droplet) and the spacer thickness. The choice and effect of each of these factors on the dispensing process is discussed below [36].

1. Electrode size - The electrode size was fixed at  $500\mu m$  and most of the other design parameters were chosen using this as the starting point.
2. Spacer thickness - Previous results [37, 44] indicate that the droplet dispensing for a water-silicone oil system requires a droplet aspect ratio (diameter:height) greater than 5. Taking this into account the spacer thickness was fixed at  $100\mu m$  for a droplet diameter of  $500\mu m$ . For this electrode size and spacer thickness combination the unit droplet volume is expected to be between 25-50nL.
3. Reservoir shape and size - The reservoir size is essentially determined by the smallest pipette-loadable volume on the lower end and chip real-estate concerns on the higher

end. In theory the reservoirs could be made as large as possible and always filled with a smaller quantity of liquid as needed. Different reservoir designs with capacities varying from 500-1500nL were tested.

4. Pull-back electrode design - A tapering pull-back electrode (wider at the dispensing end) was used to ensure that the liquid always stayed at the dispensing end of the reservoir.

In addition to the design parameters discussed above there are additional experimental factors which affect dispensing, and these include the volume of liquid in the reservoir, the length of the extruded liquid column and the voltage applied. It has been observed that the volume variation is much higher for the last few droplets generated from a reservoir i.e. when the reservoir is close to being empty [37]. The length of the extruded column also determines the volume of a unit droplet. During the necking process the liquid in the extruded column drains with half the volume going towards the reservoir and another half towards the droplet. Therefore the longer the extruded finger the larger the droplet volume. It has also been noted that the volume variation is larger when the droplet is formed farther away from the reservoir. The extruded liquid column also determines the minimum unusable dead volume in the reservoir. Figure 2.2 shows these steps in the formation of KCl droplets ( 20nL each) from an on-chip reservoir at 50V.

### **2.2.3 Fluidic Droplet Pathways**

The fluidic droplet pathways or buses connect various areas of the chip. In order to minimize the number of electrical contacts a multiphase bused design was used for the fluidic pathways. In an n-phase bus every nth electrode is electrically connected, and droplets are always spaced apart by  $k \times n - 1$  electrodes, where k is any integer. Figure 2.3 illustrates the operation of a multiphase (3-phase) bus. The use of a multiphase bus (requiring operations

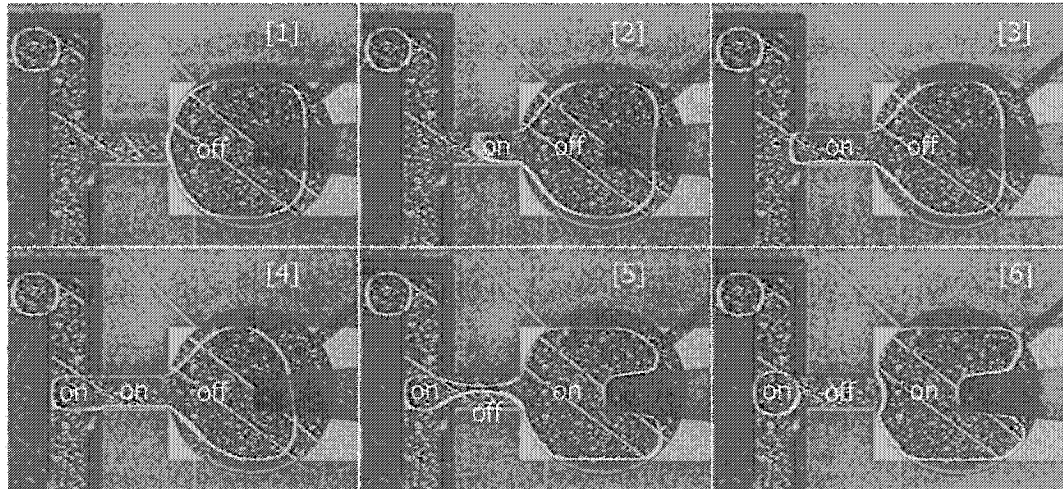


**Figure 2.2:** Droplet formation from an on-chip reservoir

to be synchronized) imposes constraints on the extent of parallelism achievable. Optimized scheduling strategies are therefore required in order to achieve maximum throughput [45].

Mixing of two droplets on the lab-on-a-chip is simply achieved by merging them and moving the merged droplet along a linear path. Droplet motion in an electrowetting system is known to create internal circulating flow patterns which enhance the mixing process. Since fluid flow in microfluidic systems is almost fully laminar these flow patterns show a high degree of reversibility [39] when the direction of the droplet motion is reversed. A linear path in one direction is therefore preferable over shuttling to avoid the demixing due to flow reversibility. The time required for complete mixing of 1.5mm x 1.5mm x 0.5mm droplets is around 2-3 seconds. In the proposed lab-on-a-chip the length scales along all the axes are 3 times smaller (0.5mm x 0.5mm x 0.1mm) and hence the mixing is expected to be significantly faster.

Chemical and biochemical reactions can be performed on-chip by merging reacting droplets and mixing them. Mixing of more than 3 droplets at a time can be a problem in the electrowetting system due to chip real-estate concerns, which means dilution factors greater than 3 would require novel strategies. One way to do this would be to use a serial-dilution approach, which consists of repeated mixing and splitting operations [37]. The

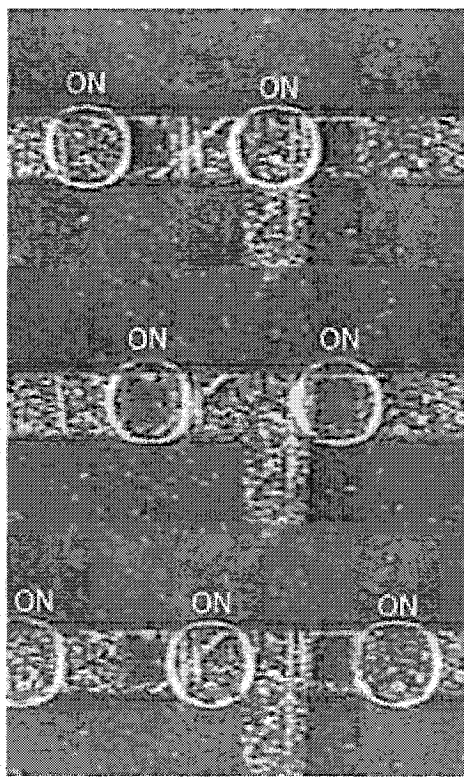


**Figure 2.3:** Figure showing the synchronized motion of two droplets on a three-phase bus

errors in dilution however increase geometrically with every additional dilution step.

Figure 2.4 shows the high-level schematic of the lab-on-a-chip for analysis of multiple analytes on a digital microfluidic platform.

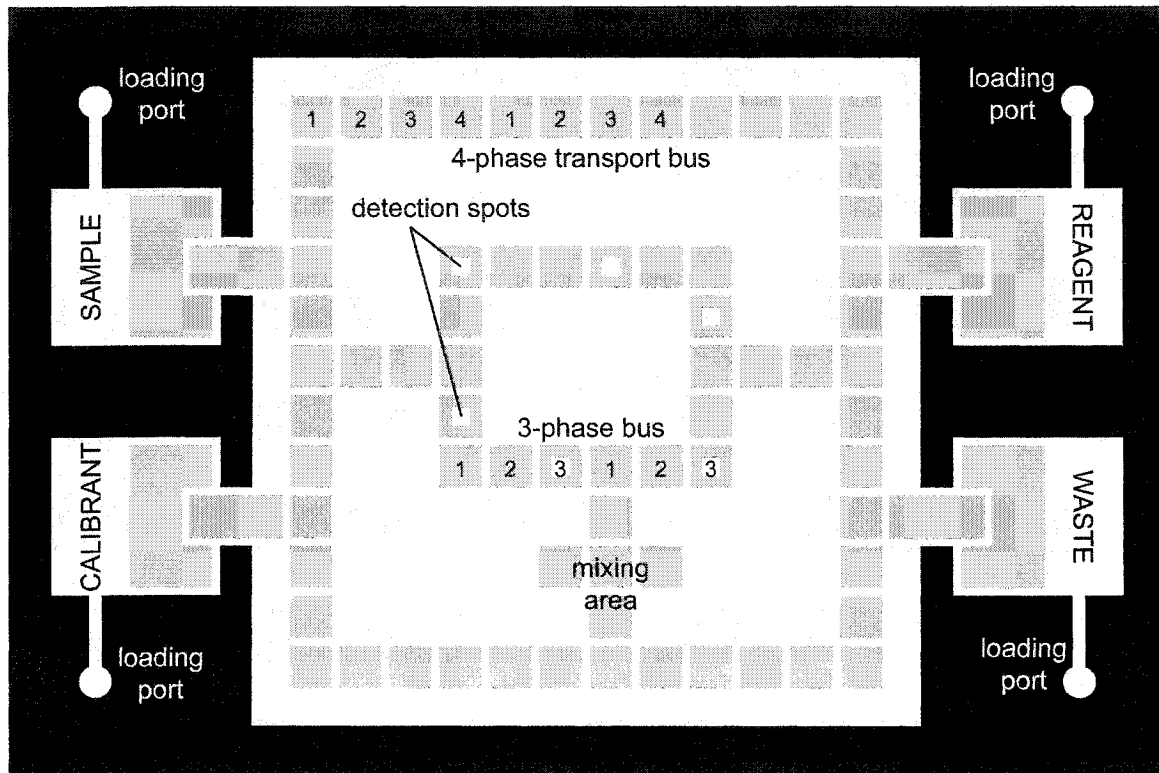


Figure 2.4: High-level architecture for clinical LoC showing the microfluidic elements

## 2.3 Fabrication of Lab-on-a-chip and System Assembly

### 2.3.1 Design specifications

A prototype lab-on-a-chip with sample injection elements, reservoirs (and waste), droplet formation structures, fluidic pathways, mixing areas and optical detection sites, was fabricated to test the various components of the architecture both individually and in an integrated fashion. The lab-on-a-chip consisted of 7 reservoirs and a waste area. The fluidic pathways consisted of a 4-phased outer transport bus, a 3-phased inner storage bus with

optical detection sites, and a mixing area, as shown in Figure 2.6. The reservoirs were 2.67 mm or 4mm in diameter, the electrode pitch  $L = 500\mu m$  and the spacer thickness  $H = 100\mu m$ . A  $100\mu m$  wide channel was defined on the spacer material to connecting the fluid input port and the reservoir. The entire chip was designed to be controlled using 22 electrical inputs.

### 2.3.2 Chip fabrication

The interconnect complexity of the electrowetting chips required a 2-layer metal process for fabrication. The interconnections were defined in the first layer and the electrode shapes were defined in the second layer. The two metal layers were separated by a inter-level dielectric, and electrical connection between the two layers was made using metallized vias. The process steps involved in the fabrication of the electrowetting chips are described below.

1. A  $2000\text{\AA}$  chrome coated glass wafer is photolithographically patterned to define the electrical contacts and interconnections to the electrodes.
2.  $6\mu m$  thick photoimageable polyimide layer is spin-coated to act as the inter-level dielectric and patterned to define  $40\mu m$  vias.
3. Indium-tin oxide is sputtered to metallize the vias and define the electrodes which were to be used for optical detection.
4. A second layer of  $1000\text{\AA}$  chrome was sputtered and patterned to define the remaining electrodes.
5. A 4mil ( $100\mu m$ ) thick photoimageable polymer ( $90\mu m$  after curing) was laminated onto the wafer to serve as the spacer material. The polymer was patterned to create the reservoirs, waste area and the loading channels.

6. 1 $\mu$ m thick Parylene C was vapor deposited to act as the primary insulating layer.
7. The Parylene surface was hydrophobized by spin-coating or dip-coating a thin (< 100nm) layer of Teflon AF (1% solids in FC-75) followed by baking at 170°C or air drying to remove the solvent.

Steps 1 through 5 were done by the Biomedical Microdevices and Sensors Laboratory at North Carolina State University, Raleigh, North Carolina. Parylene C was coated by Paratronix Inc, and the Teflon AF layer was coated in-house. Figure 2.5 shows the cross-sectional build-up of the various material layers in the two-layer fabrication process. Figure 2.6 shows the image of the top-view of the fabricated prototype lab-on-a-chip.

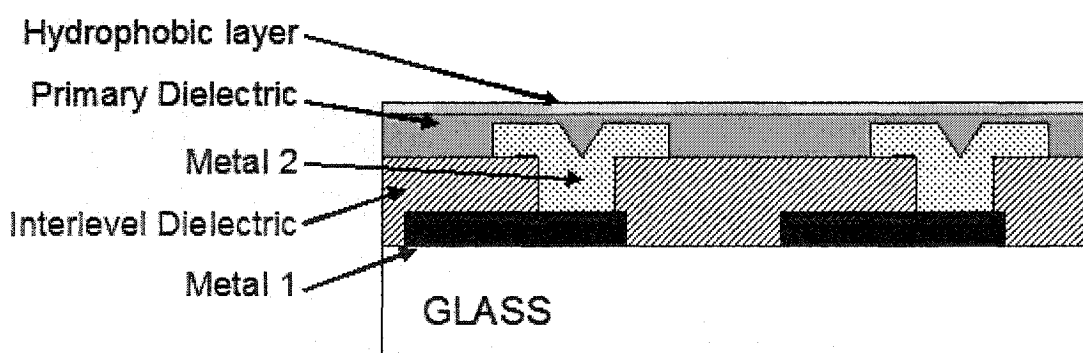


**Figure 2.5:** Two-layer metal process for fabrication a 2D lab-on-a-chip

### 2.3.3 Top plate fabrication

An indium-tin oxide coated glass slide or polycarbonate plastic acted as the ground plane. The indium tin-oxide slides were obtained from Delta Technologies. Polycarbonate plastic pieces were coated with ITO by Genvac Aerospace. Holes (aligned to the loading ports on the chip) were drilled on the ITO slide and acted as the fluidic input ports. The diameter of the holes was chosen as 1mm to fit a small volume pipette tip. The ITO slide was

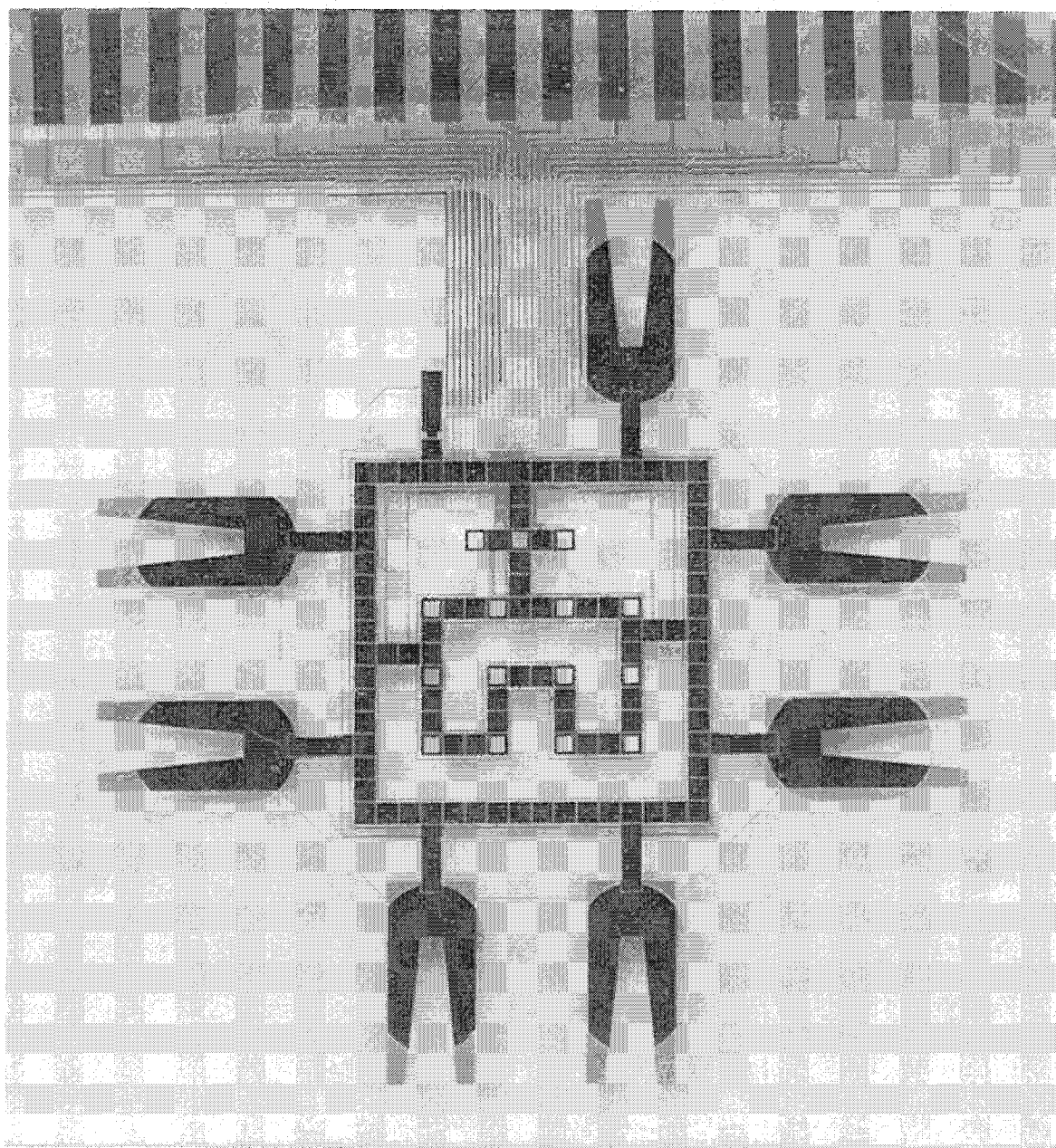


**Figure 2.6:** Top view image of the fabricated prototype lab-on-a-chip

hydrophobized by spin coating or dip coating a thin (<100nm) layer of 1% Teflon AF. The glass slides were baked at 170°C to remove the solvent. However since polycarbonate could not withstand such high temperature, the plastic top plates were left to dry overnight.

### 2.3.4 Detection Instrumentation

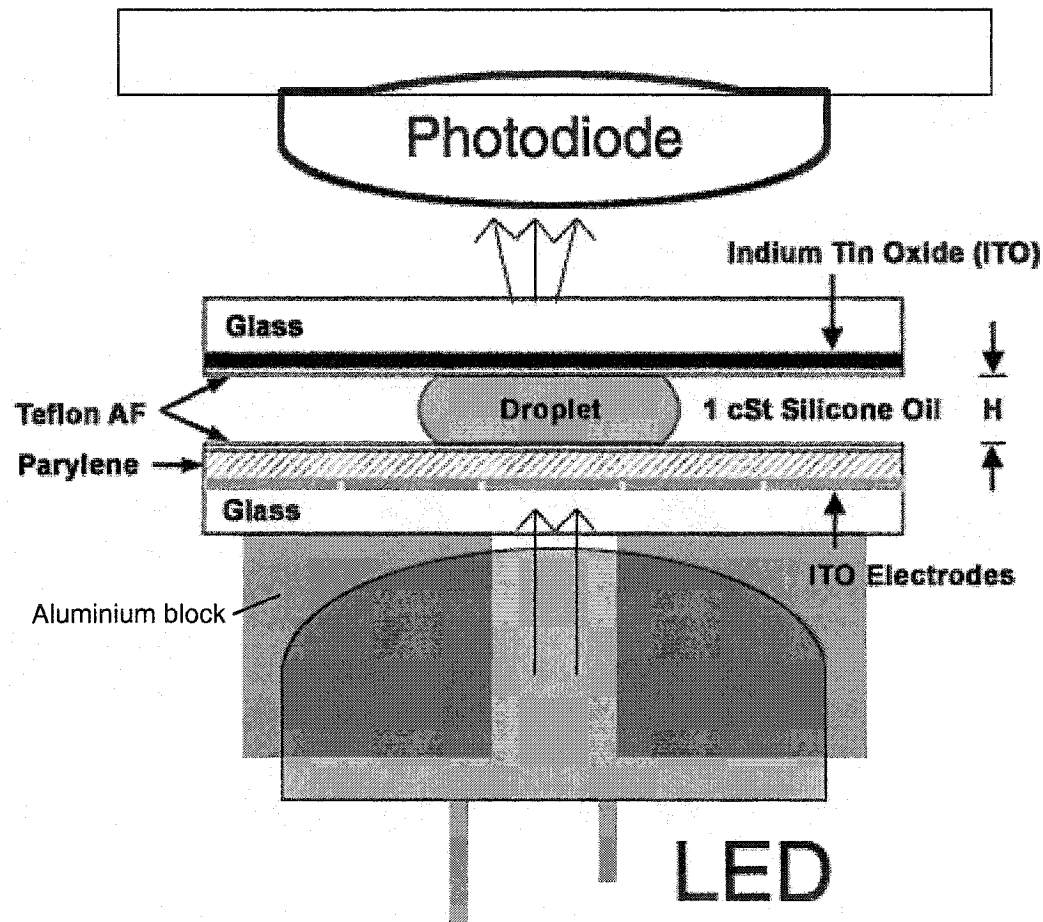
Detection in the electrowetting system is most easily done using optical techniques. This is because of the transparent nature of the materials involved in an electrowetting chip, including the electrodes which can be made out of transparent indium tin oxide. In the proposed architecture an optical absorbance measurement system, consisting of an LED and a photodiode, is integrated with the electrowetting device. The optical detection is done in a plane perpendicular to the chip. Colorimetric assays, which are very common in clinical applications, can be easily monitored using this technique. Several assays can be monitored simultaneously by either having multiple fixed detectors or by time-multiplexing a single detector.

Figure 2.7 shows the side view of the optical detection system. The output voltage of the photodiode  $V(t)$  is directly proportional to the light intensity incident  $I(t)$  on it. The absorbance  $A(t)$  is related to the intensity by the following equation.

$$A(t) = \ln\left(\frac{I(0)}{I(t)}\right) = \ln\left(\frac{V(t) - V_{dark}}{V(0) - V_{dark}}\right) \quad (2.1)$$

where  $I(0)$  and  $V(0)$  correspond to zero absorbance (or 100% transmittance), and  $V_{dark}$  is the dark voltage of the photodiode.

Equation 2.1 assumes that all the light that is incident on the photodiode passes through the liquid. Since the diameters of typical LEDs (3mm-5mm diameter) are much larger than the droplet ( $500\mu m$ ) the aperture of the light emitted by the LED was reduced by masking it using an opaque aluminium block with a  $400\mu m$  hole in the middle as shown in Figure 2.7.



**Figure 2.7:** Optical absorbance measurement instrumentation used to monitor color change

### **2.3.5 System assembly**

The electrowetting chip and the top plate were assembled such that the holes on top plate were aligned with the loading ports on the chip. The chip and top plate were clamped and held down by clips on the sides. Electrical connections to the contacts on the chip were made using a 22-pin SOIC test clip (Pomona Electronics). Voltages were applied to the test clip using an electronic controller which was essentially an array of high-voltage switches. The state of the switches (ON or OFF) was controlled by custom software through the parallel port or USB. For the absorbance measurement experiments the voltage output of the photodiode was logged on a computer using an analog data acquisition board.

## **2.4 Testing of fabricated lab-on-a-chips**

### **2.4.1 Material defects**

A small portion of the chips (3-4 in a wafer of 25) had electrical defects such as shorts and opens and since several of the electrical inputs were multiplexed, a single defect caused the entire chip to be inoperable. In the chips which were defect free the main reliability concern was the Parylene insulator. Electrolysis due to insulator breakdown was eventually seen in all the chips and almost exclusively in the reservoir (shown in Figure 2.8). Though the exact reason for the breakdown is unknown at this time it is hypothesized that this is due to mechanical cracking or failure of the Parylene film at the gasket-electrode junction in the reservoir, which exposes the metal to the liquid and causes electrolysis. This eventual breakdown in the insulator limited the time duration of a single fully-automated experiment. The longest experiment without failure lasted 10 minutes and was an exception rather than the norm. Typical lifetimes were more around 5 minutes which was not always sufficient.

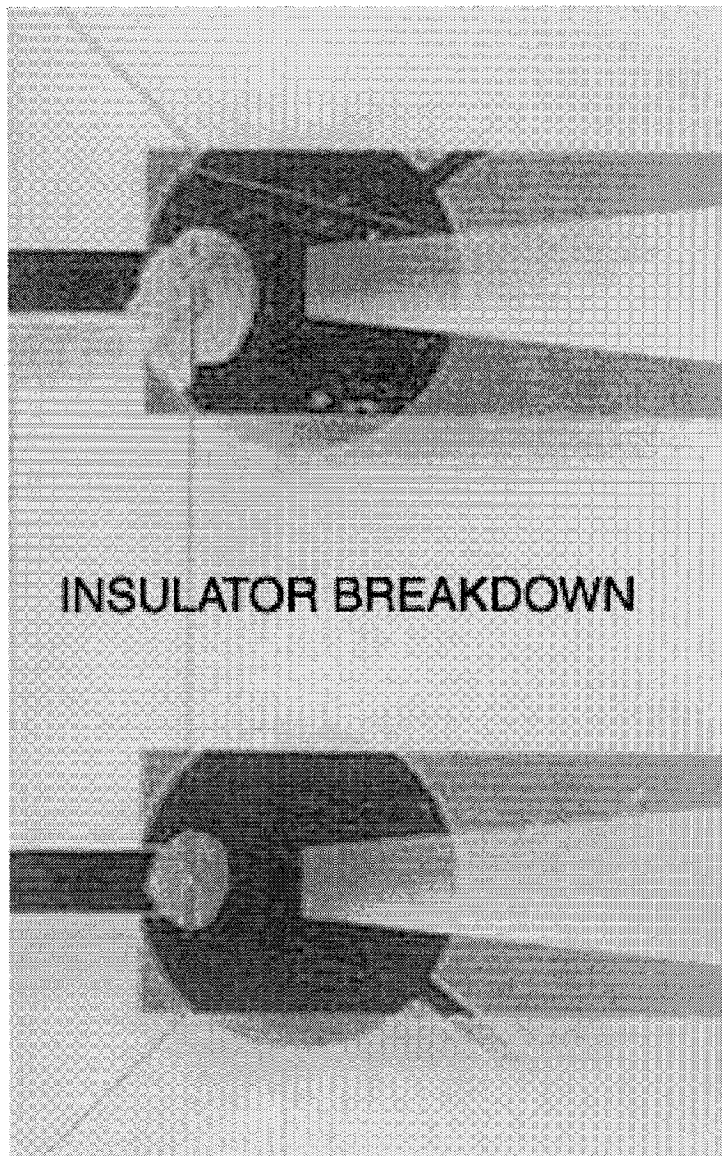


**Figure 2.8:** Electrolysis due to insulator breakdown in the reservoirs

## 2.4.2 Chip loading

Figure 2.9 shows snapshots in time during the loading of a reservoir by an external pipette. The diameter of the reservoir is 2.66mm, the channel width is  $100\mu m$  and the height of the reservoir is  $90\mu m$ . Variations in the channel width between 100 and 200 microns and the length of the channel did not affect the loading process. Silicone oil had to be injected first before the samples to avoid the trapping of air in the reservoirs. Air bubbles however still posed a huge problem during the loading of the samples and considerable operator skill was required to consistently load multiple reservoirs without any air bubbles. Significant improvement is necessary on this aspect of the design. Another problem which arose during the course of experiments was the evaporation of silicone oil through the loading holes since they were not sealed after loading.

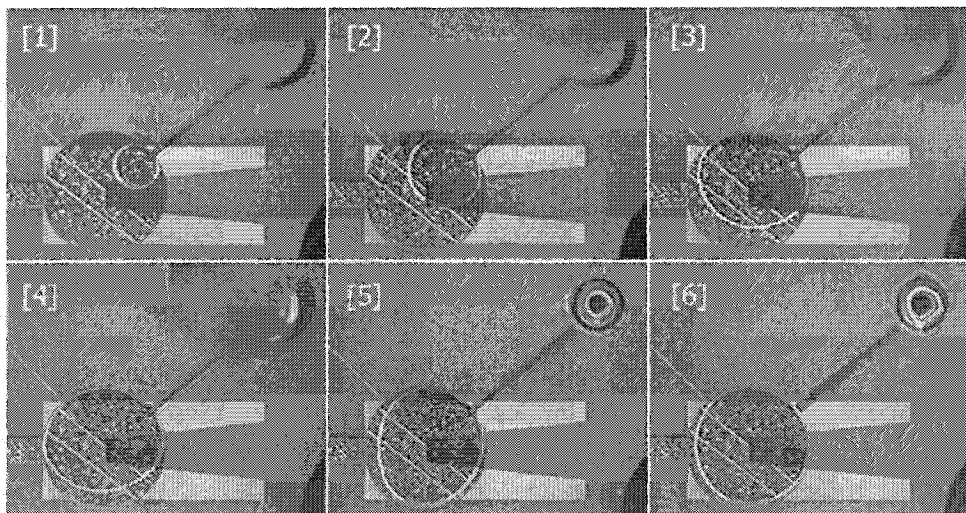


**Figure 2.9:** Sample injection into an on-chip reservoir

## 2.4.3 Droplet dispensing

Once the reservoirs were loaded without any air bubbles, droplet formation worked without any problems. Though the reservoirs were designed to hold 500nL of sample, dispensing would work only if the reservoir contained less than 500nL. This volume appeared to be

limited by the area of the pull-back electrode in the reservoir which was slightly smaller than the reservoir in the prototype lab-on-a-chip. Another design aspect which would require revision in future designs is the length of the extruded column. In the fabricated prototype the length of this column was  $1750\mu\text{m}$  (3.5 electrode widths) and resulted in the droplets being much larger ( $30\mu\text{L}$ ) than what was required for reliable transport. The larger droplets also decreased the number of droplets that could be generated from a reservoir to around 10 with the useful number being even smaller and around 8 or 9. The variation in droplet volume was calculated to be less than 3% CV [37].

#### 2.4.4 Droplet pathways

On the defect free chips the droplets were transportable in a loop around the 4-phased bus and the 3-phased bus at a maximum frequency of 50Hz. This corresponds to a speed of 2.5cm/sec. To ensure reliable operation, the maximum clock frequency that was used in other experiments was around 10Hz. The transport of two merged droplets was also tested on the two buses. A double-droplet was transportable on the 4-phase bus but not on the 3-phase bus. On the 3-phase bus the droplet was too big and caused a contention issue at the corners of the 3-phase loop. This contention caused the droplet to split into two while moving on the 3-phase bus as illustrated in Figure 2.10. This issue was not observed on the 4-phase bus.

The mixing times on the nanoliter lab-on-a-chip was evaluated by analyzing the mixing process between a fluorescein and water droplet. The two droplets were merged and moved in one direction (not shuttled) along a transport bus at 10Hz. Images of the merged droplet were captured and the time required for complete mixing was estimated to be  $\approx 0.8$  seconds.

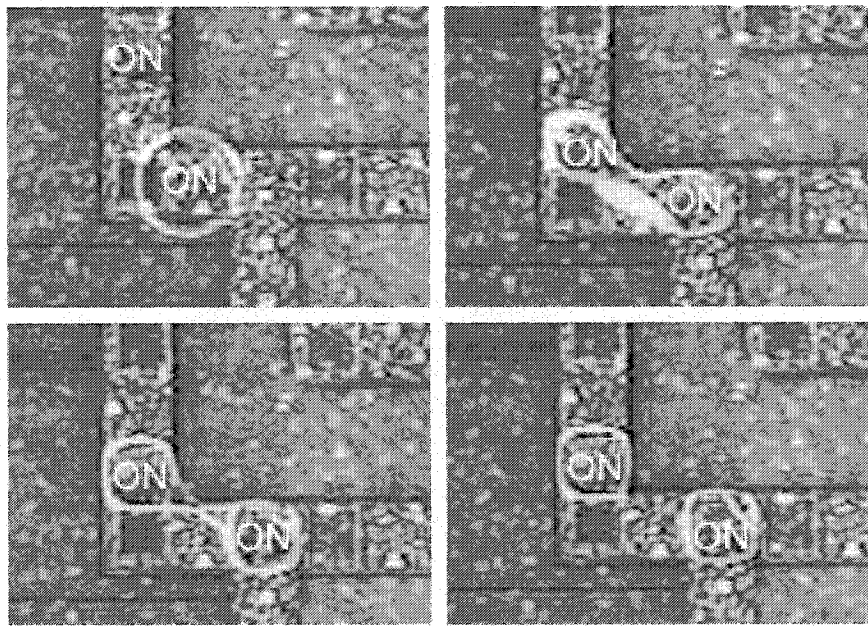


**Figure 2.10:** Bus contention causing a droplet to split while moving on the 3-phase bus

## 2.5 Chapter summary

The design and prototyping of a nanoliter lab-on-a-chip was presented in this chapter. Insulator breakdown in the reservoir caused catastrophic failure in the chips and ultimately determined the lifetime of the chip and the duration of experiments. The second biggest factor which limited experiment durations was the evaporation of silicone oil from the chip creating air bubbles during the course of an experiment. However the lab-on-a-chip was still capable of performing all the basic fluidic operations such as sample injection, droplet dispensing, transport and mixing both individually and in an integrated fashion.

# **Chapter 3**

## **Biocompatibility of the Electrowetting System**

Clinically relevant samples such as physiological fluids have always posed a major challenge to conventional microfluidic devices [17]. It is therefore important to first establish the compatibility of such fluids with the electrowetting system. The compatibility of a liquid with the electrowetting system is evaluated by testing the transportability of the droplet and the ability to form droplets from an on-chip reservoir using only electrowetting forces.

### **3.1 Transport of Biological Fluids**

All biological samples contain proteins. Proteins are not easy to handle in microfluidic systems because of their tendency to adsorb to any surface they come in contact with and contaminate them. The adsorption is more pronounced on hydrophobic surfaces and in most cases irreversible under normal conditions [46]. In the electrowetting system the liquid droplet is sandwiched between two Teflon AF coated hydrophobic surfaces. Any contact between the liquid droplet and this Teflon AF surface, will therefore contaminate the surface. In addition to contamination, protein adsorption also renders the surface permanently hydrophilic. This is detrimental to transport, since electrowetting works on the principle of modifying the wettability of a hydrophobic surface. Therefore any contact between a liquid droplet containing proteins and the Teflon surface should be avoided to prevent contamination and enable transport. As a consequence, air is not a suitable filler medium for applications involving proteins, since the droplet is always in contact with the Teflon surface. Using air as a filler medium, static electrowetting (i.e. static change in contact angle by application of a potential) of  $4\mu\text{g/mL}$  BSA droplets has been previously demonstrated in a very limited sense [46]. However dynamic transport has not been shown

in air and will indeed be a big challenge due to the reasons mentioned above. Even in the static case the reversibility of the contact angle change reduces over time due to continuous non-specific and electric field driven adsorption.

Silicone oil with its low surface tension and spreading properties appears to be an ideal alternative. From visual observations and electrical capacitance measurements during droplet transport in silicone oil, we have inferred the presence of a thin film of oil encapsulating the droplet. This oil film isolates the droplet from the Teflon surfaces, minimizing adsorption and facilitating transport.

Though the oil film is yet to be extensively characterized its stability appears to decrease with lowering of the interfacial tension between the liquid droplet and oil. Since the liquid-oil interfacial tension typically decreases with increasing protein content, the stability of the oil film is also lower in such cases. A less stable oil film implies more adsorption of proteins on the Teflon surfaces and consequently droplets having higher protein content can be expected to be more difficult to transport and may require higher voltages. The oil film may also be squeezed out by the droplet at high voltages due to electrostatic pressures. Therefore, the actuation voltage has to be carefully chosen to facilitate transport of the droplets while maintaining the oil film.

### **3.1.1 Measure of droplet transportability**

Due to the discrete nature of operation of a digital microfluidic system, the maximum switching frequency, which we define as the highest rate at which a droplet can be moved across two adjacent electrodes, is the measure of the transport performance of the system. Higher the switching frequency, more the number of discrete fluidic operations that can be performed per second and higher the throughput of the system. It has been shown previously that the average speed of a droplet at a particular voltage remains constant with physical scaling [33]. The average speed is defined as the product of switching frequency

and electrode pitch. Therefore, the switching frequency is inversely proportional to the electrode pitch and can be increased by physically scaling the system down.

### 3.1.2 Transport of Pure Protein Solution

Bovine Serum Albumin (BSA) is one of the most commonly used proteins in adsorption studies. BSA adsorbs very easily to any surface and is in fact used in many applications to protect surfaces from the non-specific binding of other proteins. The maximum switching frequency of droplets containing different concentrations of BSA (0.001-10mg/mL) was evaluated as a function of voltage.

*Materials* - Stock solution of BSA (10mg/mL) was provided by GlaxoSmithKline (Durham, North Carolina, USA) and diluted to 1 mg/mL, 0.1 mg/mL, 0.01 mg/mL and 0.001 mg/mL in deionized water. The electrode pitch was L=1mm, the gap was H=500 $\mu$ m and the droplet volume was 0.75 $\mu$ L. Silicone oil (1cSt) was used as the filler fluid.

*Methods* - The smallest voltage required to sustain motion of the physiological sample droplets across 5 electrodes was evaluated at different switching frequencies.

*Results* - The transportability was found to be sensitive to the experimental protocol that was followed. In the first protocol the droplet of BSA was first manually pipetted and the silicone oil was added next. Dispensing the BSA first caused instantaneous adsorption to the Teflon surfaces, rendering the surface hydrophilic and the droplet was not further transportable. In the modified protocol the silicone oil was first dispensed, followed by the BSA. This ensured the presence of an oil film right from the beginning of the experiment and enabled the transport of the protein solutions. Figure 3.1 plots the maximum switching frequency as a function of the voltage, for various concentrations of BSA. As expected, droplets with higher protein content are more difficult to transport and require higher voltages for operation. The concentration of BSA that is transportable is three orders of magnitude higher than what has been previously demonstrated in air [46].

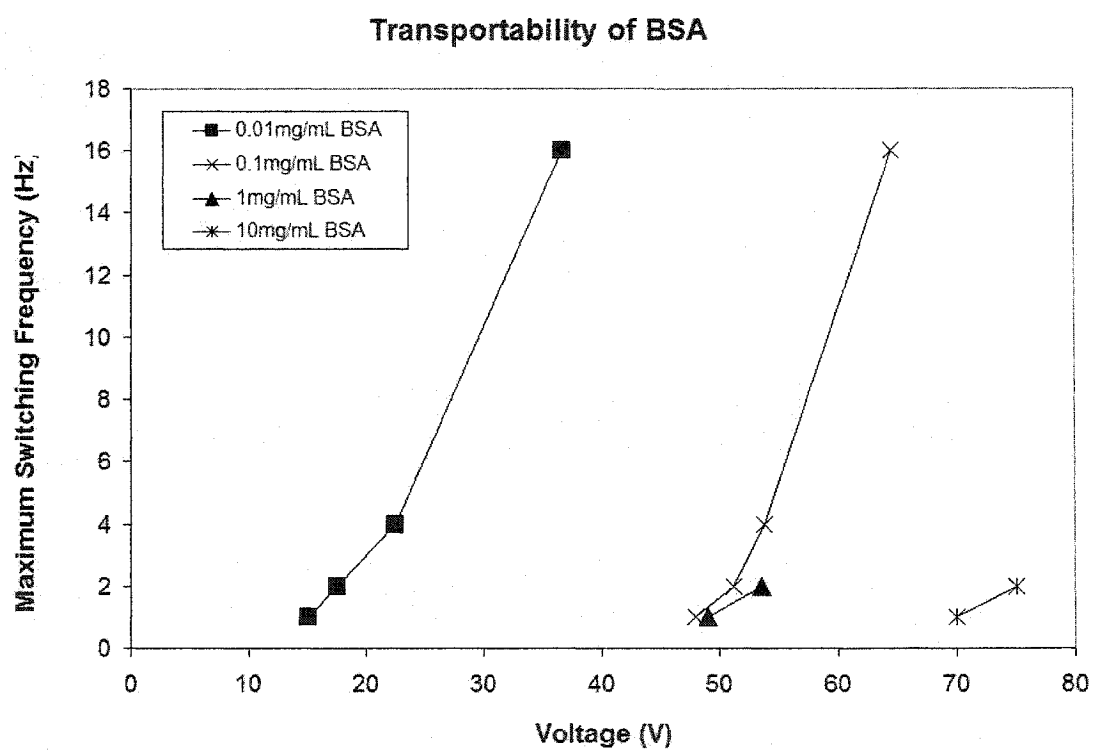


**Figure 3.1:** Switching frequency of different concentrations of BSA droplets as a function of the applied voltage

### 3.1.3 Transport of Physiological Fluids

The maximum switching frequency of a droplet of whole blood, serum, plasma, urine, saliva, sweat, tear and a buffer (0.1 M PBS, pH = 7) was evaluated as a function of the applied voltage.

*Materials* - Heparinized blood, serum and plasma samples were obtained with IRB clearance from the Duke University Medical Center. Other physiological fluids were obtained from a healthy human adult. The electrode pitch is  $L = 1.5\text{ mm}$  and the spacer height is  $H = 500\mu\text{m}$  with 1cSt silicone oil as the filler fluid. The volumes of the droplets were between  $1.3\mu\text{L}$  and  $1.5\mu\text{L}$ .

*Methods* - The smallest voltage required to sustain motion of the physiological sample droplets across 5 electrodes was evaluated at different switching frequencies.

*Results* - Figure 3.2 plots the maximum switching frequency of droplets of the various fluids as a function of the actuating voltage. All the fluids could be actuated at frequencies of 20 Hz using less than 65 V. The general trend that can be observed from the graph is that the fluids with less or no protein such as buffer and saliva transport more easily than the ones with higher protein content such as whole blood or serum, which is consistent with what we expected.

Figure 3.3 shows images of a whole blood droplet as it moves across 5 electrodes at 10Hz. The transport of the droplet of heparinized whole blood was sustainable for  $\approx 25,000$  continuous droplet transfers at 10 Hz ( $\approx 40$  min) using an actuating voltage of 52 V. After 25,000 cycles the droplet was slower to respond and required a higher voltage to maintain the same switching frequency. This performance degradation could either be due to insulator degradation or gradual adsorption of proteins on to the Teflon surface. The transport of other physiological fluids was sustainable for as much or in some cases even more cycles than whole blood, depending on the protein content. An important issue that has not been addressed is the stability of blood cells under electrowetting conditions, and

further experiments are required to evaluate any haemolysis that may occur.

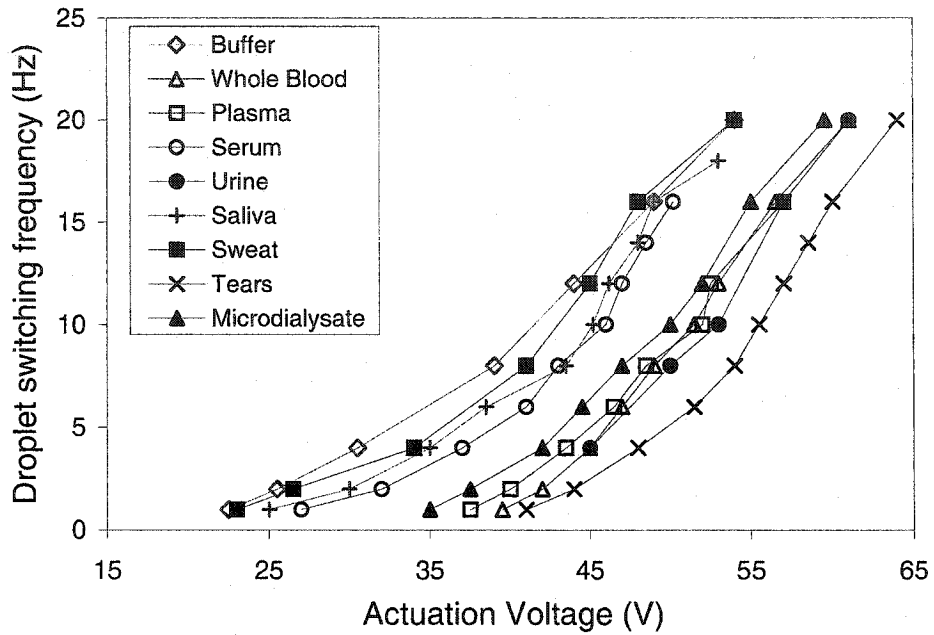


**Figure 3.2:** Switching frequency of droplets of various physiological fluids as a function of voltage applied

### 3.2 Droplet generation from on-chip reservoir

The process of generating unit-droplets from an on-chip reservoir using only electrowetting forces was described in Section 2.2.2. As in the case of transport, droplet formation also needs to be evaluated for solutions containing proteins to completely establish the compatibility of the liquid with our platform. The formation process is likely to be more severely affected by protein adsorption than transport, since the liquid in the reservoir has a much larger surface area to adsorb to than a unit droplet. Concentrations for which formation would work are therefore expected to be smaller than the maximum concentration for which simple transport would work. There are two measures of performance of droplet dispensing, reliability and repeatability. Reliability addresses the compatibility issue of whether droplets can actually be formed using only electrowetting. Repeatability

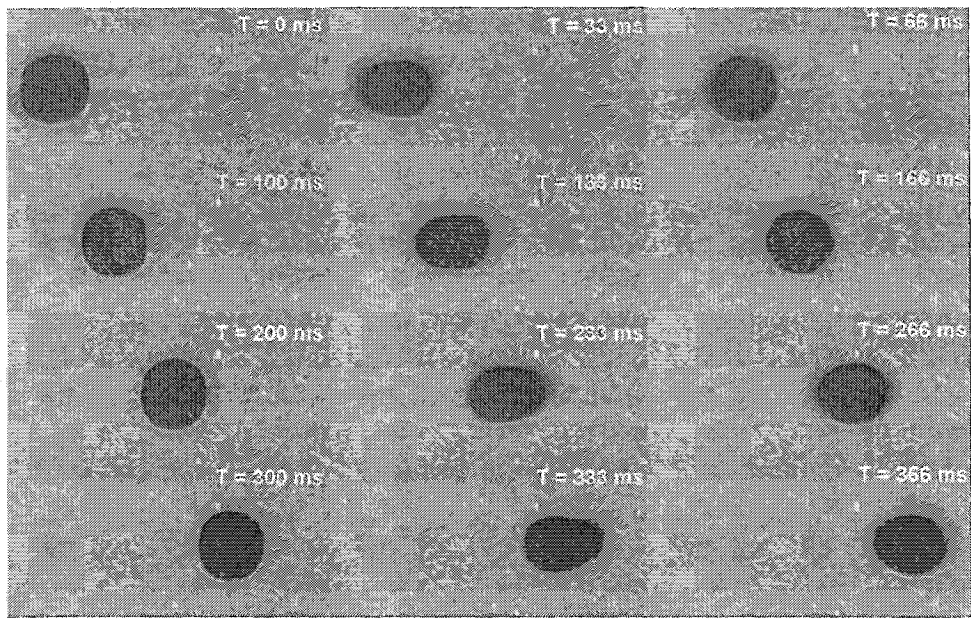


**Figure 3.3:** Transport of  $1.5\mu\text{L}$  whole blood droplet across 5 electrodes at 10Hz and 52V. The electrode material is transparent indium tin oxide

addresses the issue of droplet volume variability.

### 3.2.1 Droplet formation for pure proteins

*Materials and methods* - Bovine Serum Albumin (BSA, A-4378) was obtained from Sigma Chemicals (St Louis, Missouri, USA) and solutions of 0.1 mg/mL, 0.01 mg/mL and 0.001 mg/mL were prepared in de-ionized water. The electrode pitch was  $L=750\mu\text{m}$  and the spacer thickness was  $H=75\mu\text{m}$ . Droplet formation from BSA solutions of various concentrations (0.001-0.1 mg/mL) using only electrowetting forces was evaluated.

*Results* - Reliable on-chip dispensing was possible up to concentrations up to 0.01 mg/mL. For solutions containing higher concentrations of BSA ( $\geq 0.1\text{mg/mL}$ ) it was not possible to generate droplets using only electrowetting, despite the fact that individual droplets containing up to 10 mg/mL BSA are transportable. This is likely due to protein adsorption, since the liquid in the reservoir has a much larger surface area ( $\approx 20$  times more than a unit droplet) and therefore a higher chance of adsorbing to the surfaces of the reservoir.

### **3.2.2 Droplet formation for physiological fluids**

The reliability and repeatability of droplet formation from on-chip reservoirs was tested using human serum, plasma and whole blood and enzymatic reagents. Three serum samples having different total protein content, one plasma sample, one whole blood sample and an enzymatic glucose reagent were tested.

*Materials and methods* - All experiments were done on 2-D electrowetting chips with 2.67 mm diameter reservoirs, electrode pitch  $L = 500\mu m$  and spacer thickness  $H = 90\mu m$ . 1cSt silicone oil was used as the filler fluid. The operating voltage was fixed at 50V unless otherwise specified.

*Results* - Droplets could be reliably formed from serum, plasma and the enzymatic reagents using the standard operating voltage of 50V. Three different serum samples with different total protein contents were tested and the dispensing reliability was identical for all of them. Droplet dispensing did not work for whole blood at a maximum tested voltage of 120V.

## **3.3 Chapter summary**

The compatibility of the electrowetting system with biological samples is important to its usefulness in real-world applications. The results presented in this chapter validate the claim that the electrowetting system is compatible with a wide range of sample matrices. Pure protein solutions such as BSA and clinically relevant physiological samples such as serum and plasma were transportable and dispensable. The concentrations for which dispensing worked were however much smaller than the concentrations which were transportable. This was expected due to the significantly larger adsorption in the reservoir due to its larger surface area.

# **Chapter 4**

## **Clinical Assay on the Electrowetting Platform**

### **4.1 On-chip biological assay**

The glucose assay, which is one of the most common and frequently performed assays in clinical diagnostics, was chosen as a model assay to test the lab-on-a-chip. The in-vitro measurement of glucose in human physiological fluids is of great importance in clinical diagnosis of metabolic disorders. The most important of these disorders is diabetes mellitus (hyperglycemia) which is characterized by high levels of glucose in human physiological fluids. Diabetes is the most common metabolic disorder in the world with more than 150 million affected people, and the number is expected to double over the next two decades [47]. The assessment of glucose levels in body fluids is also used in the diagnosis of hypoglycemia (low levels of blood glucose).

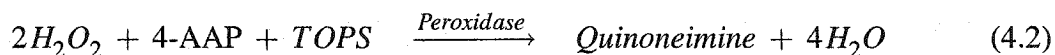
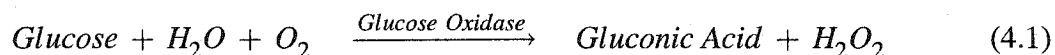
#### **4.1.1 Microfluidic glucose analyzers**

Enzymatic reactions are the most commonly used methods to assay glucose. Enzymes are protein molecules which act as catalysts for organic biochemical reactions. Glucose oxidase, due to its high specificity for glucose, is the most commonly used enzyme in a glucose assay. In the microfluidic domain glucose analyzers are usually based on continuous flow, using syringe pumps [48] or electroosmosis [49] for pumping. Microdialysis sampling has also been coupled with microfluidics [26] for real-time monitoring of glucose. The most commonly used biorecognition element is immobilized glucose oxidase [50] though enzymatic assays in solution phase [51] coupled with electrophoretic separation have also been reported. In an immobilized assay the enzyme is bound to a solid phase which is in contact with the sample that is to be analyzed. Detection is done using electrochemical

methods such as amperometry [49, 48, 26] or optical methods such as absorbance [50] or chemiluminescence [52].

## 4.2 Glucose Assay Development

Immobilized enzymatic assays are not easily adaptable to the electrowetting system because of material incompatibility and fabrication complexity. In contrast solution-phase enzymatic assays are easily implemented in the electrowetting system. A modified Trinder's reaction [53], which is a colorimetric enzyme based method, was used for glucose detection in our system. The enzymatic reactions involved in the assay are



Glucose is enzymatically oxidized in the presence of glucose oxidase to produce gluconic acid and hydrogen peroxide. The hydrogen peroxide formed reacts with 4-amino antipyrine (4-AAP) and N-ethyl-N-sulfopropyl-m-toluidine (TOPS), to form violet colored quinoneimine, which has an absorbance peak at 545nm. The absorbance is related to the concentration of quinoneimine (in Equation 4.2) by Beer's law.

$$A(t) - A_{blank} = \epsilon LC(t) \quad (4.3)$$

where  $A(t)$  is the absorbance at time  $t$ ,  $A_{blank}$  is the blank absorbance,  $\epsilon$  is the extinction coefficient of quinoneimine under the assay conditions,  $L$  is the optical path length, and  $C(t)$  is the concentration of quinoneimine at time  $t$ .

The glucose concentration is calculated from the absorbance (or the concentration of quinoneimine) using either an end-point method or a kinetic method. In the end-point method the reaction is allowed to proceed to completion. The concentration of glucose in the sample is stoichiometrically related to the concentration of quinoneimine, which is

proportional to the absorbance at the end of the reaction.

$$[\text{Glucose}] = \frac{[\text{Quinoneimine}]}{2} \times DF = \frac{A_{\text{end}} - A_{\text{blank}}}{2 \epsilon L} \times DF$$

where  $[\text{Glucose}]$  is the concentration of glucose in the sample,  $[\text{Quinoneimine}]$  is the concentration of quinoneimine at the end-point,  $DF$  is the dilution factor,  $A_{\text{end}}$  is the absorbance at the end-point.

The end-point assay typically takes 10s of minutes depending on the reagent composition and the temperature. The end-point method also uses higher concentrations of enzymes and requires a blank reading.

#### 4.2.1 Rate-Kinetic Assay

Using the kinetic method, the entire assay can be done in less than a minute. Kinetic methods also require significantly lower concentrations of enzyme as compared to end-point methods and does not require a blank reading. We have used the kinetic method in our system for the above mentioned advantages. In the kinetic method the concentration of glucose is related to the rate of the reaction. By taking the time derivative of Equation 4.3 we get

$$\text{Rate of reaction} = \frac{dC(t)}{dt} = \frac{1}{\epsilon L} \times \frac{dA(t)}{dt} \quad (4.4)$$

The Trinder's reaction obeys Michealis-Menten kinetics and therefore the effective rate equation for the glucose assay can also be written as

$$\text{Rate of reaction} = V_{\text{max}} \times \frac{[\text{Glucose}]/DF}{K_M + [\text{Glucose}]/DF} \quad (4.5)$$

where  $\text{Rate}$  is the effective initial rate of the reaction,  $V_{\text{max}}$  is the maximum rate at which the assay can proceed, and  $K_M$  is the effective Michaelis-Menten constant of the reaction.

$V_{max}$  is directly proportional to the activity (or concentration) of the enzyme. Combining Equations 4.4 and 4.5 we get

$$\text{Rate} \propto \frac{dA(t)}{dt} = \varepsilon L V_{max} \frac{[\text{Glucose}]/DF}{K_M + [\text{Glucose}]/DF} \quad (4.6)$$

#### 4.2.2 Analytical Range

From Equation 4.6 it is evident that the reaction rate is directly proportional to the glucose concentration if  $[\text{Glucose}]/DF \ll K_M$ , i.e.

$$\frac{dA(t)}{dt} = \frac{\varepsilon L V_{max}}{K_M DF} \times [\text{Glucose}] \quad \text{if } \frac{[\text{Glucose}]}{DF} \ll K_M \quad (4.7)$$

The linear range of the method is therefore dependent on the dilution factor  $DF$  and the Michaelis-Menten constant  $K_M$  and can be improved by increasing the sample dilution factor under a particular assay condition.

#### 4.2.3 Analytical Sensitivity

The analytical sensitivity is the slope of the calibration curve for the method in the linear range, and quantifies the change in measurable signal relative to the change in the concentration of analyte. For the glucose assay Equation 4.7 represents the calibration curve and the sensitivity can therefore be written as,

$$\text{Sensitivity} = \frac{d\left(\frac{dA}{dt}\right)}{d[\text{Glucose}]} = \frac{\varepsilon L V_{max}}{K_M DF} \quad (4.8)$$

From Equation 4.8 it is evident that the sensitivity is a measure of the enzyme activity ( $V_{max}$ ). For a given assay (constant  $K_M$  and  $\varepsilon$ ), the sensitivity increases with increasing enzyme activity ( $V_{max}$ ) and path length ( $L$ ), and decreases with increasing dilution factor (DF). Note that the linear range and the sensitivity have inverse dependence on the dilution factor.

#### 4.2.4 Lineweaver-Burke Plot

Equation 4.4 can also be written as

$$\frac{1}{Rate} = \frac{K_M DF}{V_{max} [Glucose]} + \frac{1}{V_{max}} \quad (4.9)$$

From Equation 4.9 it is clear that  $1/Rate$  is linearly proportional to  $1/[Glucose]$ . The plot of  $1/Rate$  versus  $1/[Glucose]$  is referred to as the Lineweaver-Burke plot, and the Michaelis-Menten constant  $K_M$  is calculated as the slope of the graph ( $K_M/V_{max}$ ) divided by the intercept on the y-axis ( $1/V_{max}$ ). If the Lineweaver-Burke plot is not linear, it means that the assay does not obey Michaelis-Menten kinetics and the kinetic method would not be applicable.

### 4.3 Experimental setup

#### 4.3.1 Chemicals

Glucose oxidase (G-6125), peroxidase (P-8125), 4-aminoantipyrine (A-4382) and TOPS (E-8506) were purchased from Sigma Chemicals (St Louis, Missouri, USA). Glucose standards (100mg/dL, 300mg/dL and 800mg/dL) were obtained from Sigma and diluted with deionized water to give stock solutions with concentrations ranging from 25mg/dl to 800mg/dL. The glucose reagent was constituted to result in the following concentrations after taking into account the dilution factor involved in the experiment: glucose oxidase (3U/mL), peroxidase (3U/mL), 4-aminoantipyrine (3mM) and TOPS (3mM) constituted in 0.1M phosphate buffered saline (Sigma, pH 7.0). The reagent was stable for 2 days when stored at  $4^{\circ}C$ .

### 4.3.2 Optical detection

Optical detection, is done in a plane perpendicular to that of the device, and the setup consisted of a green LED (545nm, from RadioShack) and a light-to-voltage converter, as shown in the schematic. The light-to-voltage converter (TSL257, Texas Advanced Optoelectronic Solutions) combines a photodiode and an amplifier on the same monolithic device. The output voltage  $V(t)$  is directly proportional to the light intensity incident  $I(t)$  on the photodiode. The voltage output is logged on a computer using a data acquisition card with a 12-bit A/D converter with a measuring range of -5V to +5V. All the data collected is analyzed in Microsoft Excel. The absorbance  $A(t)$  is calculated from the intensity using the following formula.

$$A(t) = \ln\left(\frac{I(0)}{I(t)}\right) = \ln\left(\frac{V(t) - V_{dark}}{V(0) - V_{dark}}\right) \quad (4.10)$$

where  $I(0)$  and  $V(0)$  correspond to zero absorbance (or 100% transmittance), and  $V_{dark}$  is the dark voltage of the photodiode. The slope of the absorbance versus time graph is a measure of the effective rate of the reaction (from Equation 4.6).

## 4.4 On-chip Glucose Assay

The glucose assay is performed on-chip in three steps - dispensing, mixing and detection. Droplets of the glucose sample and the reagent are first dispensed manually on the electrowetting chip using a pipettor. They are then merged and physically mixed by shuttling the coalesced droplet across 3 or 4 electrodes for 10-15 seconds, at a switching rate of 8Hz, and an actuation voltage of 50V. The time for physical mixing (10 seconds) is higher than what is required and can be reduced to less than 5 seconds [39]. At the end of the mixing phase, the absorbance is measured for at least 30 seconds using the LED-photodiode setup described earlier. The mixed droplet is held stationary by electrowetting forces, during the

absorbance measurement step. Since the absorbance measurements begin 15 seconds after the droplets are merged, the measured reaction rate may not be exactly equal to the initial rate. This difference between the measured and the actual initial rate may be noticeable for high glucose concentrations. All experiments were performed at room temperature. An increase in the reaction temperature will increase the sensitivity till an optimal value is reached. 1cSt silicone oil is used as the filler medium for all experiments. The volumes of glucose sample and reagent were chosen to result in sample dilution factors (DF) of 2 and 3. These dilution factors are orders of magnitude lower than those used in conventional colorimetric glucose sensors, which are typically greater than 100. We have not used larger dilution factors due to chip real-estate concerns and reduced mixing efficiency. For the low mixing ratios used in our system, we have also observed dissolved oxygen to be the limiting reactant. The reaction slows down once the dissolved oxygen is exhausted, and takes a long time to proceed to completion, making end-point methods infeasible. Figure 4.1 shows snapshots of a colorimetric glucose assay of a 800mg/dL sample droplet on an electrowetting chip.

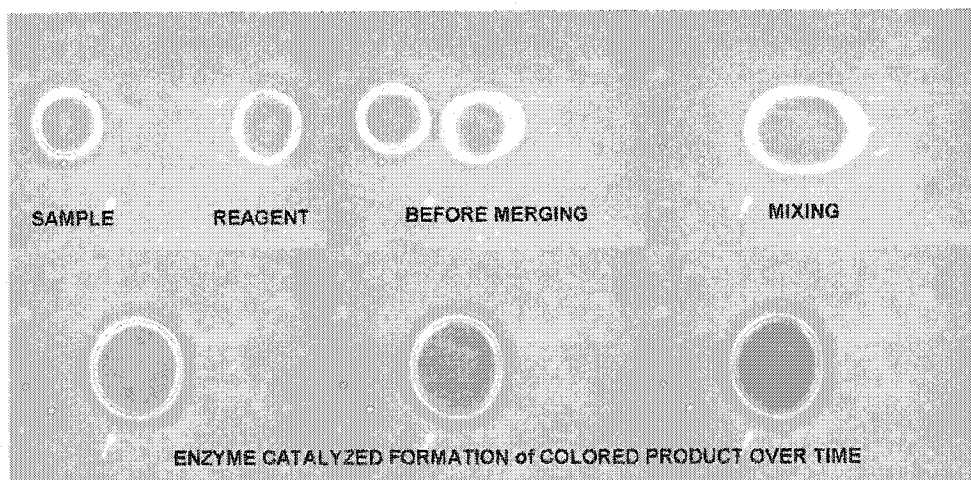


Figure 4.1: Snapshots of a colorimetric glucose assay on an electrowetting chip

#### **4.4.1 Dilution factor of 2 (DF=2)**

The dilution factor for both the sample and the reagent is 2 in this case. The constitution of the glucose reagent is chosen to account for this dilution of the reagent, and is - glucose oxidase (6U/mL), peroxidase (6U/mL), AAP (6mM) and TOPS (10mM). The volumes used are  $1.0\mu\text{L}$  for both the sample and the reagent. The absorbance  $A(t)$  as a function of time for various concentrations from 25mg/dL to 400mg/dL is shown in Figure 4.2. T=0 in the graphs corresponds to the time instant just after the sample and reagent droplets are mixed (15 seconds after merging). The slope of these curves (obtained by least-squares linear regression in Excel) gives the rate of reaction corresponding to each concentration. Figure 4.3 plots of the reaction rate as a function of the sample glucose concentration. The linear region of Figure 4.3 is shown in Figure 4.4. The linear fit is obtained by least-squares regression in Excel, with the line forced to pass through the origin. The plot shows excellent linearity up to a glucose concentration of 100mg/dL with a  $R^2$  (measure of goodness of fit) of 99.89%. The sensitivity of the assay (slope of Figure 4.4) is  $S_2 = 27.2 \mu\text{AU sec}^{-1}/\text{mg dL}^{-1}$  (AU stands for Absorbance Units).

#### **4.4.2 Dilution factor of 3 (DF=3)**

The dilution factor for the reagent is 2/3 in this case. The constitution of the glucose reagent is chosen to account for this dilution of the reagent, and is - glucose oxidase (4.5U/mL), peroxidase (4.5U/mL), AAP (4.5mM) and TOPS (7.5mM). The volume used for the sample and the reagent are  $0.7\mu\text{L}$  and  $1.4\mu\text{L}$  respectively. The rate of reaction is plotted as a function of concentration in Figure 4.5, and the linear range is shown in Figure 4.6. From the figure we can see that the reaction is linear to concentrations of 300mg/dL with a  $R^2$  of 99.76%. The sensitivity of the assay (slope of Figure 4.6) is  $S_3 = 16.6 \mu\text{AU sec}^{-1}/\text{mg dL}^{-1}$ .

Since the assay conditions (enzyme activity and path length) are the same for both experiments (DF=2 and DF=3), the sensitivities are inversely related to the dilution factors

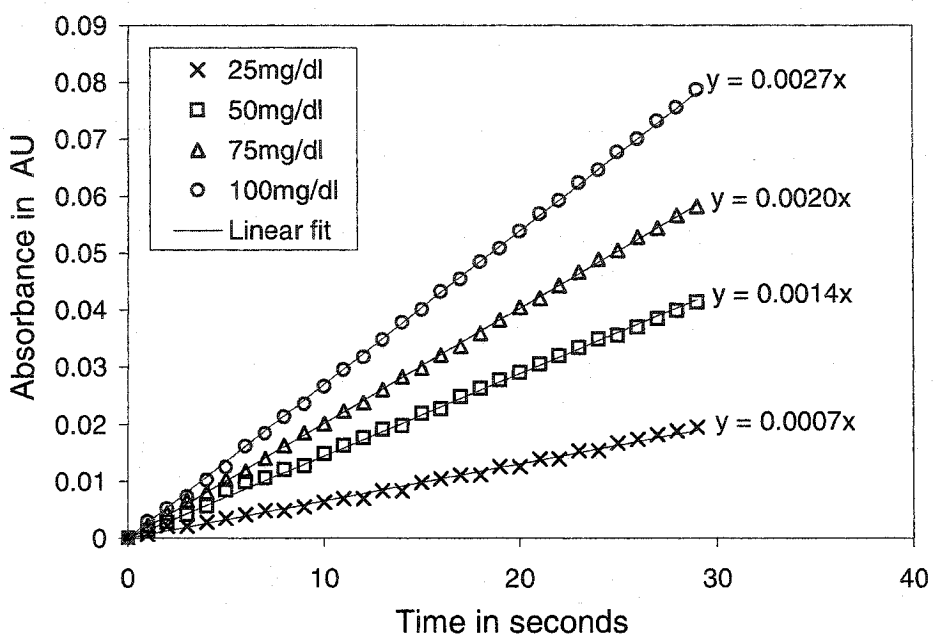


**Figure 4.2:** Absorbance versus time for Glucose concentrations from 25mg/dL to 300mg/dL, for a sample dilution factor of 2.

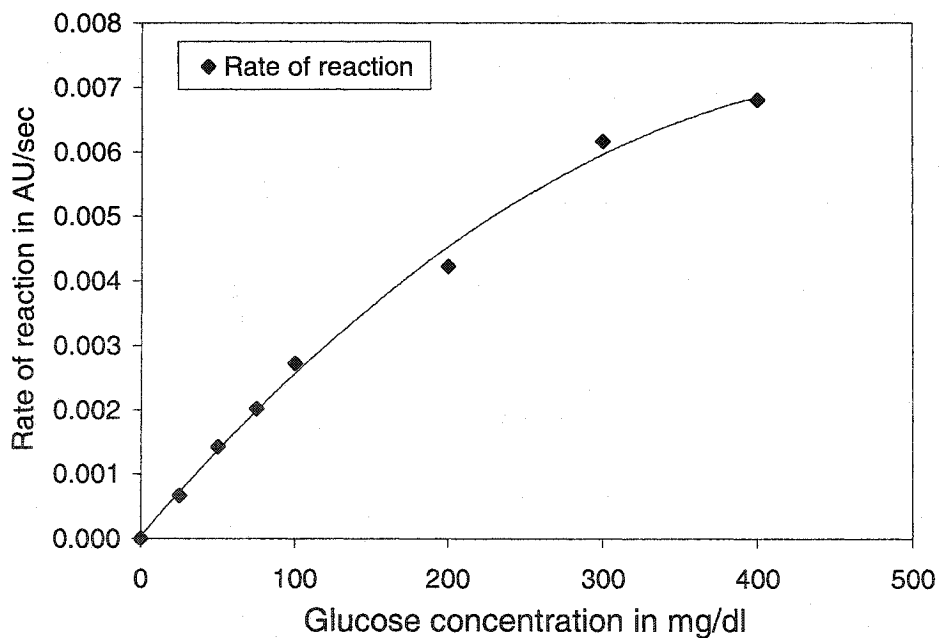


**Figure 4.3:** Rate of reaction as a function of glucose concentrations from 25mg/dl to 800mg/dl, for a sample dilution factor of 2.

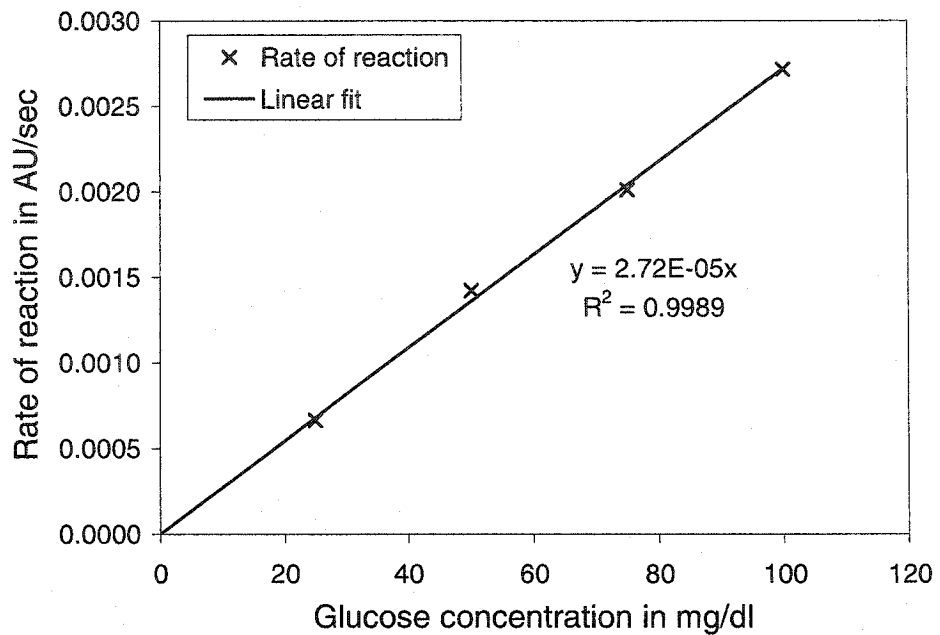


**Figure 4.4:** Rate of reaction as a function of glucose concentration in the linear range, for a sample dilution factor of 2.

(from Equation 4.8). The ratio of the sensitivities is

$$\frac{S(DF = 2)}{S(DF = 3)} = \frac{27.2}{16.6} = \frac{3}{1.83} \quad (4.11)$$

which is close to the expected value of  $3/2$ .

### Comparison with Reference Method

The assay results obtained on the electrowetting chip for a dilution factor of 3 were compared with those obtained on a commercial Gensys 20 spectrophotometer. In order for the comparison to be meaningful, the absorbance measured in the electrowetting system is multiplied by a scaling factor to account for the difference in path lengths between our system and the spectrophotometer (path length = 1cm). The scaling factor is determined by measuring the end-point absorbance of a glucose assay on both the systems. Note that since the LED light source is not collimated, the path length in the electrowetting system

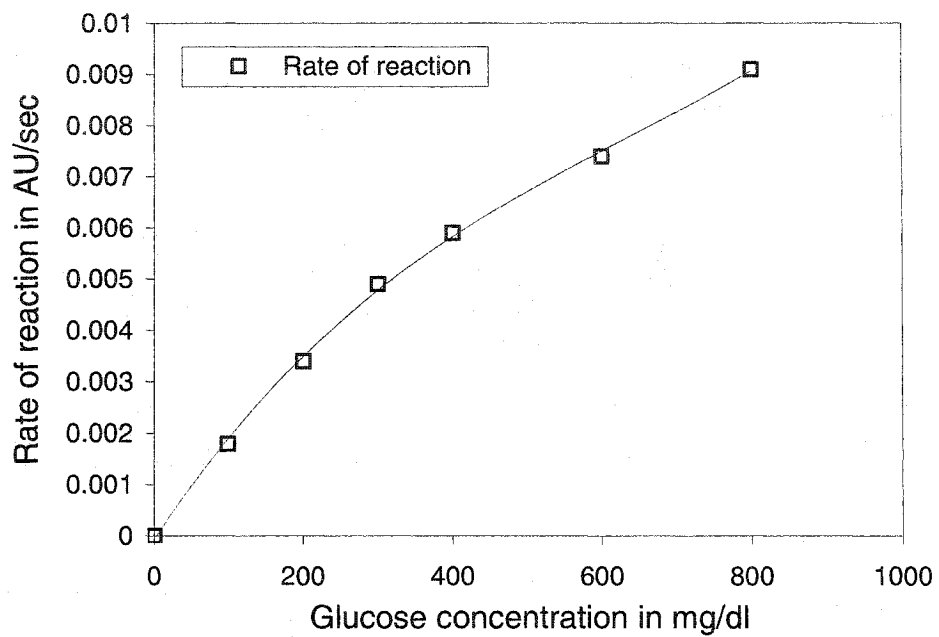


**Figure 4.5:** Rate of reaction as a function of glucose concentrations from 100mg/dL to 800mg/dL, for a sample dilution factor of 3.

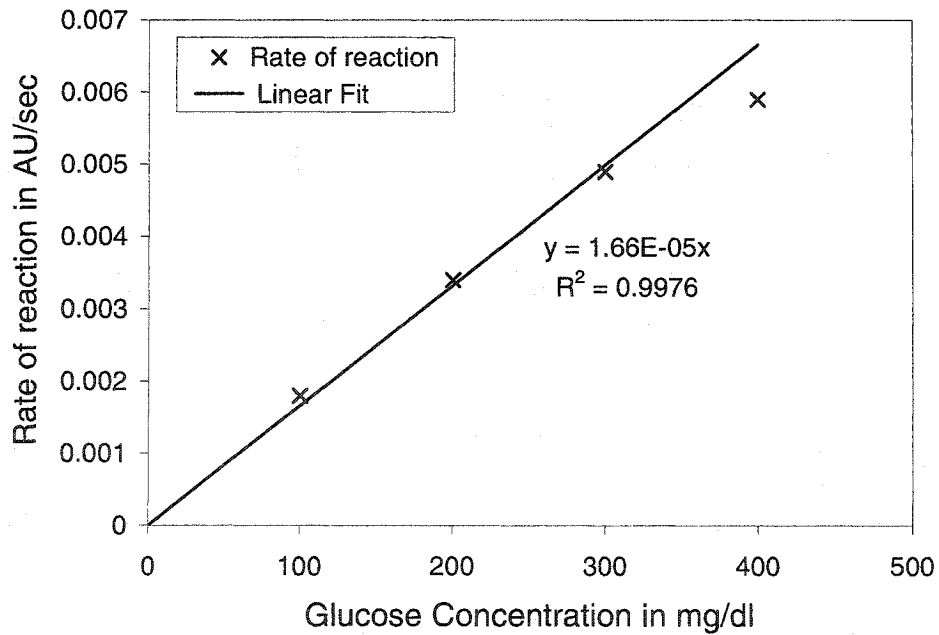


**Figure 4.6:** Rate of reaction as a function of glucose concentrations in the linear range, for a sample dilution factor of 3.

is not exactly equal to the gap spacing. Figure 4.7 compares the results from the electrowetting chip with the results obtained from identical assays on a commercial Gensys 20 spectrophotometer in Figure 4.7. From the figure we can see that the data from the spectrophotometer and from the electrowetting system are in good agreement up to 400mg/dL. The slight deviation at the higher concentrations (600mg/dL and 800mg/dL) can be attributed to the difference in the measured rate and the actual initial rate, due to the mixing delay. Figure 4.8 compares the results in the linear range. The solid and dotted lines correspond to least squares linear fits to the data points. Since the assay conditions are identical for both the experiments the sensitivities are proportional to  $V_{MAX}$  (from Equation 4.7). The nearly identical sensitivities from the figure indicate that there is no significant change in enzyme activity ( $V_{MAX}$ ) under electrowetting conditions.

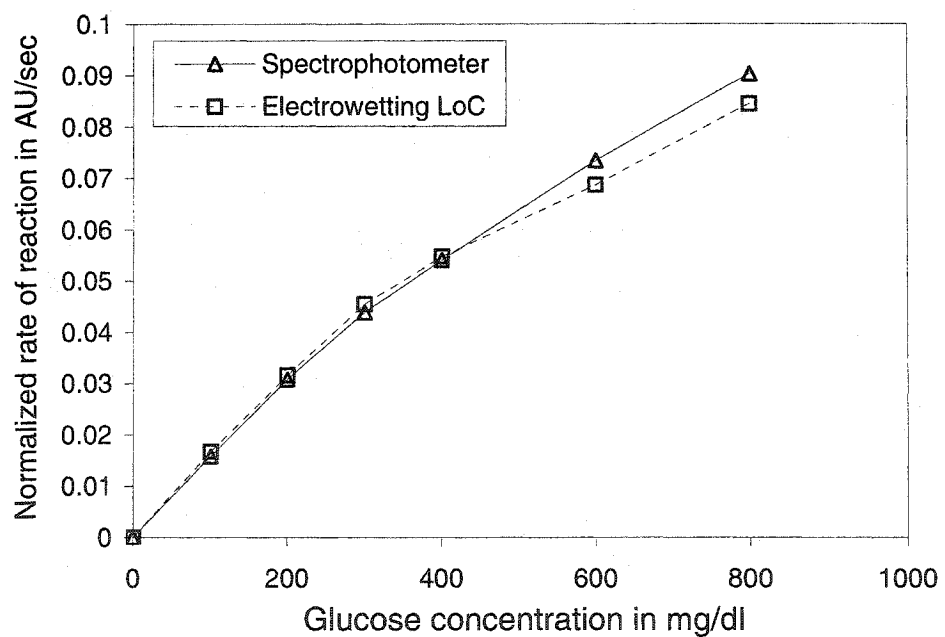


**Figure 4.7:** Comparison of results from a spectrophotometer and our electrowetting-based LoC, for a dilution factor of 3.

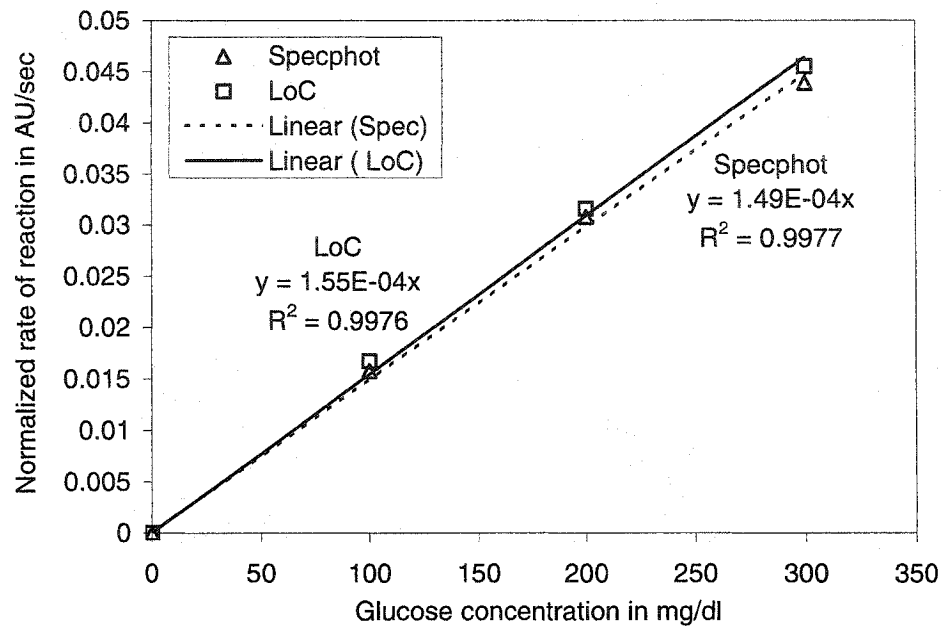


**Figure 4.8:** Comparison of results from a spectrophotometer and our electrowetting-based LoC, in the linear range, for a dilution factor of 3.

### Lineweaver-Burke plot

The Lineweaver-Burke plot (refer section 4.2.4) is used to obtain the effective Michaelis-Menten constant  $K_M$  of the reaction. The  $K_M$  value will determine the dilution factor required to achieve a certain linear range. The Lineweaver-Burke plot, for the glucose assay using a dilution factor of 3, is shown in Figure 4.9. and the  $K_M$  value is calculated using Equation 4.9 from the graph is 494 mg/dL. The  $K_M$  obtained from the plot is highly sensitive to the measured value of the reaction rate and in order to minimize the errors, the sample concentrations were chosen so that  $1/[Glucose]$  is uniformly distributed across the entire range. The excellent linearity of the Lineweaver-Burke plot validates the use of Michaelis-Menten kinetics to model the system.

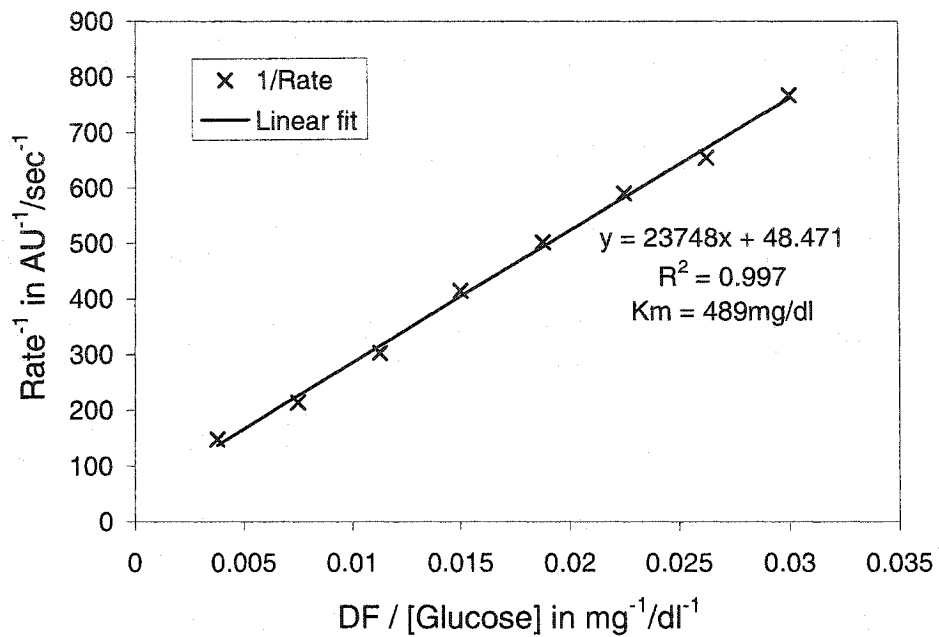


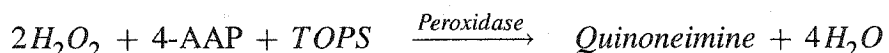
**Figure 4.9:** Lineweaver-Burke plot for Glucose Assay

#### 4.4.3 Analytical range

The normal range of glucose in human serum in a healthy adult is between 75mg/dL and 110mg/dL. These ranges are lower for children (60-100mg/dL) and even lower for neonates (30-60mg/dL). The clinical decision levels for glucose are 50 mg/dL (hypoglycemia), 126 mg/dL and 200 mg/dL (hyperglycemia) and therefore an analytical range of 25-200mg/dL is sufficient for human subjects. The results presented in the previous sections indicate that this linear range is achievable using a dilution factor less than or equal to 3. A dilution factor of 3 can be obtained by mixing one droplet of sample with two droplets of reagent. Higher dilution factors would require some sort of on-chip sample dilution such as the serial dilution method, proposed in [37].

## 4.5 Assays for Lactate and Creatinine

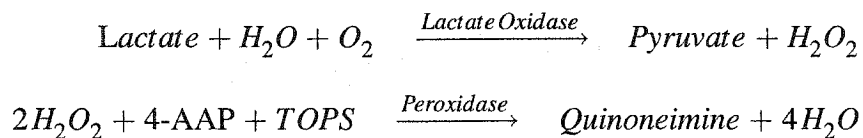
In addition to glucose, assays for other analytes such as lactate and creatinine were also developed in order to demonstrate multiplexed analysis on the electrowetting system. The assays were chosen to have a color producing step identical to the glucose assay to enable the use of a single optical detector for all the analytes.



The optical detector can be time-multiplexed for parallel detection of all the analytes.

### 4.5.1 Lactate Assay

The enzymatic reactions involved in the colorimetric lactate assay are



The lactate assay was initially tested on a spectrophotometer to determine the sensitivity and the linear range of operation. The following reagent composition was used as the starting point for the lactate assays.

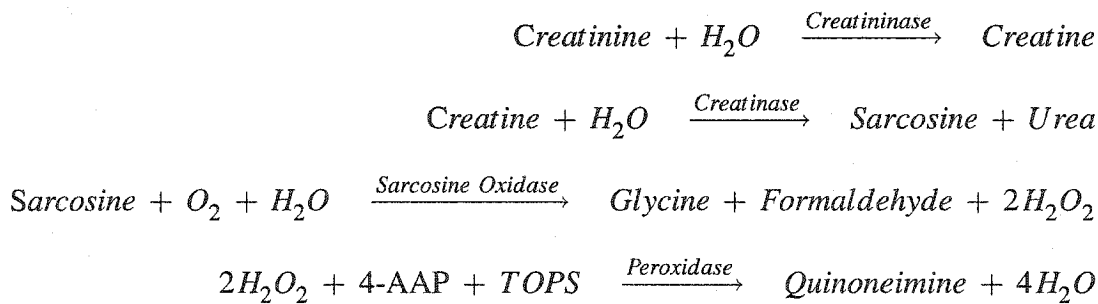
- Buffer 0.1M PIPES pH=6.8,
- Lactate Oxidase - 0.5 U/ml,
- Peroxidase - 0.5 U/ml,
- TOPS - 5mM,
- 4-Aminoantipyrine (4-AAP) - 0.5mM

Lactic acid standard solutions with concentrations in the clinical relevant range of 0.5mM-4mM were used as the sample. The initial results on the spectrophotometer were not encouraging with respect to the linearity of the assay. The calibration curve was flat with no change in the reaction rate with concentration. This was due to the very small Km of lactate oxidase under the assay conditions. In the second iteration oxalate ions which inhibit the activity of lactate oxidase was added to the reagent to improve the linearity. Sodium oxalate was tried initially but the results were not consistent between experiments due to its poor solubility in water. Potassium oxalate was much more soluble in water and was used at a concentration of 15mM in the reagent as the source of oxalate ions in the modified reagent.

Figure 4.10 shows the calibration curve obtained using the reagent with the inhibitor for a 1:1 mixing ratio. Though the linearity improved significantly from the initial experiment, it was still not sufficient in the range relevant to human samples. Increasing the concentration of potassium oxalate beyond 15mM had a negligible effect on improving the linearity.

#### 4.5.2 Creatinine Assay

The enzymatic reactions involved in the creatinine assay are the following [54].



The enzymatic creatinine assay as developed by Fossati et al [54] is an end-point reaction and not a kinetic assay. The time to completion for the end-point reaction was

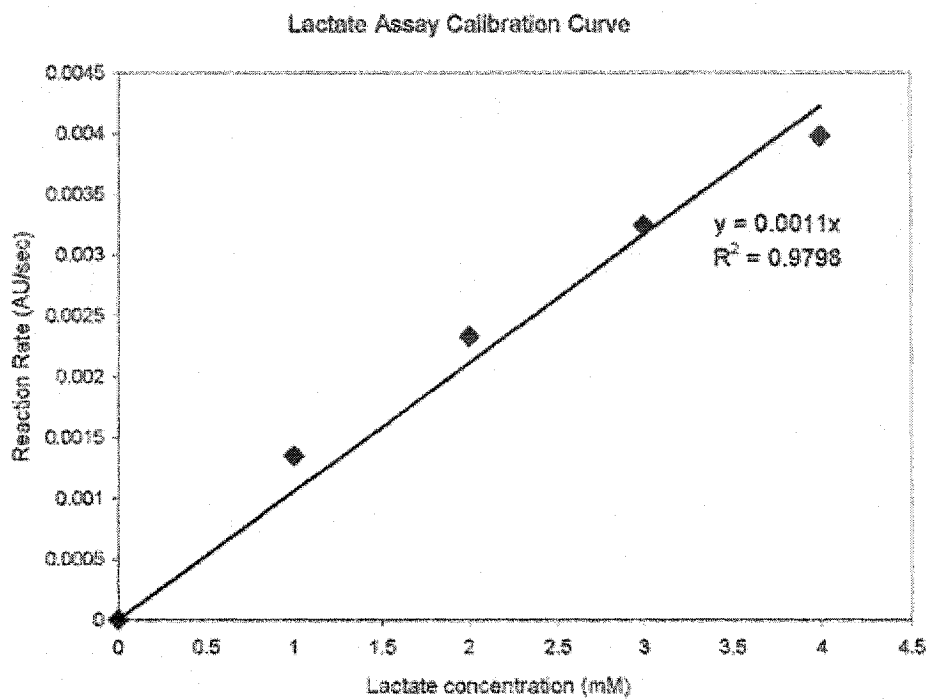


**Figure 4.10:** Calibration curve for a lactate assay done on a spectrophotometer

20 minutes at an elevated temperature of 37°C. Such long assay times are not currently feasible on the electrowetting lab-on-a-chip, so the kinetics of the enzymatic creatinine assay was evaluated to see if a rate-kinetic method could be used.

The reagent composition was 3mM TOPS, 0.6mM AAP, 12U/mL peroxidase, 10U/mL sarcosine oxidase, 20U/mL creatinase, 20U/mL creatininase in 0.1M PBS (pH=7.4). Standard solutions of creatinine in the range of 0.5-2mg/dL (human range in serum) were used as the sample.

Figure 4.11 shows the kinetics of a creatinine assay over a 10 minute time period. The reaction is very slow at the beginning and requires a little more than 3 minutes before a measurable color change is observed. Figure 4.12 plots the slope of the linear region of the kinetic curve (from 300-500 seconds) as a function of the concentration. The assay is linear up to the tested concentration of 2mg/dL however the sensitivity is very poor ( $2e-4$  AU/sec/mg/dL) even for the 1cm path length. For a  $100\mu m$  path-length this sensitivity

translates to an absorbance change of 8e-4 in 300 seconds for a concentration of 2mg/dL. Such small absorbance changes are not detectable with the current setup. For this reason the creatinine assay was not tested on the microfluidic lab-on-a-chip.

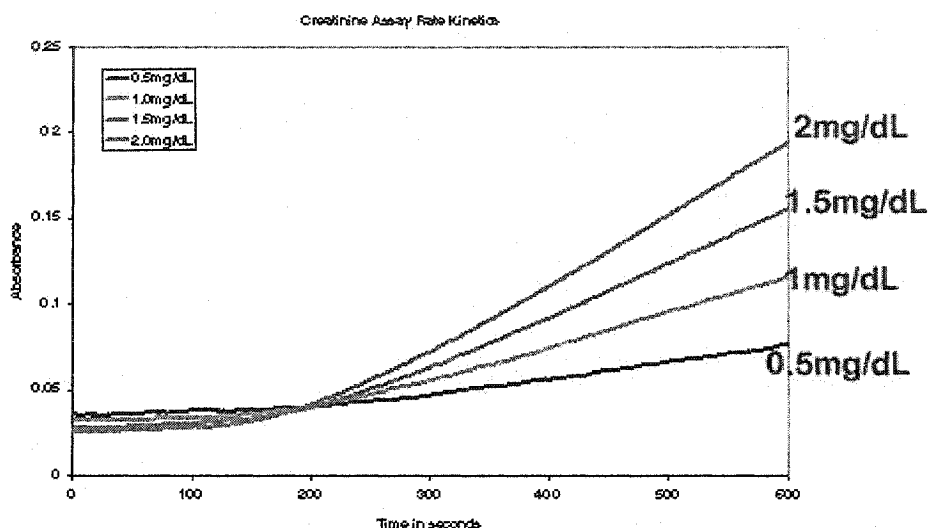


**Figure 4.11:** Kinetics of an enzymatic creatinine assay on a spectrophotometer

## 4.6 Chapter summary

A glucose assay protocol suitable for a droplet-based lab-on-a-chip was designed in this chapter. The assay is linear up to concentration of 100mg/dL for a sample:reagent ratio of 1:1 and up to 300mg/dL for a sample:reagent ratio of 1:2. The assay was tested manually on an electrowetting chip and the results compared well with those that were obtained using a conventional method. Enzymatic assays for lactate and creatinine were also developed using the same color producing step as the glucose assay. The lactate assay suffers from poor linearity in the human range. The creatinine assay exhibited poor sensitivity even at path lengths of 1cm and would not be detectable on the microfluidic lab-on-a-chip.

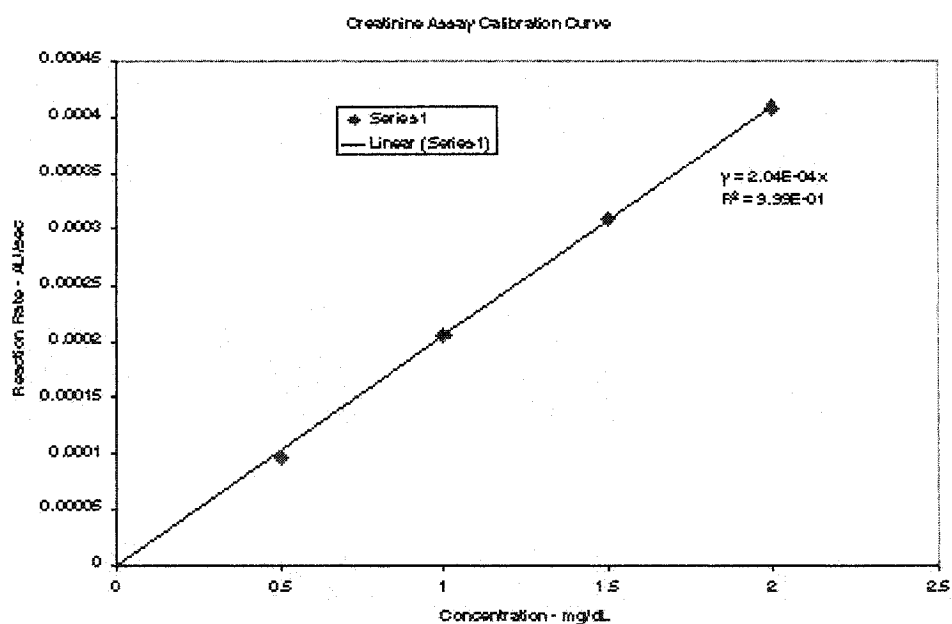


**Figure 4.12:** Calibration curve for the creatinine assay done on a spectrophotometer

# **Chapter 5**

## **Automated and Integrated Assays on a Lab-on-a-chip**

The basic toolkit required to perform fully automated and integrated analytical assays was developed in the previous chapters of this thesis. Glucose assays were demonstrated on an electrowetting chip using manual pipetting of droplets that were microliters in volume. In this chapter the glucose assay protocol is transferred to a fully automated nanoliter lab-on-a-chip.

Three different aspects of the lab-on-a-chip operation are addressed in this chapter - microfluidic automation, assay repeatability, and analysis of a human physiological sample (serum). The prototype nanoliter lab-on-a-chip described in chapter 2 was used in all the experiments reported in this chapter. The glucose assay developed in chapter 4 was used as the model system to evaluate the repeatability of clinical assays.

### **5.1 Microfluidic automation**

The automation of a clinical assay protocol from “sample injection to result” on the lab-on-a-chip requires the integration of droplet dispensing, transport, mixing, detection and disposal.

#### **5.1.1 Pipelined Glucose Assays**

It has been previously discussed that the use of multiphase buses on the lab-on-a-chip requires the use of pipelining strategies for partially parallel operation. Two pipelined glucose assays were performed on the prototype lab-on-a-chip and the flowchart of the

experiment is shown in Figure 5.1. Two droplets each of glucose samples and reagent were formed from 4 different reservoirs in a serial fashion. While the first sample and reagent were being mixed the second set of droplets were transported towards the mixing area. The mixed droplet was split into two and one droplet was moved to a storage area for detection while the other droplet was sent to waste. The second sample and reagent were mixed while the color change in the first assay occurred.

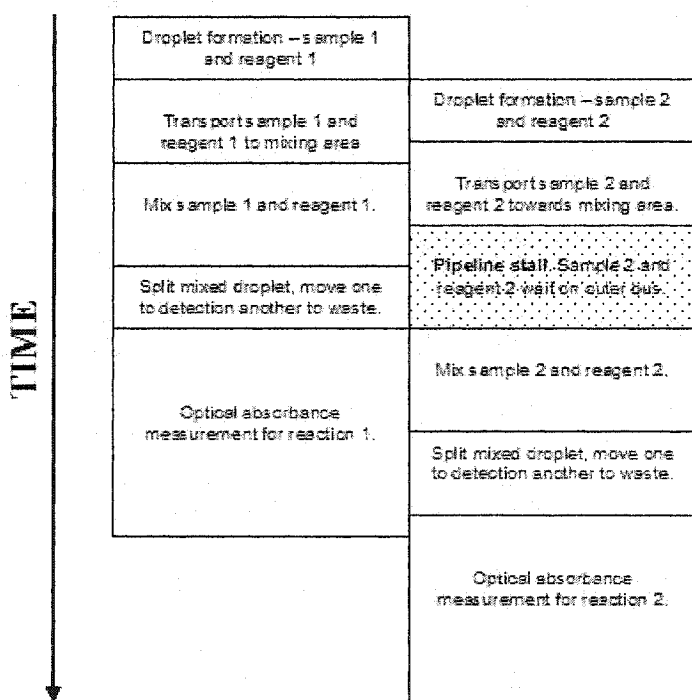


**Figure 5.1:** A flowchart describing the pipelined operation of two glucose assays

Figure 5.2 shows a snapshot of the chip during the operation of the pipelined assay. The figure shows colorimetric reactions on two droplets in the 3-phase inner storage bus, sample and reagent mixing, another sample and reagent droplet being transported on the outer 4-phase bus towards the mixing area, and a droplet being moved to the waste area - all occurring parallel in time. This experiment demonstrates the full capability of the lab-on-a-chip with high-level of integration and automation.

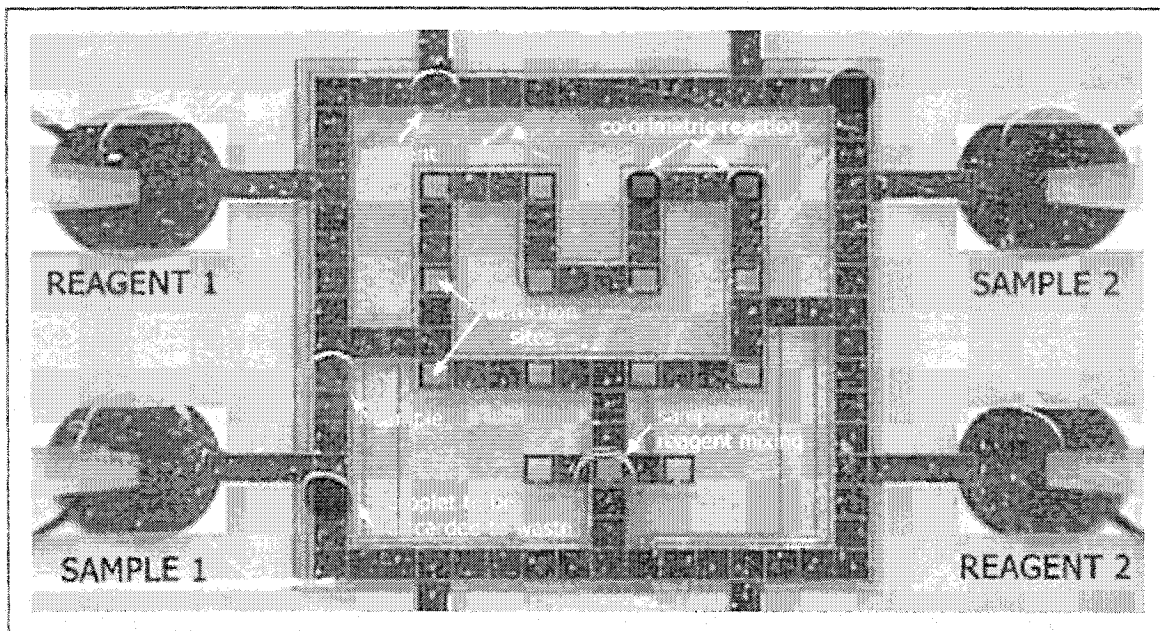


**Figure 5.2:** A snapshot during the course of a pipelined glucose assay on a digital microfluidic lab-on-a-chip

The experiment described above required a complex program for execution and was difficult to setup and execute for repeated use. For the repeatability experiment and to demonstrate the multianalyte assaying capabilities of the lab-on-a-chip a simpler assay protocol was developed. In the revised assay protocol multiple samples were analyzed in a serial fashion - one sample at a time.

## 5.2 Assay Repeatability

The repeatability of a measurement or the precision is one of the most important performance metrics of a analytical method. There are two aspects of precision in a clinical method, within-run precision and day-to-day precision. A within-run precision test is performed by analyzing the same control sample at least 20 times in a repetitive manner within a short interval. Day-to-day precision is calculated by analyzing the same control sample over several days.

In the electrowetting system the within-run precision is mainly affected by errors in

droplet volumes, cross contamination between experiments, and errors in measurement. The within-run precision was evaluated by performing multiple automated assays on glucose samples.

### 5.3 Serial Assays on Multiple Glucose Samples

Three different concentrations of glucose (40mg/dL, 80mg/dL and 120mg/dL) were assayed in a serial fashion. Droplets of sample and reagent were formed in succession, merged and mixed by simply moving the droplet on the bus. The absorbance was monitored for 60 seconds using the LED-photodiode setup described previously and the droplet was discarded to a waste area on-chip. Three assays were performed on each sample for a total of nine assays. The entire experiment was fully automated and lasted a little more than 10 minutes. The absorbance as a function of time for the 9 assays is shown in Figure 5.3. The rate of change of absorbance for each assay was estimated by linear curve fitting in Excel and the calibration curve as a function of concentration is shown in Figure 5.4.

#### 5.3.1 Within-run variation

The percentage coefficient of variation for the three different concentrations is shown in Table 5.1.

**Table 5.1:** Coefficient of variation for the three different glucose concentrations

Glucose Concentration (mg/dL)	Coefficient of variation
40	1.81
80	1.86
120	0.72

From Table 5.1 we can see that there is less than 2% within-run variation in the assays. The excellent reproducibility of the results indicates minimal volume variability and negligible cross-contamination. The reproducibility is the best (0.72%) for the highest

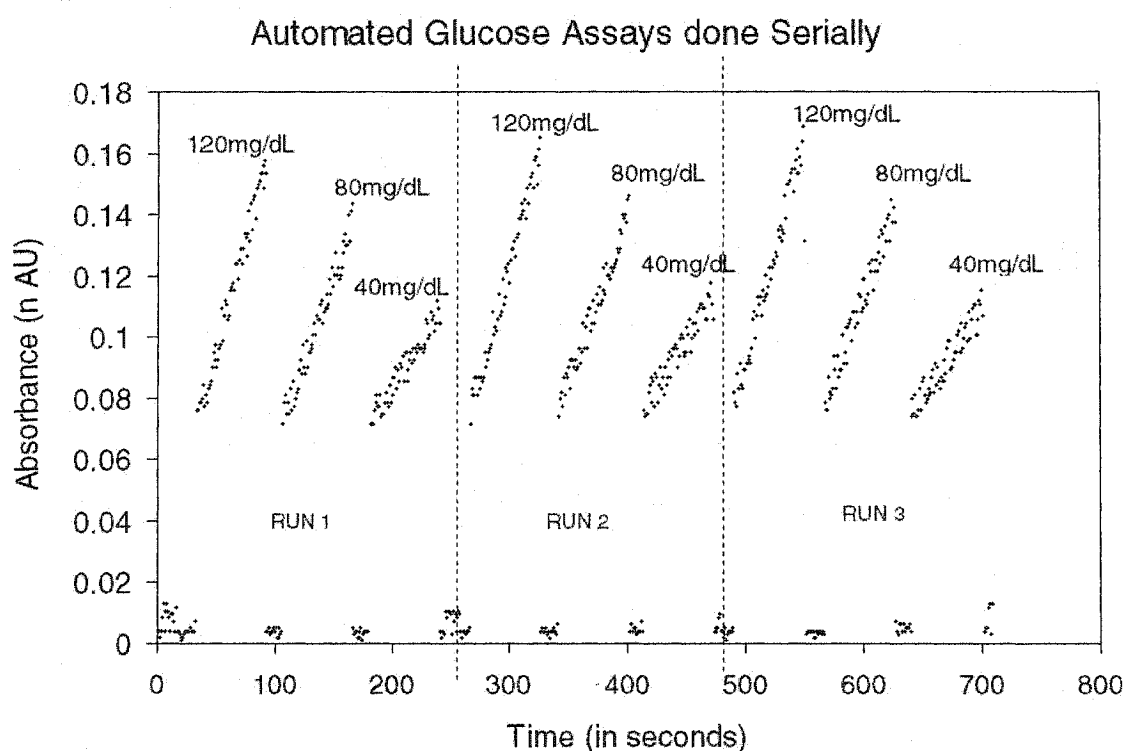


**Figure 5.3:** The absorbance measured as a function of time for nine serial glucose assays - three different glucose concentrations assayed three times each

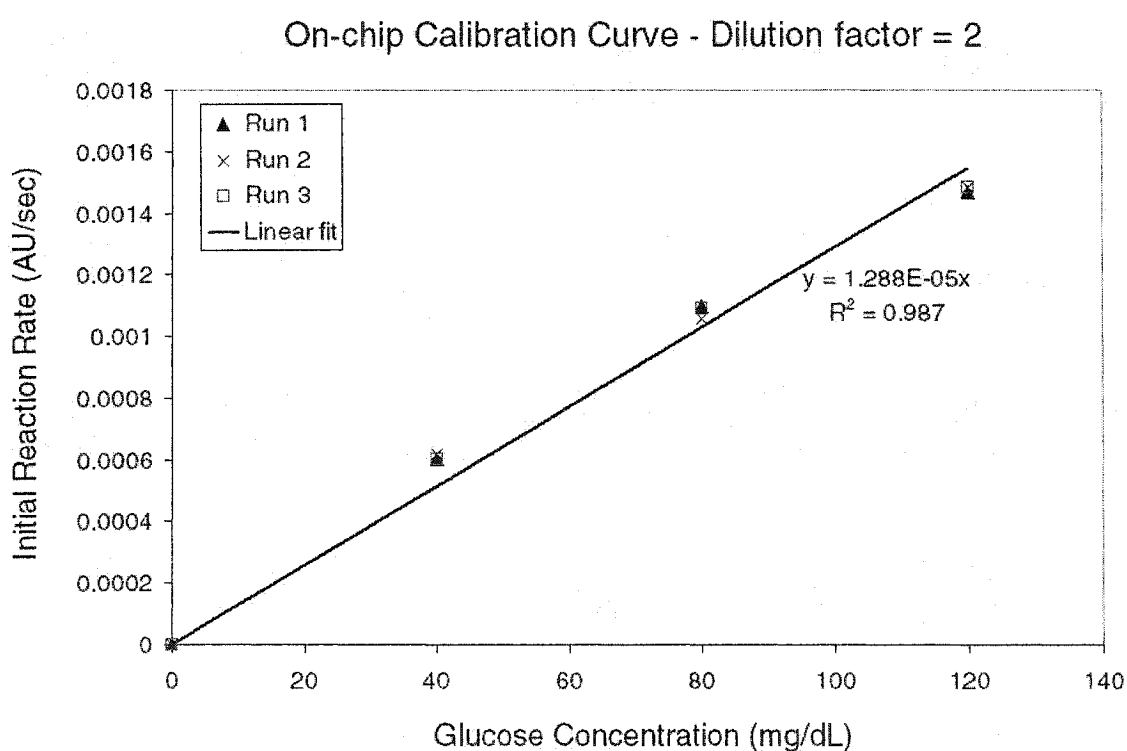


**Figure 5.4:** On-chip calibration curve for multiple glucose assays

concentration (120mg/dL) and is lower (1.8%) for the smaller concentrations. This can be explained due to a larger component of error due to measurement noise at the lower concentrations. The higher noise at 40 and 80mg/dL is evident from Figure 5.3.

### 5.3.2 Comparison with off-chip results

The results obtained on-chip were compared with those obtained on a spectrophotometer to verify that there is no change in the behavior of the assay under electrowetting. Since the path lengths for the two systems were different and the calibration curve was not linear in the range of concentrations tested, the Michaelis-Menten constant was used as a figure of merit of the assay. Figure 5.5 shows the Michaelis-Menten curve for the glucose assays done on-chip. The effective  $K_m$  for the assay from the curve is 147.7mg/dL. The excellent linearity of the Michaelis-Menten curve also validates the use of the rate-kinetic model for the glucose assay. Figure 5.6 shows the Michaelis-Menten curve for identical assays done on a spectrophotometer. The effective  $K_m$  for the assay is 136.7mg/dL and compares very well with the  $K_m$  obtained from the on-chip assays, indicating negligible change in behavior of the assay on-chip.

## 5.4 Serial Assays on Same Glucose Sample

A 120mg/dL glucose sample was analyzed nine times serially to further evaluate the within-run variation. Droplets of the sample and the reagent were dispensed, mixed and the absorbance change monitored for 30 seconds. Figure 5.7 plots the absorbance measured as a function of time for all the nine experiments. The solid line represents the least-squares linear fit to the data points. Figure 5.8 plots the initial rate of the reaction (slope of the linear fit) against the run number. The coefficient of variation for the entire experiment is 5.7%. The CV drops to 2.2% if only the first 6 data points are considered. The reason for the larger error in the last 3 runs is due to the wider variation in the droplet volumes

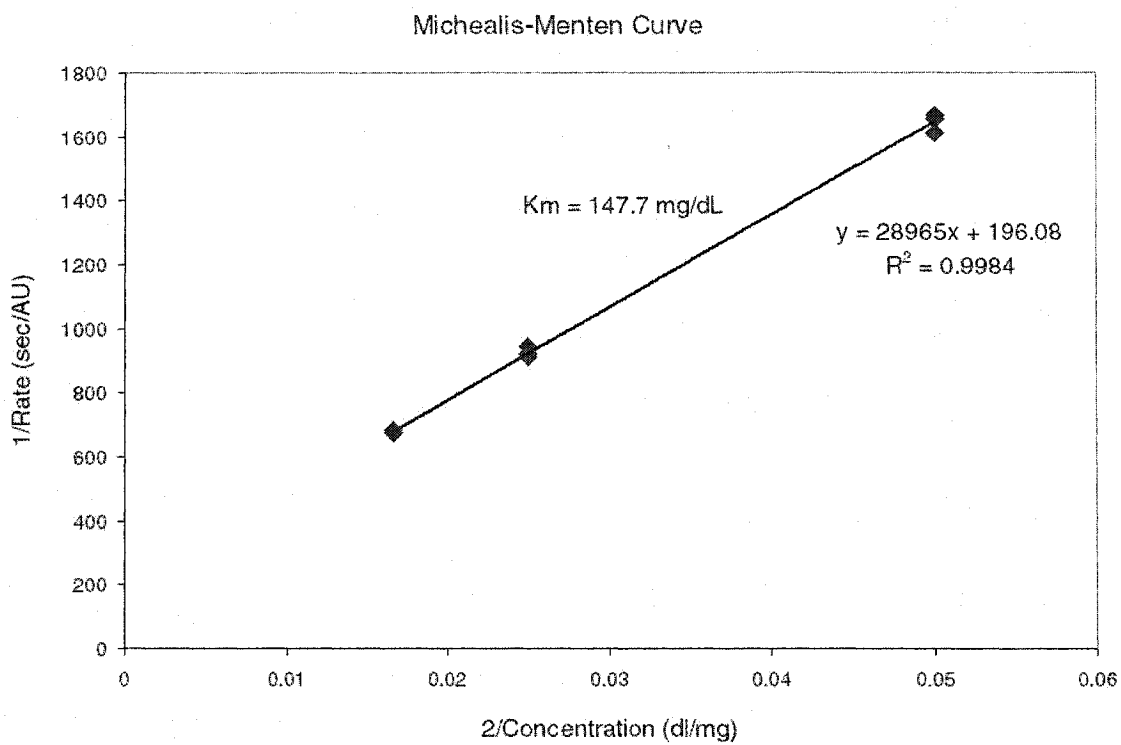


**Figure 5.5:** Michaelis-Menten Curve (on-chip assays)

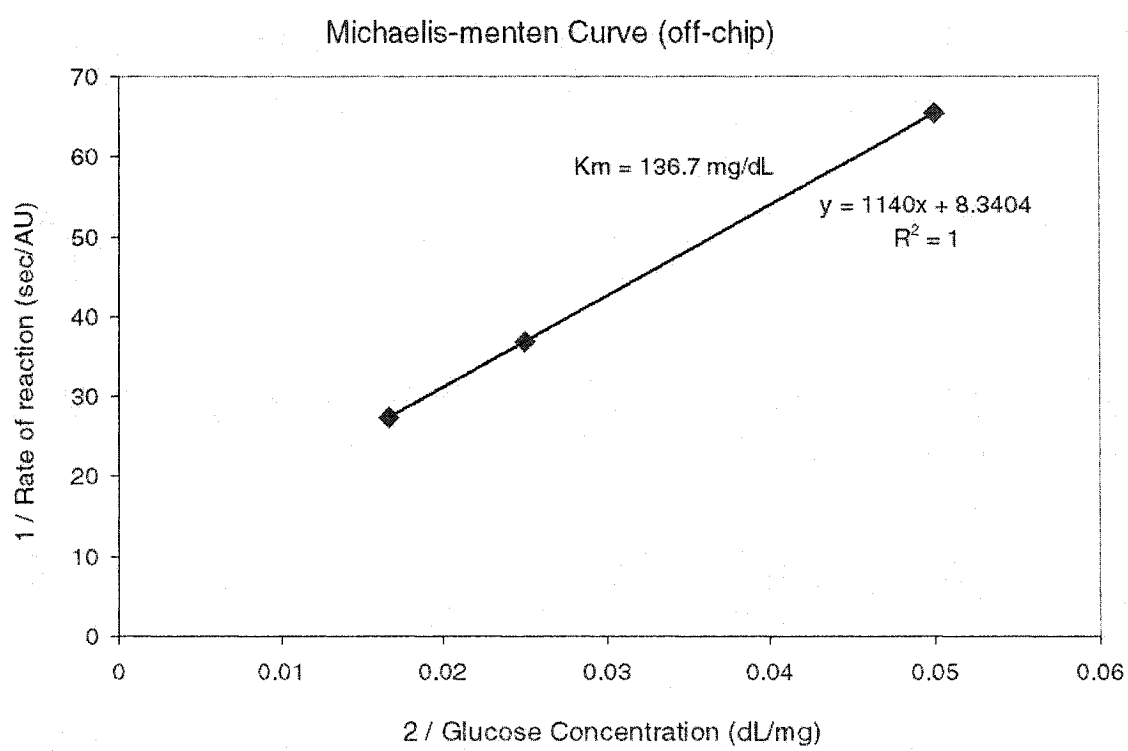


**Figure 5.6:** Michaelis-Menten Curve (off-chip spectrophotometric assay)

as the reservoir becomes empty. Another reason for the increased variation in this experiment is the shorter data collection period. Since data is collected only for 30 seconds (as compared to 60 seconds in the previous experiment) the change in absorbance (signal) measured is correspondingly smaller. The smaller change in measured signal implies a larger signal-to-noise ratio.

### Kinetics of serial assays on 120mg/dL glucose sample

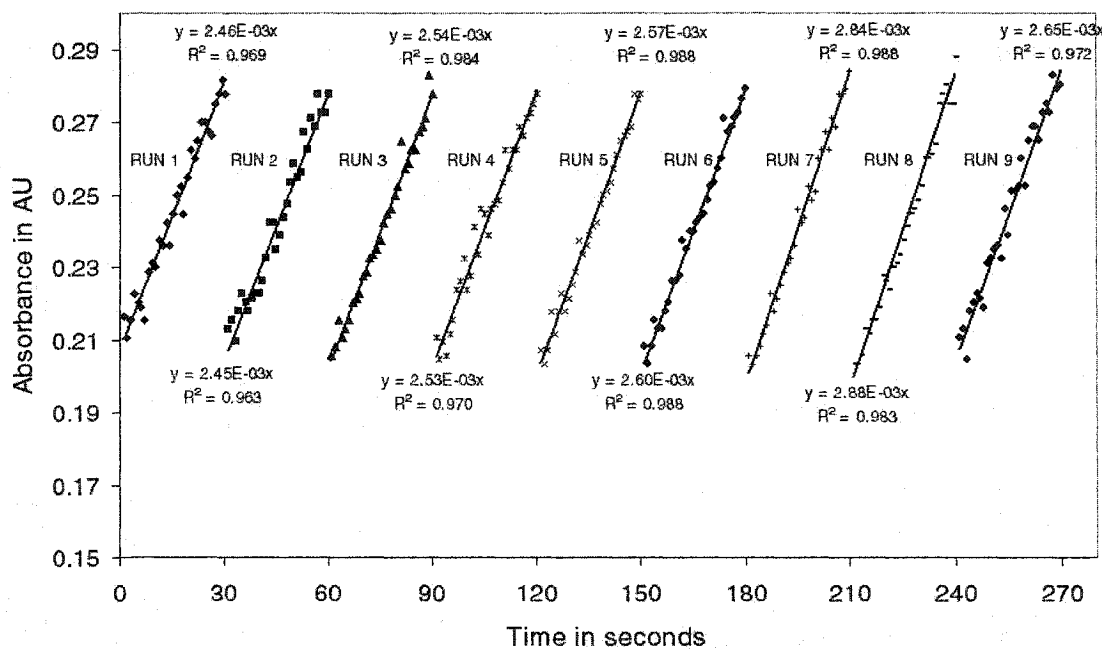


**Figure 5.7:** Absorbance as a function of time for multiple glucose assays on the same 120mg/dL sample

The within-run experiment was repeated with a 40mg/dL glucose sample. Five sample droplets were assayed in a serial fashion using the same assay protocol as the 120mg/dL sample. Figure 5.9 plots the absorbance measured as function of time for all the five experiments. The solid line represents the least squares linear fit. From the figure one can observe that the  $R^2$  values are very poor (95% to 97%) which indicates that the measurement errors are significant for this experiment. Figure 5.10 plots the initial rate of the reaction

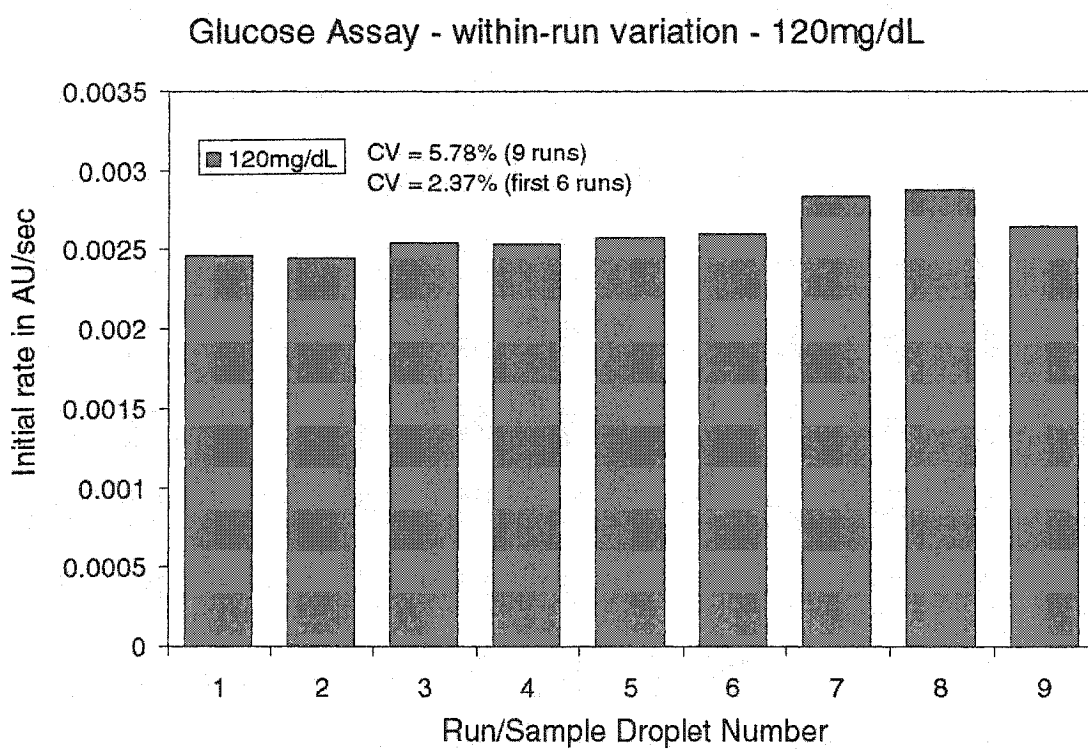


**Figure 5.8:** Reaction rate versus the run number for multiple glucose assays on the same 120mg/dL sample

against the run number. The coefficient of variation for the experiment was 10.5%. The error is significantly larger compared to previous results, and most of it is attributed to measurement errors rather than droplet volume variations.

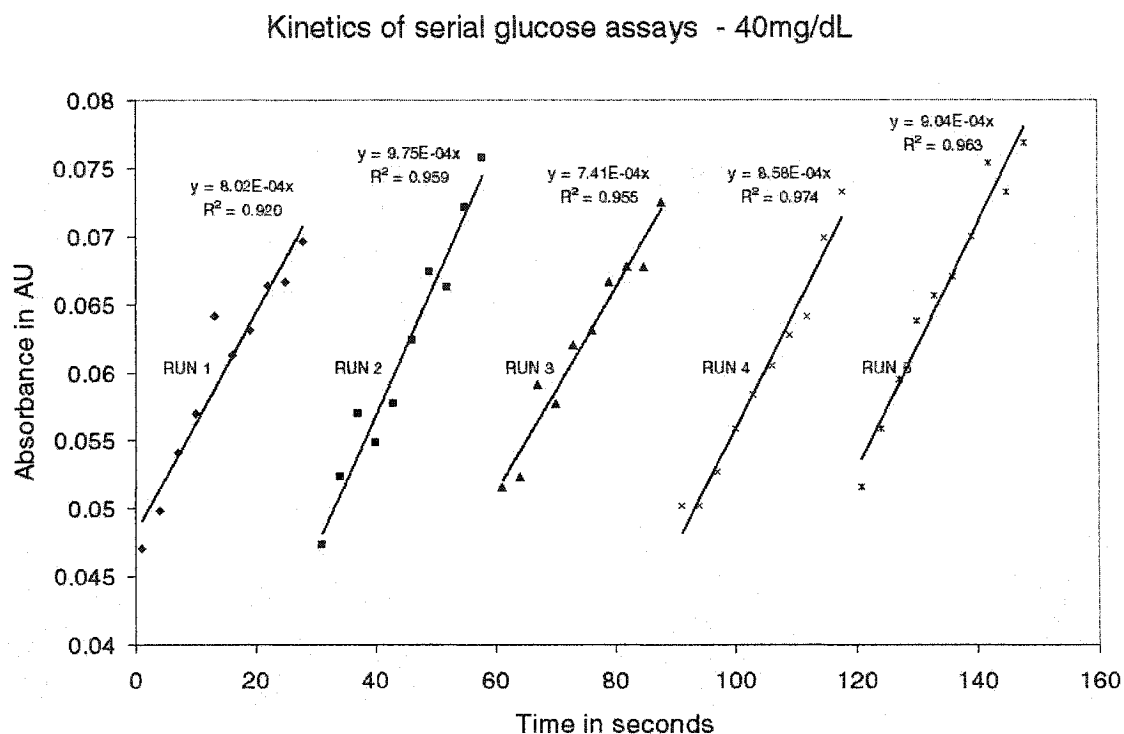


**Figure 5.9:** Absorbance as a function of time for multiple glucose assays on the same 40mg/dL sample

## 5.5 Glucose assay on serum

An on-chip automated assay was performed on a serum sample and compared to results obtained using a reference methodology. The assay protocol was similar to the ones used previously. The glucose assay is first performed on a 100mg/dL calibrant sample and the rate of reaction was noted as the reference reading ( $Rate_{100}$ ). The reaction rate for the serum sample was then measured ( $Rate_{serum}$ ) and the unknown concentration ( $[Glucose]_{serum}$ )

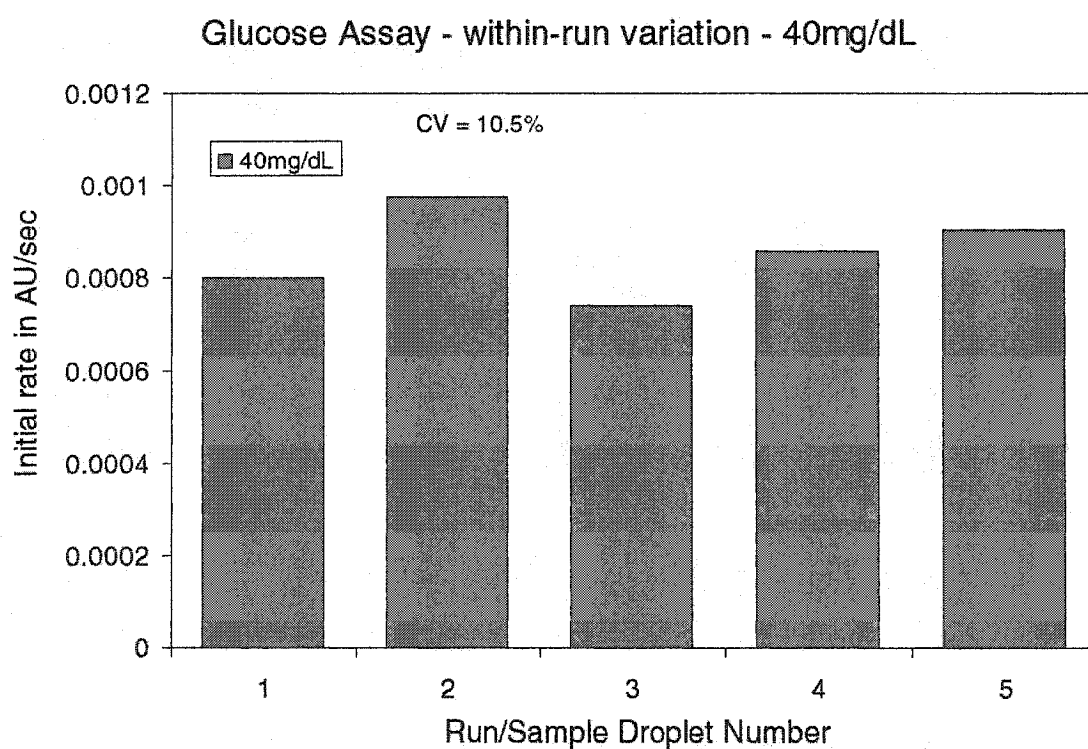


**Figure 5.10:** Reaction rate versus the run number for multiple glucose assays on the same 40mg/dL sample

was inferred using the following equation.

$$[Glucose]_{serum} = \frac{Rate_{serum}}{Rate_{100}} \times 100 \text{mg/dL} \quad (5.1)$$

The unknown glucose concentration was measured to be 35mg/dL. The reference method was done on a spectrophotometer using a dilution factor of 100 and a dilution factor of 2 (to simulate on-chip conditions). The glucose concentration obtained using the reference methodology was 63mg/dL for a dilution factor of 100 and 33mg/dL for a dilution factor of 2. The huge difference in the glucose concentrations measured for dilution factors of 100 and 2 is attributed to interference. One of the important reasons for using a high dilution factor is to reduce the effect of interfering substances in the sample to insignificant levels. So the role of interferents could be significant if small dilution factors are used. The discrepancy between the results for dilution factors of 2 and 100 was also observable for other serum samples which were tested on the spectrophotometer as indicated in Table 5.5. From the table we can see that the glucose concentration measured using a dilution factor of 2 is at least 30 to 40mg/dL smaller than the value obtained using a more conventional dilution factor of 100.

**Table 5.2:** Comparison of serum glucose values obtained using dilution factors of 2 and 100

Glucose concentration in mg/dL	
Dilution factor = 2	Dilution factor = 100
32.5	63.8
27	63
37	80
32	70.3

## **5.6 Lactate assay on-chip**

The lactate assay developed in the previous chapter was also tested on the lab-on-a-chip. It was not possible to obtain a measurable signal change irrespective of the lactate concentration and the duration of the assay. This was unexpected since the sensitivities obtained using 1:1 mixing ratio on the spectrophotometer indicate that a measurable color change should be produced on the lab-on-a-chip. However scaling the system up to a 1.5mm pitch, 500 $\mu$ m gap and microliter volumes produced good color in short times. The only difference between the nanoliter scale lab-on-a-chip and the microliter scale experiment was the significantly larger surface area of the oil-droplet interface in the latter case. Since silicone oil is permeable to oxygen this means that the oxygen concentration available for the reaction is higher in the microliter scale than the nanoliter scale. Though this evidence is inconclusive it leads us to suspect that the unexpected behavior on the nanoliter lab-on-a-chip had something to do with oxygen limitation.

## **5.7 Chapter summary**

The complete automation and integration from sample injection to result was demonstrated by performing multiple glucose assays using pipelined and serial assay protocols. The within-run reproducibility was excellent suggesting that the droplet-volume variability and the effects of cross-contamination are minimal. Glucose assays on serum performed poorly on-chip due to high interference at small dilution factors. The interference could be reduced by increasing the dilution factor. A higher dilution factor however means a lower sensitivity and requires alternative detection methodologies.

# **Chapter 6**

## **Conclusions and Future Work**

### **6.1 Conclusions**

A fully programmable digital microfluidic lab-on-a-chip (LoC) was developed in this thesis. The digital microfluidic platform is based on discrete microdroplets actuated in a programmable fashion by electrowetting. The lab-on-a-chip integrates and automates all the operations from sample injection to detection to provide sample-in-result-out functionality.

#### **6.1.1 Lab-on-a-chip Architecture**

A high-level architecture for the lab-on-a-chip, integrating previously developed digital microfluidic components, was first designed for integrated and automated analysis of multiplexed analysis on a monolithic device. The lab-on-a-chip integrates fluidic input ports for sample injection, on-chip reservoirs for droplet formation, fluidic pathways for transport and mixing areas and optical detection sites on the same monolithic substrate. The functional requirements of each of these individual components were elaborated and each component was designed taking these requirement into consideration.

A prototype lab-on-a-chip with sample injection elements, reservoirs (and waste), droplet formation structures, fluidic pathways, mixing areas and optical detection sites, was fabricated to test the various components of the architecture both individually and in an integrated fashion. The interconnect complexity of the electrowetting chips required a 2-layer metal process for fabrication. The interconnections were defined in the first layer, the electrode shapes in the second layer and metallized vias were used to connect the two. Insulator breakdown in the reservoir area was the major cause of failure of these chips and reduced the average lifetime of a chip to 5 minutes of continuous operation. Though the

exact reason for the breakdown is unknown at this time it is surmised that this is due to mechanical cracking or failure of the Parylene film at the gasket-electrode junction in the reservoir, which exposes the metal to the liquid and causes electrolysis.

The fluidic input port was designed for manual loading using a small volume pipette through a loading hole in the top plate. The formation of air bubbles during the loading process was the main challenge and considerable operator skill and practise was required. Droplets were formed from a reservoir on-chip using only electrowetting forces. The droplet volume and the formation process was dependent on several factors including the reservoir shape, electrode dimensions, and liquid properties. The reproducibility in the droplet volume was excellent and less than 3% (CV). The reproducibility is independent of the scale of the device and is the same for microliter or nanoliter droplets.

A multi-phased bus architecture was used for the droplet pathways to minimize the electrical signals to chip and simplify programming. 25nL droplets of water were transportable at 50Hz, corresponding to an average speed of 2.5cm/sec, on the lab-on-a-chip. Mixing was simply achieved by transporting the merged droplet on the bus at a high frequency. The droplets were moved in a single direction and not shuttled, to prevent unmixing due to flow reversibility. 25nL droplets of fluorescein and water were completely mixed in  $\approx$ 0.8 seconds. An optical absorbance measurement system, consisting of an LED and a photodiode, was also integrated with the electrowetting device to monitor colorimetric assays.

### 6.1.2 Biocompatibility

The compatibility of a liquid with the electrowetting system was evaluated by testing the transportability of the droplet and the ability to form droplets from an on-chip reservoir using only electrowetting forces. Using air as the filler media was incompatible with protein solutions due to non-specific adsorption. Silicone oil on the other hand formed a thin

film between the droplet and the chip surfaces and minimized the non-specific adsorption. Using silicone oil as the filler fluid rapid and repeatable transport of human physiological fluids such as whole blood, serum, urine and plasma, and other proteins such as bovine serum albumin, was achieved. All the physiological fluids could be actuated at frequencies of 20 Hz using less than 65 V. The general trend that was observed is that the fluids with less or no protein moved more easily than the ones with higher protein content. The transport of a droplet of heparinized whole blood was sustainable for  $\approx$ 25,000 continuous droplet transfers at 10 Hz ( $\approx$ 40 min) using an actuating voltage of 52 V. After 25,000 cycles the droplet was slower to respond and required a higher voltage to maintain the same switching frequency. This performance degradation could either be due to insulator degradation or gradual adsorption of proteins on to the Teflon surface.

Protein concentrations for which droplet formation worked were much smaller than the maximum concentration that was transportable. Reliable on-chip dispensing was possible up to concentrations up to 0.01mg/mL, which is three orders of magnitude smaller than the concentration for which transport would work (10mg/mL). This is likely due to non-specific protein adsorption in the reservoir due to its much larger surface area ( $\approx$ 20 times more than a unit droplet). Droplets could be reliably formed from serum, plasma and the enzymatic reagents using the standard operating voltage of 50V. Three different serum samples with different total protein contents were tested and the dispensing reliability was identical for all of them. However droplet dispensing did not work for whole blood up to a voltage of 120V.

### **6.1.3 Biological assays**

A colorimetric enzyme-kinetic assay (based on the Trinder's reaction) was also developed for the detection of glucose in physiological fluids to act as a model system. The glucose assay was linear up to 100mg/dL using a sample to reagent (volume) ratio of 1:1 and up

to 300mg/dL using a ratio of 1:2. There was also no significant change in the activity of the enzymes under electrowetting conditions. Assays were also developed for lactate and creatinine for use on the lab-on-a-chip. Lactate assays suffered from poor linearity in the human range for a dilution factor of 2. The linearity of the creatinine assay was excellent in the human range, however, the sensitivity was very poor even at a path length of 1cm.

#### **6.1.4 Integrated and automated lab-on-a-chip**

The automation of a clinical assay protocol from “sample injection to result” was demonstrated on the prototype lab-on-a-chip. Two different assay protocols were implemented on the lab-on-a-chip - a pipelined protocol and a serial protocol.

Two pipelined glucose assays were performed on the prototype lab-on-a-chip. Two droplets each of glucose samples and reagent were formed from 4 different reservoirs in a serial fashion. While the first sample and reagent were being mixed the second set of droplets were transported towards the mixing area. The mixed droplet was split into two and one droplet was moved to a storage area for detection while the other droplet was sent to waste. The second sample and reagent were mixed while the color change in the first assay occurred. This is the first time such complex fluidic protocols have been implemented in a programmable, automated and integrated fashion on any microfluidic lab-on-a-chip.

Using a serial assay protocol, three assays were each done on three samples each of 40, 80 and 120mg/dL glucose standards, to automatically generate a calibration curve and to study the within-run variation. The entire experiment was done in an automated and integrated fashion. The within-run reproducibility was less than 2% which indicated that both the volume variation and the cross-contamination was negligible. The reproducibility was the best (0.72%) for the highest concentration (120mg/dL) and was lower (1.8%) for the smaller concentrations. This was due to a larger component of error due to measurement noise at the lower concentrations. The results obtained on-chip were compared with

those obtained on a spectrophotometer and it was verified that there was no change in the behavior of the assay under electrowetting.

A 120mg/dL glucose sample was analyzed nine times serially to further evaluate the within-run variation. The coefficient of variation for all the 9 samples was 5.7%. The CV dropped to 2.2% if only the first 6 data points were considered. The reason for the larger error in the last 3 runs was due to the wider variation in the droplet volumes as the reservoir became empty.

Serum samples were also assayed on-chip but the results did not compare favorably to reference measurements due to interferences which become significant at lower dilution factors. Assays done on-chip and off-chip using identical dilution factors however compared well, indicating that the electrowetting chip was not responsible for the lower values obtained on-chip.

In summary - the microfluidic capability of the electrowetting-based lab-on-a-chip platform has been significantly expanded in this thesis to now achieve high-levels of integration and operation. The basic biocompatibility of the electrowetting system has also been established. The most challenging technology component that is currently missing from the digital microfluidic toolkit is a good detection methodology and future research should focus on this aspect of the technology.

## 6.2 Future Work

The three main issues that need to be addressed to make an electrowetting-based lab-on-a-chip useful for analytical applications are the dilution factor, detection methodology and system integration.

### **6.2.1 Dilution factor**

Most established biochemistry assay protocols require the reagent to be at least a few 10s of times in excess of the sample. Dilution factors of a 100 or 200 are most common. There are several reasons for using such high dilution factors.

1. Having the reagent in excess buffers any variations in the composition (concentration, pH, ionic strength) of the reagent due to the addition of the sample. The reagent will therefore be usable with samples with widely varying physical and chemical properties.
2. For enzyme-kinetic assays a larger dilution factor increases the linear range of operation of the assay.
3. Having the reagent in excess (or effectively diluting the sample) effectively enables reactions requiring oxygen which pose a problem on our system due to the presence of oil.
4. The most significant benefit of dilution is the suppression of interfering substances.

The main drawback of using high dilutions is the loss in sensitivity of the assay since sample concentrations are effectively reduced. This is significant on the electrowetting-based lab-on-a-chip due to poor scaling of optical detection methodologies. However sample dilution is imperative for correct operation of assays and cannot be compromised.

There are a couple of ways of realizing large dilution factors on the electrowetting chip. The first way is to serially dilute the sample and then add the reagent. This is not preferable since errors in dilution increase geometrically with every additional dilution step. A better alternative would be to use different sized electrodes and consequently droplets, for the sample and the reagent.

### **6.2.2 Detection methodologies**

Optical detection is easiest to integrate with the electrowetting-based lab-on-a-chip platform. However optical systems scale very poorly with miniaturization [55]. For example the path length for the lab-on-a-chip (0.1mm) presented in this thesis is 100 times smaller than conventional systems (10mm). The absorbances to be measured are therefore 100 times smaller on the electrowetting system and this poses serious sensitivity issues. Other optical methods such as fluorescence and chemiluminescence have orders of magnitude better sensitivities than absorbance. However these methods are not as common for blood chemistry applications. Electrochemical detection is a more suitable detection methodology but has the drawback of adding to the fabrication complexity in the device. However electrochemical methods are unavoidable if whole blood analysis at the point-of-care is required [56]. Future research should focus on increasing the path length for absorbance to the more conventionally used 1cm and integrating electrochemical detection on-chip.

### **6.2.3 System integration**

The lack of good sample preparation methods is currently the biggest impediment to the commercial acceptability of microfluidic technologies and considerable research effort is required in this area [57] to integrate this critical operation on-chip. The main topics under sample preparation would be the separation of cells from whole blood to obtain serum or plasma, and sample preconcentration. Sample preconcentration becomes essential in assays where the molecules which are to be detected are very small in number - causing errors in sampling at small volumes.

Packaging also become critical if the device is to be used in widely varying environmental conditions. The role of temperature fluctuations on the performance of the chip also needs to be evaluated and ways to maintain the temperature of the system constant is absolutely necessary for field operation. Reagent storage and shelf life is another impor-

tant system design issue if these devices are to be used in a clinical setting as disposable cartridges.

## **Appendix A**

### **Protein Stamping for MALDI Mass Spectrometry using an Electrowetting-based Microfluidic Platform**

#### **A.1 Abstract**

MALDI-MS (matrix-assisted laser desorption/ionization mass spectrometry) is one of the most commonly used techniques for protein analysis. In conventional systems sample preparation is typically done in well-plates and transferred onto a MALDI target by robotic systems, which are complex, huge, expensive and slow. In this paper, we present a droplet-based microfluidic interface to transfer protein samples from a well-plate format onto a MALDI target for MS analysis. The droplets are actuated using the electrowetting phenomenon, and are immersed in silicone oil which prevents non-specific adsorption and enables the manipulation of high concentrations of proteins. Droplet transport and droplet formation were evaluated as a function of protein concentration using bovine serum albumin (BSA) as a test system. Droplet transport was possible for BSA concentrations up to 10mg/mL which is three orders of magnitude higher than previously reported results on handling proteins by electrowetting. Droplet formation from on-chip reservoirs, using only electrowetting forces and no external pressure assistance, was possible up to concentrations of 0.01mg/mL. An interface between a well-plate format and the electrowetting chip, and a scheme to passively stamp droplets onto a target substrate was then designed and tested by stamping BSA solutions. In two separate experiments 3.6fmoles and 16fmoles of BSA were stamped onto a glass slide using 0.001mg/mL and 0.01mg/mL samples respectively. A protein mixture with known constituents (ABI 4700 proteomics analyzer calibration

solution) was stamped onto a MALDI plate and the individual proteins were correctly identified in the mass spectrum obtained using MALDI-TOF- MS. The preliminary results establish the feasibility of using an electrowetting-based microfluidic system to handle proteins especially for protein stamping applications. The proposed system has a small footprint, is easy to control, and is very fast compared to conventional robotic systems. In addition, there are no moving parts and the associated mechanical reliability issues. Future work involves scaling to a larger number of samples and integration of sample preparation steps on-chip.

## A.2 Introduction

Mass spectroscopy (MS) is increasingly becoming the method of choice for protein analysis in biological samples [58]. Among the various MS methods, MALDI-TOF (Matrix Assisted Laser Desorption-Ionization Time of Flight) is the most commonly used due to its simplicity, high sensitivity and resolution. A typical MALDI-MS protocol for protein identification involves sample preparation, stamping onto a MALDI target and analysis on a MALDI-TOF mass spectrometer. Sample preparation steps (such as digestion and concentration) are usually done in the well-plate format and last for several hours at the least. The stamping is done using complex robotic systems which are huge, expensive and immobile. Sample volumes required are also very high, which is a concern for proteins available in very small quantities.

The emerging paradigm of microfluidic lab-on-a-chip systems can alleviate these drawbacks by reducing volume requirements to nanoliters, decreasing sample preparation time (due to more efficient kinetics on the microscale) and by providing a simpler interface to MALDI-MS instrumentation without moving parts. Several microfluidic platforms have been proposed for protein analysis using MALDI-MS. Ekstrom et al [59] integrated a microchannel immobilized enzyme reactor (for protein digestion of  $1\mu\text{L}$  samples within 3

minutes) with a piezoelectric microdispenser for stamping in a high-density format. The microfluidic device used a syringe pump for inducing fluid flow. Brivio et al [60] developed a continuous flow lab-on-a-chip consisting of an on-chip microfluidic device with reaction microchannels and integrating the microdevice with a MALDI-TOF MS standard sample plate. A pressure driven pumping mechanism using the vacuum of the instrument was used as a driving force in the reaction microchannel. Gyros AB (Uppsala, Sweden) [61, 28] has developed a system to integrate sample concentration, elution and crystallization on a CD platform for MALDI analysis.

All the microfluidic devices discussed above are based on continuous flow in fixed microchannels, offering very little flexibility in terms of scalability and reconfigurability. An alternative approach is to manipulate the liquid as discrete microdroplets. This approach, referred to as digital microfluidics, has several advantages over continuous-flow systems, the most important being the ease of fabrication, and reconfigurability and the scalability of architecture.

Electrowetting is one of several techniques that have been proposed to actuate microdroplets. Electrowetting refers to the modulation of the interfacial tension between a conducting liquid phase and an insulated solid electrode, by the application of an electric potential between the two. Kim et al [62] have proposed an electrowetting-based system for analysis of peptides and proteins by MALDI using the electrowetting chip itself as the MALDI target. However since the droplets are manipulated in air, non-specific protein adsorption problems arise and only sufficiently hydrophilic proteins or ultra low concentrations of other proteins ( $<< \mu\text{g/mL}$ ) would work. The system proposed in this paper uses silicone oil to encapsulate the droplet and minimize adsorption, enabling the manipulation of very high concentrations of protein solutions. Using this technique we have previously demonstrated the manipulation of real physiological samples containing proteins for a clinical diagnostic application [63]. In this paper we extend our system to

format protein samples for MALDI-MS analysis and present preliminary results to establish the proof of concept. Droplet transport and formation from an on-chip reservoir is first evaluated as a function of the protein concentration using bovine serum albumin (BSA) as a test system. An interface between a well-plate format and an electrowetting chip, and a scheme to passively stamp droplets onto a target substrate is then designed and tested using water and BSA solutions. Finally droplets of a known protein mixture are stamped on to a standard MALDI target plate and analyzed on an ABI 4700 MALDI-MS TOF system.

## A.3 Materials and Methods

### A.3.1 Chip fabrication

The electrowetting system comprises of a photolithographically patterned metal electrode array (chrome or indium tin oxide) on a glass substrate and a continuous ground plane (indium tin oxide on glass or polycarbonate) parallel to it. A spacer of known thickness ( $H$ ) separates the electrode array and the ground plane and the droplets are sandwiched between the two. The spacer material is also used to physically define the on-chip reservoir. 1cSt silicone oil (DMS-T01, Gelest, Morrisville, Pennsylvania, USA) is used as the filler medium surrounding the droplets to prevent evaporation and facilitate transport. The electrode array is insulated from the droplet by layer of Parylene C ( $\approx 800\text{nm}$ ) and both the surfaces are hydrophobized by a thin layer of Teflon AF 1600 ( $\approx 50\text{nm}$ ). Figure A.1 shows the vertical cross-section of a typical electrowetting device. The fabrication and operation of the electrowetting system are described in detail in [33].

### A.3.2 Chemicals

Bovine Serum Albumin (BSA, A-4378) was obtained from Sigma Chemicals (St Louis, Missouri, USA) and stock solutions of 0.1 mg/mL, 0.0 mg/mL and 0.001 mg/mL were prepared in de-ionized water. BSA (10mg/mL) was also provided by GlaxoSmithKline

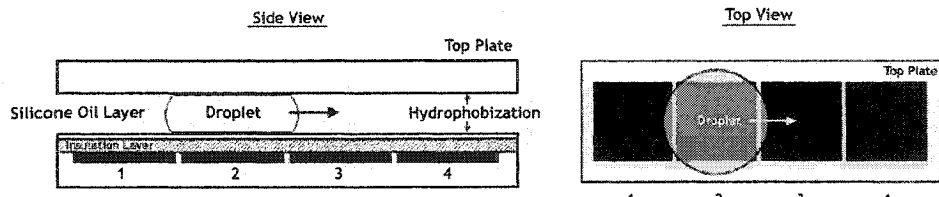


**Figure A.1:** Top and side views of a typical electrowetting setup

(Durham, North Carolina, USA) and diluted to 1 mg/mL, 0.1 mg/mL, 0.01 mg/mL and 0.001 mg/mL in deionized water. ABI 4700 proteomics analyzer calibration solution was provided by the Duke University Proteomics Center (Durham, North Carolina, USA) and consisted of 1.0 $\mu$ M des-Arg1-Bradykinin, v Angiotensin I, 1.3 $\mu$ M Glu1-Fibrinopeptide B, 2.0 $\mu$ M ACTH (1-17 clip), 1.5 $\mu$ M ACTH (18-39 clip), and 3.0 $\mu$ M ACTH (7-38 clip) in a-cyano-4-hydroxycinnamic acid/acetonitrile/TFA matrix.

#### A.4 Manipulation of Protein Samples by Electrowetting

The manipulation (droplet formation, transport etc) of non-biological electrolytes using electrowetting has been demonstrated both in air [44] and in other immiscible media such as silicone oil [33]. However dealing with fluids containing proteins is not as straightforward, since they tend to irreversibly adsorb to hydrophobic surfaces such as the Teflon AF surface in the electrowetting setup. Any contact between the protein sample and the Teflon AF surface will therefore contaminate the surface and also render the surface permanently hydrophilic [46]. This is detrimental to electrowetting since electrowetting works on the principle of reversible modification of the wettability of a hydrophobic surface. Therefore any contact between a liquid containing proteins and the Teflon surface should be avoided to prevent contamination and not inhibit transport. As a consequence, air is not a suitable filler medium for applications involving proteins, since the droplet is always in contact with the Teflon surface. Silicone oil with its low surface tension ( $\approx$ 20dynes/cm) and spreading

property is an ideal alternative. From visual observations we have inferred the presence of a thin film of oil, encapsulating the droplet. This oil film isolates the droplet from the Teflon surfaces, minimizing adsorption and facilitating reversible electrowetting. However, we need to evaluate if lipophilic proteins in droplets would partition into the surrounding oil.

The stability of the oil film, though yet to be extensively characterized, appears to decrease with increasing protein content which causes lowering of the interfacial tension between the liquid (droplet) and oil. A less stable oil film implies more adsorption of proteins on to the Teflon surface and consequently liquids having high protein concentrations are more difficult to manipulate and require higher actuation voltages. The droplet transport and droplet formation processes are therefore studied as a function of protein concentration using bovine serum albumin (BSA) as a test protein. We have previously shown the transport of a variety of biological fluids including whole blood, serum, plasma and urine on our system using silicone oil as the filler fluid [63].

#### A.4.1 Protein Droplet Transport

Due to the discrete nature of operation of a digital microfluidic system, the maximum switching frequency (defined as the highest rate at which a droplet can be completely moved across two adjacent electrodes) is the measure of the transport- performance of the system. Higher the switching frequency, more the number of discrete fluidic operations that can be performed per second and higher the throughput of the system. The maximum switching frequency is evaluated for droplets containing different concentrations of BSA as a function of the applied voltage. Droplets are manually dispensed using a pipette in order to nullify the effect of the concentration dependency of automated droplet formation.

#### A.4.2 Protein Droplet Formation

Unit droplet generation from a larger volume liquid of is a very important component of the world-to-chip interface of any droplet-based microfluidic device. In an electrowetting system, droplets can be generated from on-chip reservoirs using purely internal electrowetting forces, from external reservoirs using active pressure sources, or a combination of the two. We have previously demonstrated droplet generation with and without external pressure assistance for aqueous electrolytes [63, 33]. However, as in the case of transport, droplet formation also needs to be evaluated for protein solutions to completely establish the compatibility of the liquid with our platform. The formation process is likely to be more severely affected by protein adsorption than transport, since the liquid in the reservoir has a much larger surface area to adsorb to than a unit droplet. Concentrations for which formation would work are therefore expected to be smaller than the maximum concentration for which simple transport would work. Droplet formation using only electrowetting forces is tested for BSA solutions with concentrations ranging from 0.001-0.1mg/mL.

### A.5 Passive Protein Stamping

Stamping refers to the process of transferring a protein droplet on to a MALDI substrate which can be analyzed on a MALDI MS system. Figure A.2 shows a high level schematic of an electrowetting-based stamping system which interfaces a standard well-plate format and a MALDI target substrate. The electrowetting chip consists of an on-chip reservoir (physically defined by the spacer material) and a set of contiguous electrodes connecting it to the stamping site. A polycarbonate sheet (coated with conductive indium tin oxide to act as the ground plane) is clamped to the electrowetting chip, and has holes for injecting liquid into the reservoir from a well-plate and for extraction (stamping) onto the MALDI target. By designing the diameter of the stamping hole to be much larger than the spacer thickness (which is also the droplet height), the liquid is passively pushed out

of the stamping hole. The larger diameter creates a lower pressure at the stamping hole as compared to the transport layer on the chip, which forces the droplet out spontaneously without active forces [64]. However some liquid is still expected to be left behind in the hole as dead volume. Preliminary stamping experiments are done with water or protein solutions containing 0.01mg/mL or 0.001mg/mL bovine serum albumin. Sample is injected into the on-chip reservoirs either from a well-plate (using a syringe pump to apply pressure) or a pipette. Droplets are then automatically generated from the reservoir, configured on the chip by electrowetting, and vertically stamped onto a MALDI target. To complete the feasibility study, a known protein mixture (AB1 4700 proteomics analyzer calibration solution) is stamped on to a standard MALDI target plate and analyzed on an ABI 4700 MALDI-MS TOF system to determine if any proteins are lost on the electrowetting platform or the stamping hole. We would like to note that though the eventual objective is to do sample preparation on-chip, the well-plate format still represents a standardized high-throughput input format. Hence the emphasis on interfacing the electrowetting chip to the well-plate format.

## A.6 Results and Discussion

### A.6.1 Transport of BSA droplets

The maximum switching frequency of droplets containing different concentrations of BSA (0.001-10mg/mL) was evaluated as a function of voltage. The electrode pitch was  $L=1\text{mm}$ , the gap was  $H=500\mu\text{m}$  (refer to Figure 1 for definition of L and H), and the droplet volume was  $0.75\mu\text{L}$ . Silicone oil (1cSt) was used as the filler fluid. Figure A.3 plots the maximum switching frequency as a function of the voltage, for various concentrations of BSA. As expected, droplets with higher protein content are more difficult to transport and require higher voltages for operation. This is the first time such high concentrations of protein have been demonstrated to transport on an electrowetting system. Using air as a filler medium,

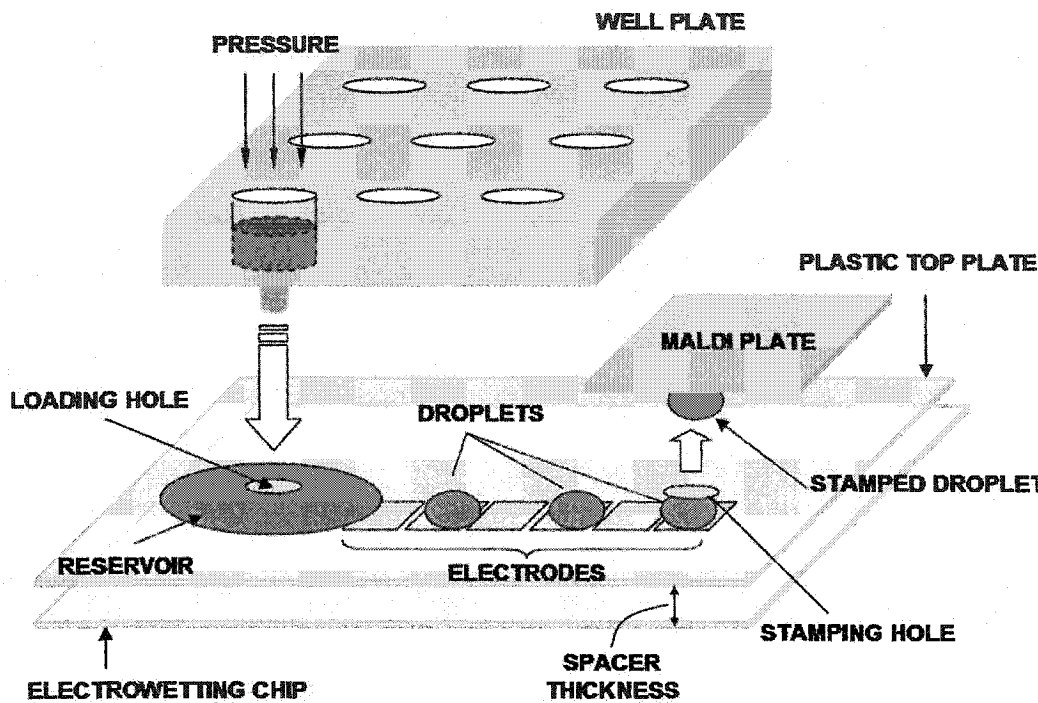


**Figure A.2:** High level schematic of the droplet stamping setup

static electrowetting (i.e. static change in contact angle by application of a potential) of  $4\mu\text{g/mL}$  BSA droplets has been previously demonstrated in a limited sense [46]. However dynamic transport has not been shown in air and will indeed be a big challenge due to the reasons mentioned previously. Even in the static case the reversibility of the contact angle change reduces over time due to continuous non-specific and electric field driven adsorption.

### A.6.2 BSA Droplet Formation

Droplet formation from BSA solutions of various concentrations (0.001-0.1mg/mL) using only electrowetting forces was evaluated. The electrode pitch was  $L=750\mu\text{m}$  and the spacer thickness was  $H=75\mu\text{m}$ . For concentrations up to 0.01mg/mL reliable on-chip dispensing was possible. For solutions containing higher concentrations of BSA ( $\geq 0.1\text{mg/mL}$ ) it was not possible to generate droplets using electrowetting alone, despite the fact that

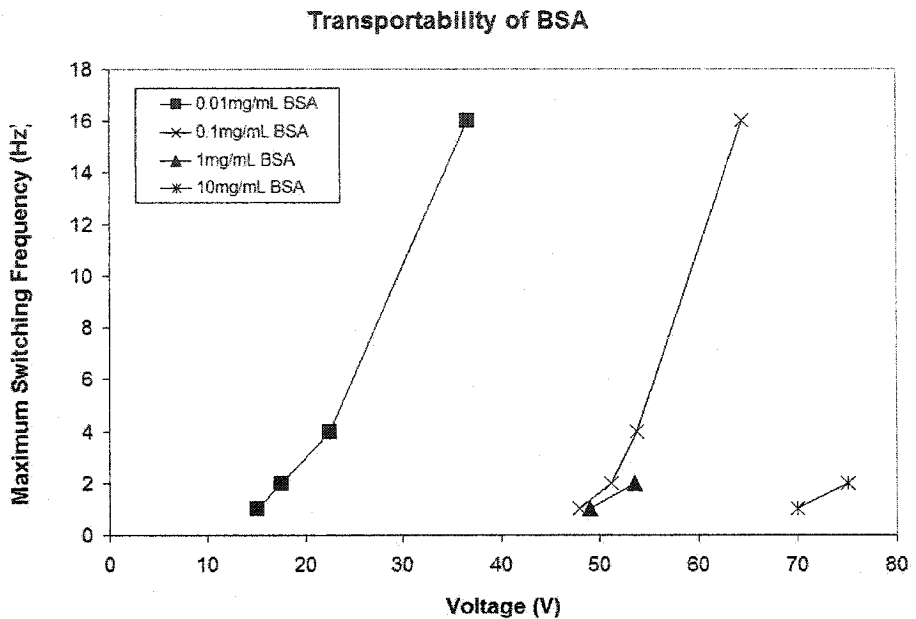


**Figure A.3:** Maximum switching frequency of a BSA droplet as a function of the voltage for various concentration of BSA

individual droplets containing up to 10mg/mL BSA have been transported previously. This is likely due to protein adsorption, since the liquid in the reservoir has a much larger surface area ( $\approx 20$  times more than a unit droplet) and therefore a higher probability of adsorbing to the surfaces of the reservoir.

### A.6.3 Protein Stamping

Preliminary experiments were conducted with water, and protein solutions containing 0.01 mg/mL or 0.001 mg/mL bovine serum albumin. The electrode pitch was  $L=750\mu\text{m}$  and the spacer thickness was  $H\approx 75\mu\text{m}$ , resulting in a unit droplet volume of  $\approx 40\text{nL}$ . The thickness of the top plate of polycarbonate sheet was  $500\mu\text{m}$ , and the diameter of the stamping hole was  $600\mu\text{m}$ . A hydrophobic glass slide with a hydrophilic patch (aligned to the stamping hole) was used as the stamping target. The spacing between the stamping target and the polycarbonate top plate was  $\approx 90\mu\text{m}$ . Liquid was loaded from a well-plate (for water samples) or using a pipette (for protein solutions). Droplets were then automatically generated

from the reservoir, routed to the stamping hole, and vertically stamped onto the stamping target. Figure A.4 shows the time lapsed images of an experiment where 10 droplets ( $\approx 40\text{nL}$  each) of  $0.001\text{mg/mL}$  were dispensed from the reservoir, of which 6 droplets ( $\approx 240\text{nL}$  corresponding to  $3.6\text{fmoles}$ ) was stamped onto the glass slide. The remaining 4 droplets ( $\approx 160\text{nL}$ ) were left behind in the stamping hole as dead volume. In a similar experiment, an estimated  $16\text{fmoles}$  of BSA was stamped using  $0.01\text{mg/mL}$  BSA solution. The number of moles stamped can be further increased by increasing the concentration of the protein solution or the volume of liquid i.e. the number of droplets stamped.

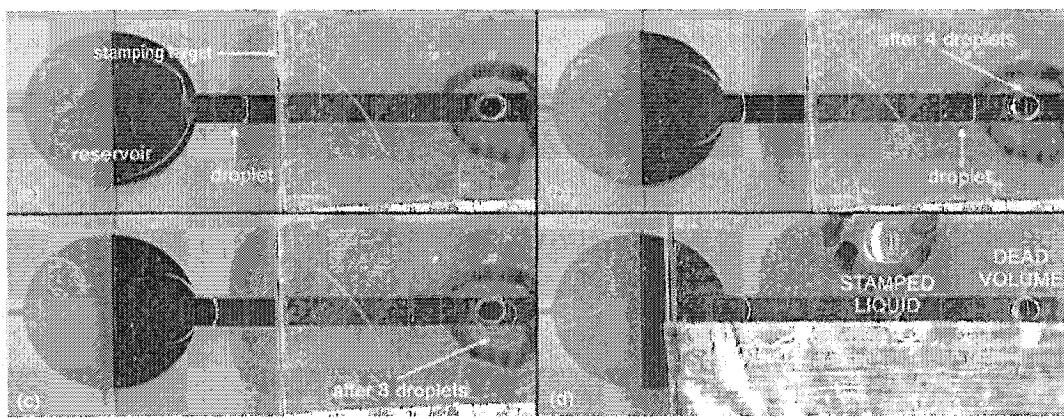


**Figure A.4:** Time lapsed images of a protein stamping experiment

#### A.6.4 MALDI-MS on protein calibration solution

To complete the feasibility study, a protein stamping experiment was performed using ABI 4700 calibration solution as a test protein sample. The electrode pitch was  $L=1.5\text{mm}$  and the spacer height was  $H=300\mu\text{m}$ . The calibration solution contained the following proteins.

- des-Arg-Bradykinin (mol. Wt. = 904.468 Daltons)
- Angiotensin I (1296.685 Da)
- Glu-Fibrinopeptide B (1570.677 Da)

- ACTH (1-17) (2093.087 Da)
- ACTH (18-39) (2465.199 Da)
- ACTH (7-38) (3657.929 Da).

Two  $1\mu\text{L}$  droplets of the calibration solution were dispensed manually onto chip, transported by electrowetting, and passively stamped through the polycarbonate top plate on to a MALDI plate. The MALDI plate was then analyzed on an ABI4700 MALDI TOF/TOF system and the spectrum obtained is shown in Figure A.5. The figure shows that all the proteins in the calibration solution are detectable in the spectrum even after on-chip operations of transport and passive stamping were performed. ACTH (7-38) does not appear on the graph since the mass spectroscopy was done only till a molecular weight of 3400 Daltons as suggested by the manufacturer protocol. The preliminary results establish the feasibility of using an electrowetting-based microfluidic system for protein stamping applications. Further work is required to integrate sample preparation on-chip which would reduce the total analysis time significantly. Mechanical design issues also need to be considered at the injection and ejection orifices, such as air bubbles and dead volume. Ways to increase the total amount of protein stamped also need to be investigated. This could be done by spotting more number of droplets at the same location, by increasing the concentration of the protein in solution or by scaling the system up in dimensions. Eventually the system also needs to be scaled to accommodate an actual 96-well plate or 384-well plate.

## A.7 Conclusions

An electrowetting-based microfluidic platform for protein stamping applications was described in this paper. Protein droplet transport and formation from an on-chip reservoir was initially evaluated to establish the compatibility of the protein with the electrowetting system. Bovine serum albumin (BSA) was used as a test protein, and concentrations

### MALDI-MS spectrum for Protein Calibration Solution

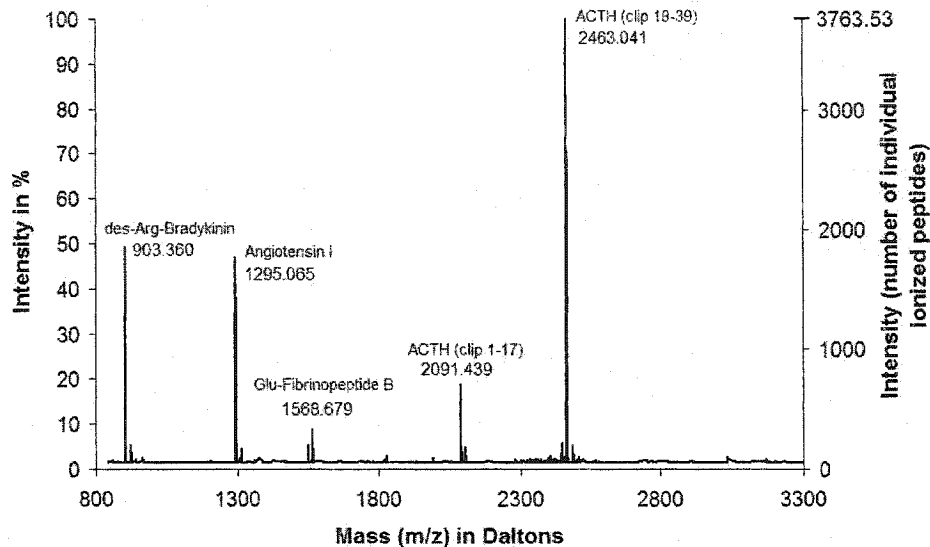


Figure A.5: Mass spectra of the ABI4700 MALDI calibration solution

up to 10mg/mL were transportable, which is more than three orders of magnitude higher than previously reported results. Droplets formation was possible up to concentrations of 0.01mg/mL using only electrowetting forces. We were able to manipulate droplets containing such high concentrations of proteins due to the presence of an oil film encapsulating the droplet and minimizing non-specific adsorption to Teflon AF. A passive stamping scheme was designed to vertically actuate droplets onto a MALDI target and tested using BSA and water. Liquid was loaded from a well-plate (for water samples) or using a pipette (for protein solutions), and droplets were automatically generated from the reservoir and configured on the chip by electrowetting to be vertically stamped onto the stamping target. By designing the diameter of the stamping hole to be much larger than the spacer thickness, a lower pressure is created at the stamping hole as compared to the transport layer on the chip, which forces the droplet out spontaneously without active forces. In two separate experiments 3.6fmoles and 16fmoles of BSA were stamped onto a glass slide using 0.001mg/mL and 0.01mg/mL samples respectively. MALDI-MS was also performed on

an ABI 4700 proteomics analyzer calibration solution and from the mass spectra the proteins in the calibration solution were correctly identified. The preliminary results establish the feasibility of using an electrowetting-based microfluidic system for protein stamping applications. The proposed system has a small footprint, is easy to control, and is very fast compared to conventional robotic systems. In addition, there are no moving parts and the associated mechanical reliability issues. Future work mainly involves integration of sample preparation on-chip and scaling the system to a larger array.

## A.8 Acknowledgements

We acknowledge John van Arnold at the Duke University Proteomics Center for providing us with the MALDI calibration samples and assistance with mass spectrometry, Dr. Hugh Crenshaw at GlaxoSmithKline for providing BSA samples and for partly funding the research, and BioMachines and Leap Technologies for partly funding this project.

## **Appendix B**

# **A Droplet-based Lab-on-a-chip for Colorimetric Detection of Nitroaromatic Explosives**

### **B.1 Abstract**

Portable and automated field screening equipment would be very effective in detecting and quantifying explosives at various sites. A droplet-based microfluidic lab-on-a-chip utilizing electrowetting is presented for the colorimetric detection of TNT (trinitrotoluene). The method uses the reaction between nitroaromatics and a strong base which forms the highly colored Jackson- Meisenheimer complex. Microliter-sized droplets of TNT are programmed to transport, mix, and react with potassium hydroxide (KOH) on the microfluidic chip. Colorimetric reactions of TNT are characterized both on a spectrophotometer and on the microfluidic chip. The detection of TNT on the chip is linear in the range of  $4\text{-}20\mu\text{g/mL}$  with a time-to-result of 2.5 minutes. It is also observed that the absorbance peaks of DNT (dinitrotoluene) and TNT are mutually independent and that the presence of DNT does not affect the detection of TNT. Electrowetting also does not seem to influence the colorimetric complex as observed from a comparison of results between a spectrophotometer and on-chip.

### **B.2 Introduction**

Recent thrusts in counterterrorism efforts have led to an increased interest in technologies for the detection of explosives. Explosives need to be detected in a variety of complex environments such as mail, luggage, urban areas of high population density (such as airports, subways, stadiums), soils (from munitions manufacturing sites, military bases, land mine

fields, post-blast sites), and water (ground, surface, and sea).

Nitroaromatics (TNT, DNT, DNB) form one of the most commonly used class of explosive compounds, with TNT being the most widely used explosive [65]. TNT poses a health risk to humans even at very low parts per billion concentrations in ground water [66] and is suspected to be a carcinogen besides being highly toxic for humans, plants, and animals [67].

TNT is currently analyzed in the laboratory using the high performance liquid chromatography -based U.S. EPA SW-846 Method 8330 [68]. Several commercial field screening test kits are also available for the detection of TNT, based either on immunoassays [69, 70] or colorimetric methods [71, 72]. In a comparison of all on-site TNT analysis methods, the colorimetric method as detailed in EPA Method 8515 was found to be the most suitable for on-site detection based on accuracy, detection limits, precision, ease of use, cost per sample, and the ability to detect classes of explosives [73]. The EPA 8515 method is based on the reaction between a nitroaromatic and a strong base which forms the highly colored Jackson- Meisenheimer anion, and has a detection limit of partsper- million.

Current laboratory methods for trace analysis of nitroaromatics have long turnaround times (3 days), are expensive (1000 dollars) and require skilled technicians [74]. Commercial field screening test kits have a shorter turnaround time but still require a skilled on-site technician. There is therefore a need for on-site explosive detection systems that would be fully-automated in addition to being inexpensive, sensitive, reliable, and compatible with a broad range of samples. The advent of microfluidic labon- a-chip technology offers such detection systems due to the advantages in portability, reduction of the volumes of the sample and reagents, faster analysis, increased automation, mass manufacturability, and high throughput.

Most microfluidic devices are based on continuous flow which are rigid in design and have limited reconfigurability and scalability in architecture. An alternative approach,

which offers a more generic microfluidic platform, is to manipulate the liquid as unit-sized discrete microdroplets. Electrowetting is one of several techniques that have been successfully used to implement a digital microfluidic lab-on-a-chip. Electrowetting refers to the modulation of interfacial tension between a conducting liquid and a solid electrode, by the application of an electric field between them. We have previously utilized electrowetting to demonstrate a fully integrated and automated colorimetric assay for glucose [63]. In this paper, while sample extraction is still manual, we extend the utility of our electrowetting platform by automating the chemical analysis and detection of droplets containing nitroaromatic explosives. The proposed digital microfluidic platform for the detection of TNT is shown in Figure B.1. This platform could be used to perform simultaneous optical detection on multiple droplets.

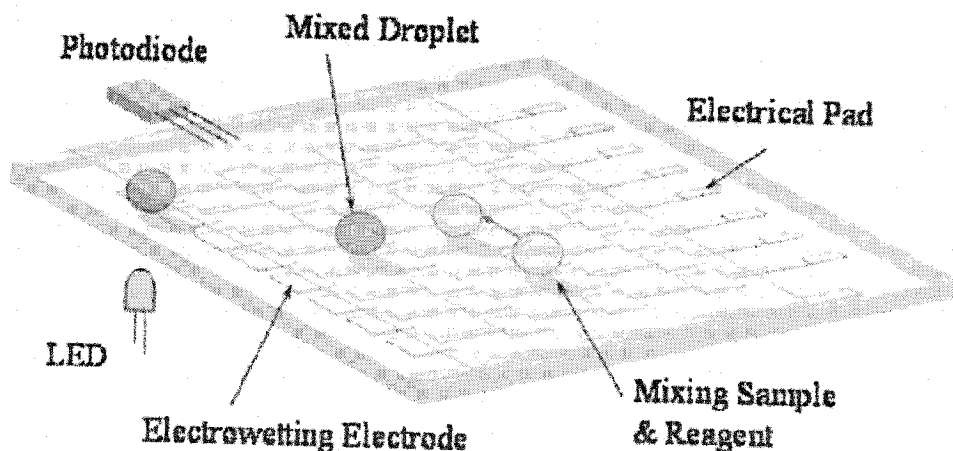


**Figure B.1:** Schematic of the electrowetting lab-on-a-chip integrated with optical detection

## B.3 Materials and Methods

### B.3.1 Chemicals

Commercial grade 2,4,6-trinitrotoluene (TNT) and pure 2,4-dinitrotoluene were obtained from Sandia National Labs. KOH and DMSO were reagent grade.  $20\mu\text{g/mL}$  stock solu-

tions of TNT and DNT were freshly prepared in DMSO and diluted to obtain various sample concentrations between  $4\text{-}20\mu\text{g/mL}$ . Since KOH does not dissolve readily in DMSO, a 0.36M KOH solution was first prepared in deionized water and then diluted 2000 times with DMSO to obtain a stock concentration of  $180\mu\text{M}$ . The KOH stock solution finally ended up with less than 0.05% water.

### B.3.2 Electrowetting setup and Chip Fabrication

The electrowetting system consists of two parallel electrode plates, a continuous ground plate on top and an addressable electrode array (pitch = L) on the bottom plate as shown in Figure 1. A spacer separates the top and bottom plates, yielding a fixed gap (H). The droplet is sandwiched between the two plates, and surrounded by immiscible silicone oil, which prevents evaporation of the droplets and also reduces the voltages required for transporting the droplets. The electrode array is insulated (Parylene C) from the liquid and both surfaces are hydrophobized (Teflon AF). Indium Tin Oxide (ITO), a transparent conductor, is used as the material for the electrodes, to enable easy integration of optical detection methods. In the experiments reported in this paper, we have used electrowetting chips with an electrode pitch (L) of 1.5 mm and a gap spacing (H) of 600  $\mu\text{m}$ .

### B.3.3 Colorimetric method for the detection of TNT

Nitroaromatic compounds such as TNT/DNT react with nucleophiles (bases) such as hydroxides and alkoxides, to form colored Jackson-Meisenheimer complexes. Acetone, acetonitrile and methanol have been the most popular choices for TNT analysis even though this reaction has been demonstrated in various organic solvents. These solvents are miscible with silicone oil in the current setup. DMSO is another versatile solvent which dissolves most aromatic hydrocarbons, including nitroaromatics such as TNT, and yet is immiscible with silicone oil, making it a compatible solvent with our current setup. Also

DMSO is completely miscible with water in all proportions and has a low order of toxicity for use in the field. For these reasons we chose to use DMSO as the solvent to develop the TNT reactions. DMSO is also known to enhance the stability of the Jackson-Meisenheimer complex [75]. In the experiments reported in this paper, potassium hydroxide (KOH) was used as the base to react with TNT to produce the colored complex. To the best of the authors' knowledge the reaction between TNT/DNT and KOH using DMSO as the solvent has not been characterized in terms of the absorbance peaks of the colored complexes, and is therefore reported in this paper.

### B.3.4 Optical Detection

The colored Jackson-Meisenheimer complex is detected using a simple absorbance measurement system comprising of an LED (505nm) and a photodiode, perpendicular to the plane of the electrowetting chip, as shown in Figure B.1. The absorbance is calculated from the equation  $A=\ln(V/V_0)$ , where V is the photodiode voltage output using TNT as the sample and  $V_0$  corresponds to the blank absorbance.

### B.3.5 System Operation Protocol

The reactions were performed on the chip in three steps: dispensing, electrowetting-enabled mixing, and colorimetric detection. Droplets of TNT and KOH are dispensed manually by a pipette on the electrowetting chip. These two droplets are merged by applying voltages to the appropriate electrodes. The merged droplet is further mixed by shuttling it across four electrodes for 30 seconds at an actuation voltage of 50 V. Our earlier results indicate that mixing should be complete in less than 30 seconds for this pattern of mixing [39]. At the completion of mixing, the absorbance is measured using the LED (light emitting diode)/photodiode setup described earlier. All the reactions were performed at room temperature.

## B.4 Results and Discussion

### B.4.1 Absorbance spectra of colored product

The absorbance spectrum of the colored product resulting from the reaction between TNT (or DNT) and KOH, in DMSO is shown in Figure B.2. TNT has absorbance peaks ( $\lambda_{max}$ ) at 336 nm and 510 nm, while DNT has peaks at 407 nm and 657 nm. It should also be noted that TNT has absorbance minima close to the absorbance peaks of DNT and vice-versa. The TNT reaction was monitored at 505 nm (close to  $\lambda_{max}=510\text{nm}$ ), which is the peak emission wavelength of the LED used in the on-chip optical measurements.

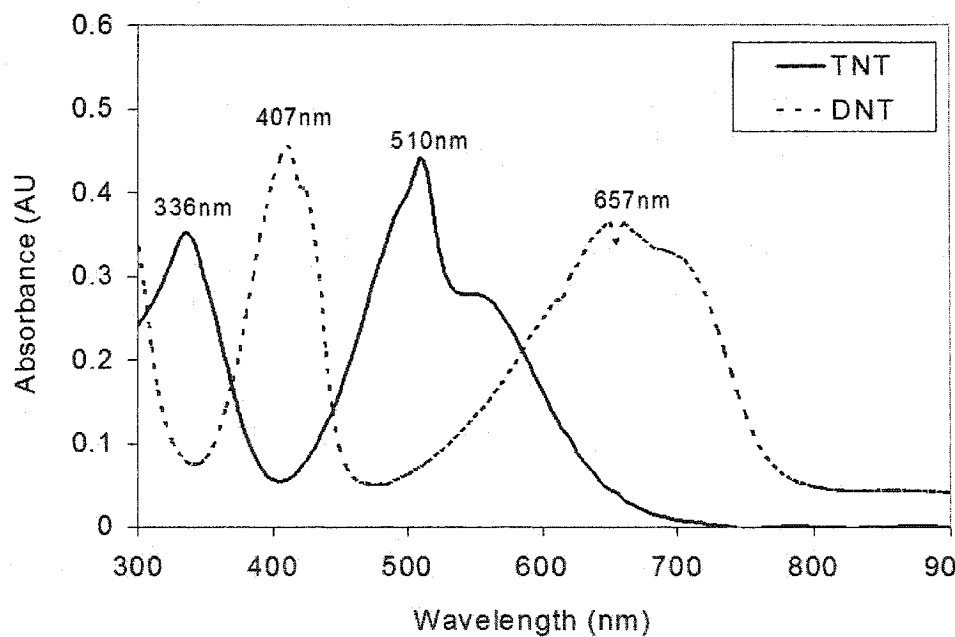


**Figure B.2:** Absorbance spectra of colored complexes formed in the reaction between TNT/DNT and KOH using DMSO as the solvent

### B.4.2 TNT reaction on a spectrophotometer

The TNT reaction was initially characterized on a bench top spectrophotometer (Gensys 20). 500 $\mu\text{L}$  of 180 $\mu\text{M}$  KOH was added to 500 $\mu\text{L}$  of the sample (4-20 $\mu\text{g/mL}$ ) at T=0s and the absorbance was monitored at 505nm on the spectrophotometer. Figure B.3 shows

the absorbance of the colored complex, as a function of time. From the figure note that the absorbance remains stable after  $T=120$ s. Figure B.4 plots the absorbance obtained at  $T=150$ s (after stable color is reached) as a function of the TNT concentration. The absorbance is linear up to  $20\mu\text{g/mL}$  which was the highest concentration tested, with an  $R^2$  (measure of goodness of fit) of 99.94%.

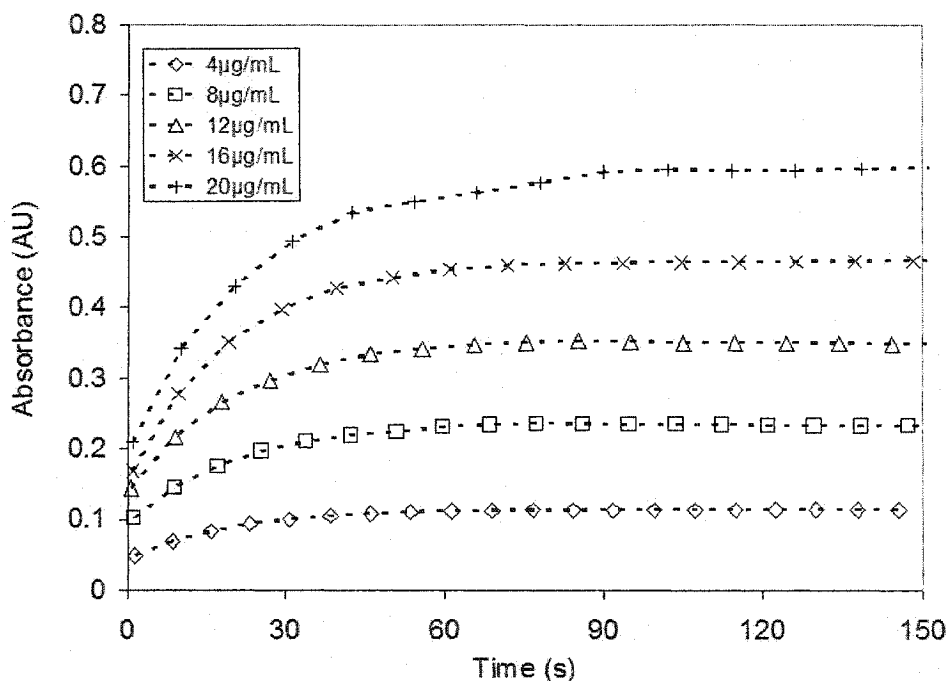


**Figure B.3:** Absorbance of the colored complex for various concentrations of TNT as a function of time on the spectrophotometer

#### B.4.3 Detection of TNT on-chip

A  $1.5\mu\text{L}$  droplet of the TNT sample ( $4\text{-}20\mu\text{g/mL}$ ) and a  $1.5\mu\text{L}$  droplet of  $180\mu\text{M}$  KOH was dispensed and mixed to react on the chip. The blank absorbance is measured with the KOH droplet. Figure 5 shows absorbance under the reaction conditions as a function of time.  $T=0$ s corresponds to the time instant at which the droplets were merged. From the figure it can be observed that the color stabilizes around  $T=150$ s. The absorbance measurements are therefore taken 150s after the droplets were merged. A comparison of

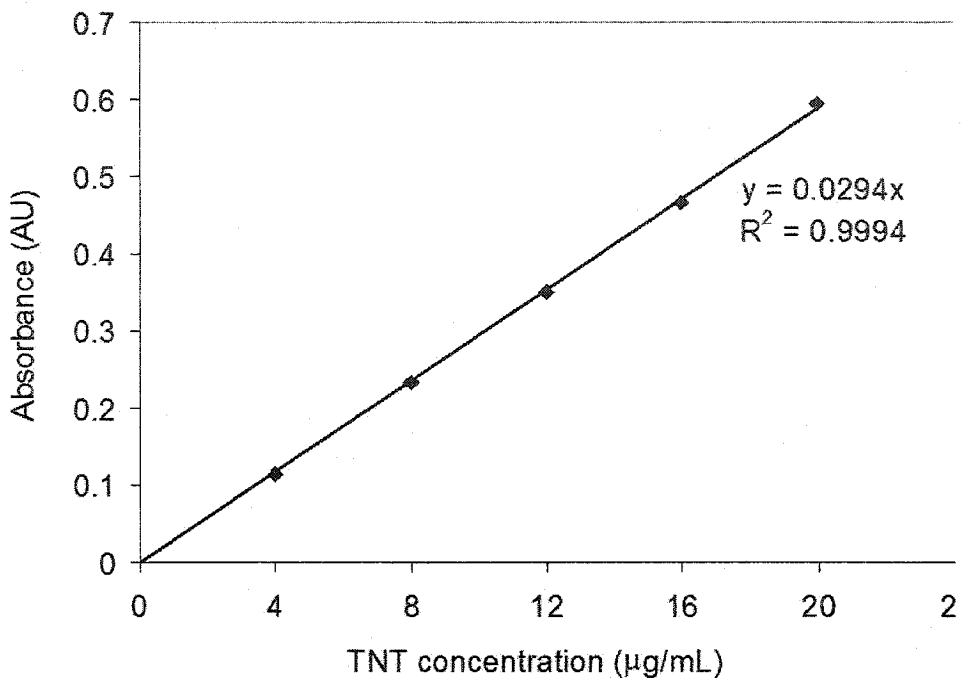


**Figure B.4:** Calibration curve of absorbance with respect to the concentration of TNT demonstrating a linear relation on the spectrophotometer

reaction kinetics after 30s in Figure 3 and Figure B.5 shows that qualitatively the trends are similar. On-chip reaction kinetics data are not available before 30s because the droplets are being shuttled for mixing during that time. It should be noted that the absorbance values are not the same, due to the different optical path lengths for each case. From Figure B.6, the absorbance is linearly related to TNT with an  $R^2$  of 98.63% up to 20  $\mu\text{g/mL}$  (the highest concentration tested).

#### B.4.4 Detection of TNT in a mixture of TNT and DNT

From Figure B.2 we can see that the absorbance spectra for TNT and DNT are mutually independent. This means that TNT can be quantitatively estimated even in the presence of DNT. To verify this hypothesis, mixtures of TNT and DNT were analyzed in various ratios on a spectrophotometer at 505nm (absorbance peak of TNT), and the results are shown in Figure B.7. 100% TNT or DNT corresponds to a concentration of 20  $\mu\text{g/mL}$ . From Figure

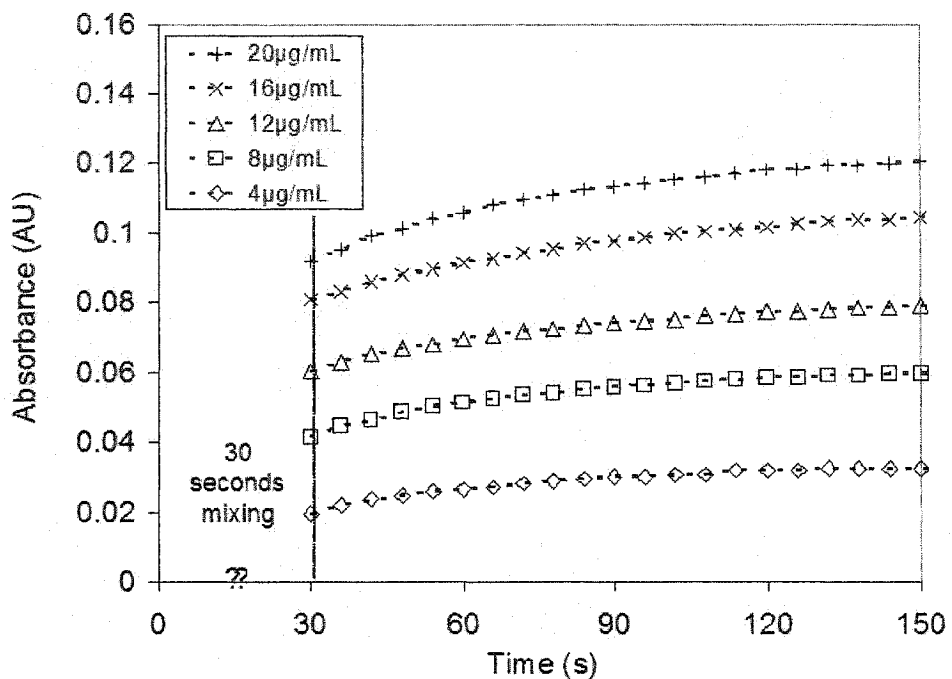


**Figure B.5:** Absorbance of the colored complex for various concentrations of TNT as a function of time on the electrowetting chip

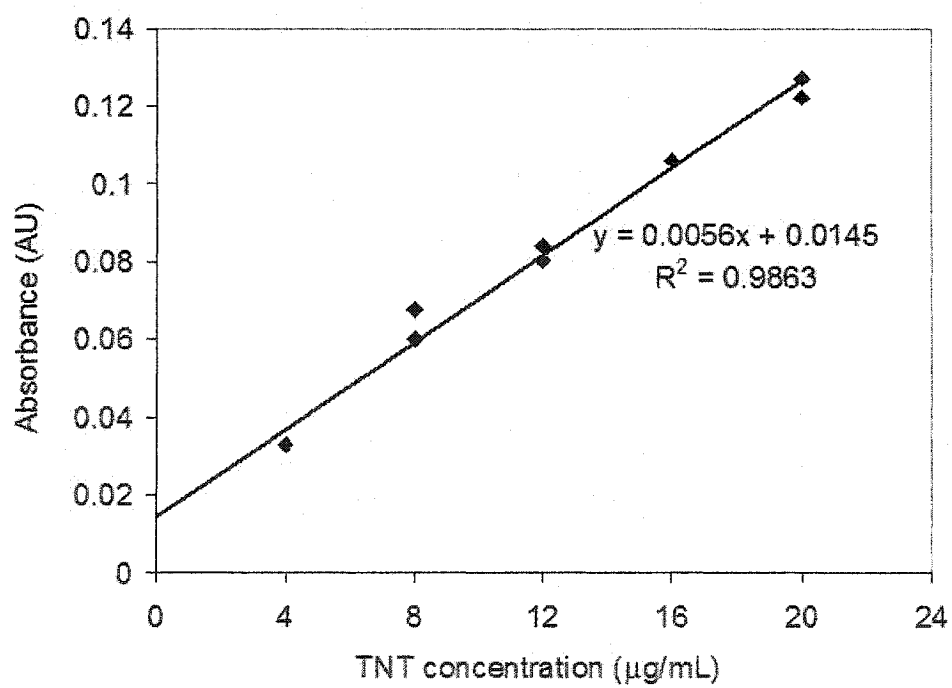


**Figure B.6:** Calibration curve of absorbance with respect to the concentration of TNT demonstrating a linear relation on the electrowetting chip

7, the absorbance at 505 nm is linear with varying concentrations of TNT in the TNT+DNT mixture and is negligible for 100% DNT and 0% TNT. Therefore, using this colorimetric reaction, TNT can be detected even in the presence of DNT.

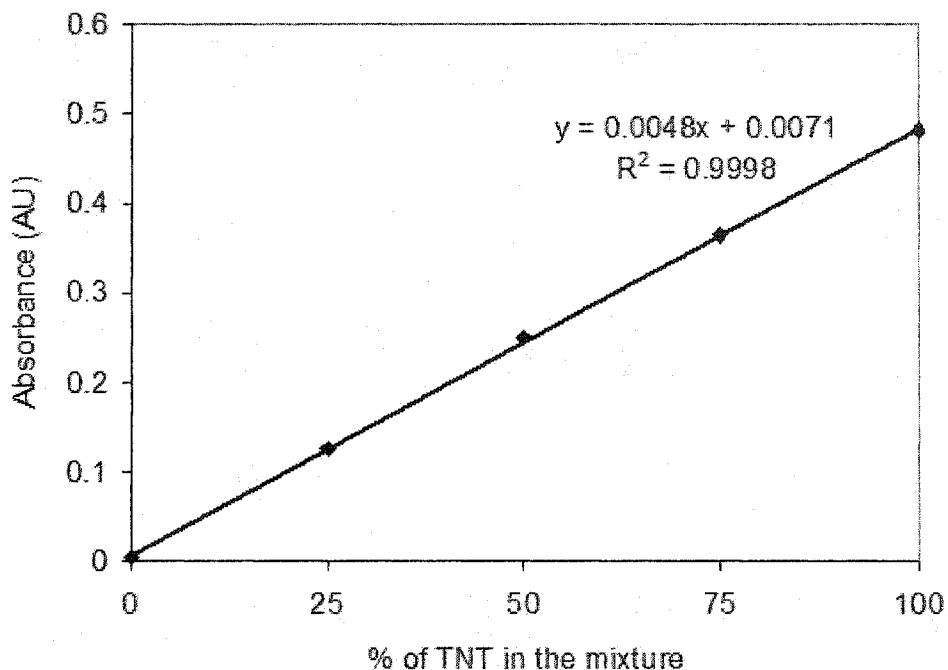


**Figure B.7:** Absorbance of TNT at 505 nm with varying amounts of TNT+DNT demonstrating the noninterference of DNT with the TNT reaction. At 0% TNT in the mixture, DNT is 100%

## B.5 Conclusions

A digital microfluidic lab-on-a-chip based on electrowetting actuation of droplets has been demonstrated for the detection of 2,4,6-trinitrotoluene (TNT) in DMSO. The colorimetric detection is based on the absorption of the Jackson-Meisenheimer complex formed as a result of the reaction between the nitroaromatics and a strong base. We have demonstrated a linear range of detection for TNT between  $4\mu\text{g/mL}$  to  $20\mu\text{g/mL}$  and the time for each reaction-to-detection is about 2.5 minutes. The lab-on-a-chip can handle multiple samples in parallel, so the detection time would still be 2.5 minutes for simultaneous detection of a

number of samples. Advantages of such a lab-on-a-chip system include complete automation and integration, on-chip calibration, nanoliter sample/reagent consumption, increased parallelism, and portability. Since the current lab-on-a-chip platform is being developed as a generic analytical platform, analysis of a broader range of samples encompassing both chemical and biological realms can be integrated on the same platform. Future work would involve improving the detection limits of the system from  $\mu\text{g/mL}$  to  $\text{ng/mL}$ . Also, experiments need to be performed on nitroaromatic samples extracted from soil and post-blast residues to establish the suitability of a digital microfluidic system for field screening of nitroaromatics. Methods will also be adapted for the colorimetric detection of nitramines and nitrate esters. The system will also need to work with a wider range of solvents including acetone and acetonitrile, which are more commonly used solvents. Even though we have automated analysis, extraction is still manual therefore extraction procedures need to be automated in order to have a fully automated system.

## B.6 Acknowledgements

We thank Dr. Phil Rodacy of Sandia National Labs for providing the DNT and TNT samples. The authors also thank Dr. Michael Pollack for assistance with device design, Phil Paik for software programming, and Stefan Ufer at BMMSL, NC State for fabricating the devices.

# **Appendix C**

## **3-D Imaging of Moving Droplets for Microfluidics Using Optical Coherence Tomography**

### **C.1 Abstract**

We present the use of optical coherence tomography (OCT), an interferometric 3-D imaging technique, to visualize microdroplets in an electrowetting-based microfluidic device. Vertical cross-sectional images of stationary and moving microdroplets are obtained using this technique, to provide information on static and dynamic contact angle changes and flow profiles inside the microdroplet during transport. The initial results are encouraging and OCT appears to be a promising method to study fundamental, yet poorly understood electrowetting phenomena such as contact angle saturation and contact angle hysteresis. OCT can also be used in visualizing 3-D flow profiles in droplet-based microfluidics.

### **C.2 Introduction**

There has been considerable interest lately in electrowetting-based microfluidic systems. Electrowetting refers to the electrical modulation of the interfacial tension between a conducting liquid phase and a solid electrode [33]. Though there have been considerable advances from a technology perspective, the science behind electrowetting is not understood completely, and several fundamental questions still remain unanswered [76], partially owing to the lack of good visualization tools.

Current visualization techniques in an electrowetting system have been limited to observation of the top and side views of droplets using CCD microscope cameras, with vary-

ing degrees of sophistication in automation and optics [39, 77]. This technique, though sufficient for observation from the top, can pose severe constraints on materials and system design for imaging from the side. Another drawback is that these techniques do not provide 3-D tomographical information.

Optical coherence tomography (OCT) is an emerging real-time, in-situ, and noninvasive imaging technique based on low-coherence interferometry, with micrometer resolution [78]. Though most of its applications have been for cross-sectional tissue imaging in biological systems, OCT has recently been used to image flow patterns in a continuous flow microfluidic device [79]. In this paper we present the use of OCT to image microdroplets in an electrowetting-based microfluidic system. Unlike the CCD microscope-based methods, OCT obtains tomographical images by non-invasively scanning the droplet from above, circumventing the design constraints mentioned before.

### C.3 Experimental Setup

**Electrowetting Actuator** - The electrowetting system consists of two parallel electrode plates - a continuous ground plate and an addressable electrode array. The droplet is sandwiched between the two plates, and is surrounded by immiscible 1cSt silicone oil. The electrode array is insulated from the liquid and both surfaces are hydrophobized. The spacing between the electrode array and the ground plane is  $520\mu\text{m}$  in all experiments described in this paper. The fabrication details of the electrowetting chip can be found in [33]. The liquids used in the OCT experiments are required to scatter light; therefore droplets of skim milk or an aqueous solution of 1m polystyrene beads are used.

**Optical Coherence Tomography Imaging** - The details of the OCT setup are described in detail in [78]. The high speed OCT system used in this study has an axial and lateral resolution of  $\approx 20\mu\text{m}$ . The axial scan range (vertical field-of-view) is set to 1.5mm, and the lateral scan range (horizontal field-of-view) is set to 1mm for the static experiments and to 2mm for

the dynamic experiments. All images and videos are captured at the center of the droplet though in practice any cross-section of the droplet can be visualized. Video images are captured at a rate of 8 frames per second.

## C.4 Results and Discussion

### C.4.1 Static Contact Angle

OCT is used to visualize the change in “apparent” contact angle of a 400nL polybead droplet with the bottom plate at different voltages. We use the term apparent contact angle since a thin oil film can exist underneath the droplet under certain conditions, resulting in a two-phase system for which contact angles are not defined. Figure C.1 shows images of the droplet at various voltages. The contact angle increases with applied voltage and saturates beyond a certain voltage, as seen in the images. Saturation of contact angles at higher voltages is a very important contact angle phenomenon of interest in the fundamental study of electrowetting. Using OCT, this phenomenon can be visualized very clearly under different conditions.

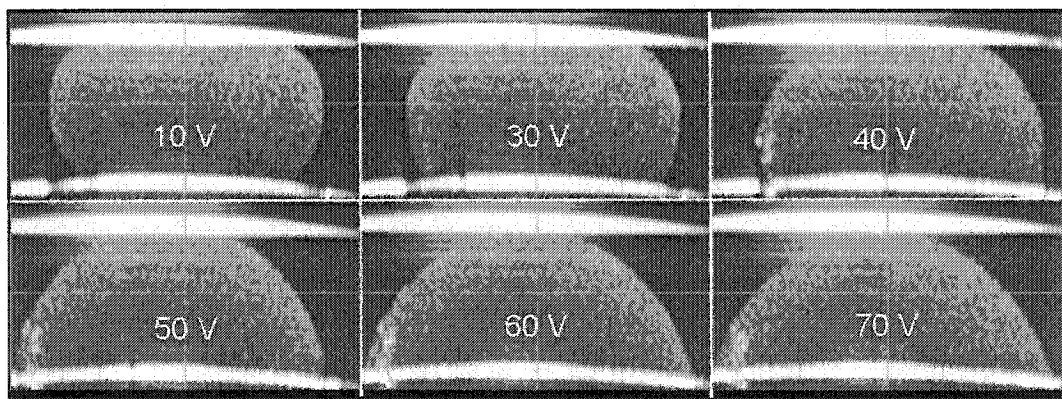


**Figure C.1:** Images showing the change in static contact angle of a droplet containing beads as the voltage is changed

#### C.4.2 Dynamic Contact Angle

Dynamic contact angle changes are visualized using OCT while the droplet is in motion. Figure C.2 shows snapshots of a 500nL skim milk droplet as it moves across two 1mm electrodes. The arrow indicates the direction of droplet motion. The dynamic contact angle information can be used to study the effect of contact angle hysteresis on the droplet transport.

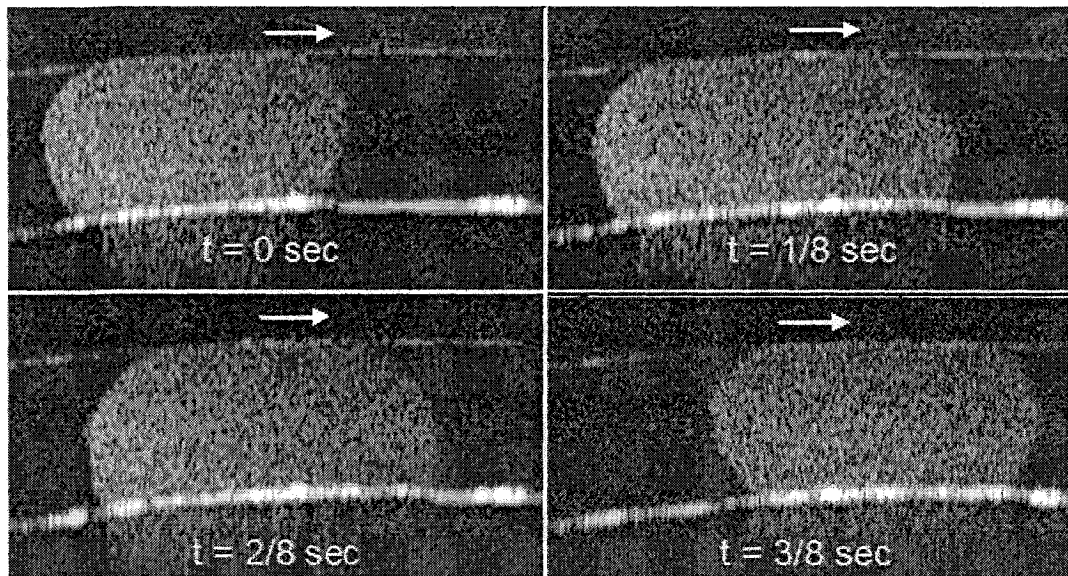


**Figure C.2:** Images showing the change in dynamic contact angle of a milk droplet as it moves from one electrode to another

#### C.4.3 Flow Patterns during Transport

Flow profiles inside the droplet can be obtained by imaging a moving droplet loaded with beads. A 500nL KCl droplet (0.1M) is loaded with a small volume (<50nL) of the polybeads. The droplet is then shuttled across two 1mm electrodes. Figure C.3 shows snapshots of the droplet as it moves across the two electrodes. Complete flow reversibility is evident from the images, corroborating the observations in [39].

Comparing the results from the static and dynamic experiments, we can see that the non-linearities at the edges of the image are more pronounced while using a 2mm lateral

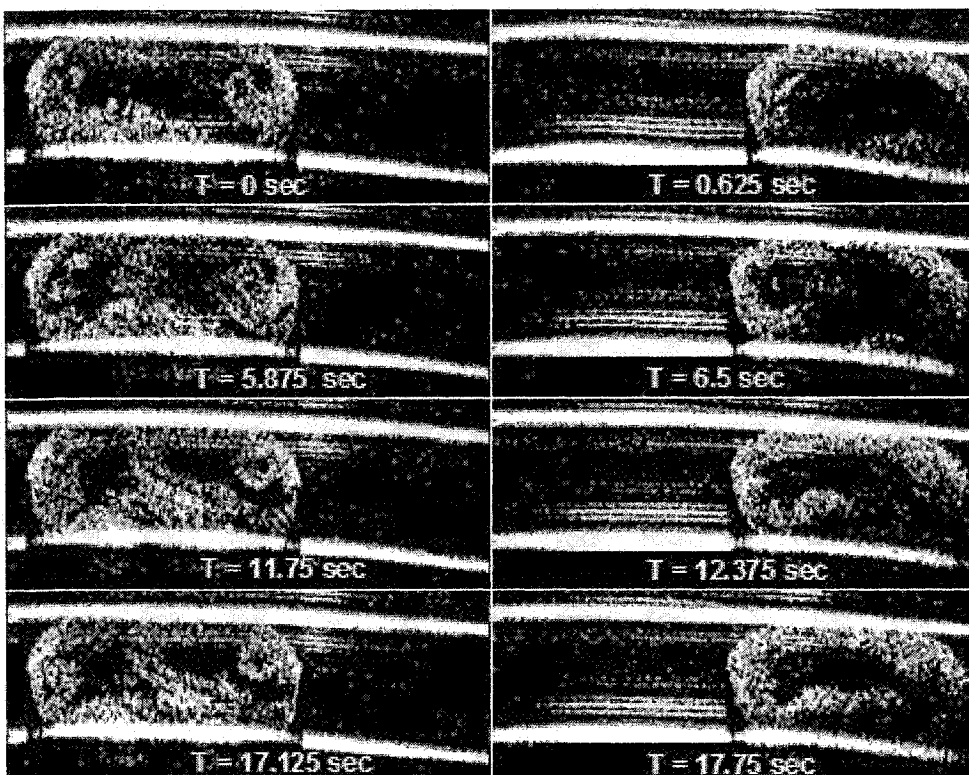


**Figure C.3:** Flow profiles inside a moving droplet illustrating complete reversibility of flow

scan. The lateral scan should be limited to 1mm to obtain good linearity, which means that smaller electrodes need to be used.

#### C.4.4 Quantitative Contact Angle Data

The most accurate method of determining the contact angle from the OCT images is by fitting the outline of the droplet to the Laplace- Young equation;  $\delta P = \gamma(1/R1 + 1/R2)$ , where  $\delta P$  is the pressure difference across the droplet-oil interface,  $\gamma$  is the interfacial tension, and R1 and R2 are the principal radii of curvature of the droplet-oil interface. This is because the contact angle measured from the OCT images is very sensitive to the location of the (apparent) 3-phase contact point, which is difficult to determine accurately. The images also need to be compensated to account for changes in effective path length that arise due to differences in refractive indices between the droplet and the oil. Therefore, significant post-processing of these images is required to obtain useful quantitative data.

### C.5 Conclusions and Future Work

We have demonstrated the use of OCT to image microdroplets in an electrowetting-based microfluidic system. OCT was used to obtain static and dynamic contact angle information, which is of use in studying important electrowetting phenomena such as contact angle hysteresis and saturation. Flow profiles were visualized inside a droplet with beads. The flow visualization can be further extended to study droplet mixing. The initial results yielded qualitative information on the utility of OCT to image droplets. Further analysis is needed to obtain quantitative results.

### C.6 Acknowledgement

We thank Michael Choma, Department of Biomedical Engineering., Duke University, for help with the OCT setup.

## Bibliography

- [1] P. Gwynne and G. Heebner. Lab automation and robotics: the brave new world of 24/7 research. <http://www.sciencemag.org/feature/e-market/benchtop/robotfinal.shtml>.
- [2] M. Bissell and F. Sanfilippo. Empowering patients with point-of-care testing. *Trends in Biotechnology*, 20(6):269–270, 2002.
- [3] T. Chapman. Lab automation and robotics. *Nature*, 421:661–666, 2003.
- [4] <http://www.allegro-technologies.com>.
- [5] <http://www.caliperls.com>.
- [6] D. R. Reyes, D. Iossifidis, P-A. Auroux, and A. Manz. Micro Total Analysis Systems. 1. Introduction, Theory, and Technology. *Analytical Chemistry*, 74(12):2623–2636, 2002.
- [7] D. Iossifidis, D. R. Reyes, P-A. Auroux, and A. Manz. Micro Total Analysis Systems. 2. Analytical Standard Operations and Applications. *Analytical Chemistry*, 74(12):2637–2652, 2002.
- [8] B. H. Weigl and R. L. Bardell. Microfluidics for clinical diagnostics - promise and current reality. *Laboratory Medicine*, 35(4):233–237, 2003.
- [9] N. Lion, F. Reymond, H. H. Girault, and J. S. Rossier. Why the move to microfluidics for protein analysis. *Current opinion in Biotechnology*, 15(1):31–37, 2004.
- [10] P. R. Selvaganapathy, E. T. Carlen, and C. H. Mastrangelo. Recent progress in microfluidic devices for nucleic acid and antibody assays. *Proceedings of the IEEE*, 91(6):954–975, 2003.
- [11] H. Andersson and A. van den Berg. Microtechnologies and nanotechnologies for single-cell analysis. *Current opinion in Biotechnology*, 15(1):44–49, 2004.
- [12] A. J. Tudos, G. A. J. Besselink, and R. B. M. Schasfoort. Trends in miniaturized total analysis systems for point-of-care testing in clinical chemistry. *Lab on a chip*, 1(1):83–95, 2001.
- [13] C. F. Streckfus and L. R. Bigler. Saliva as a diagnostic fluid. *Oral Diseases*, 8:69–76, 2002.

- [14] R. P. Taylor and T. J. James. Enzymatic Determination of Sodium and Chloride in Sweat. *Clinical Biochemistry*, 29(1):33–37, 1996.
- [15] R. Aller. Chemistry analyzers branching out. *CAP Today*, pages 84–106, June 2002.
- [16] C. A. Burtis and E. R. Ashwood, editors. *Tietz Textbook of Clinical Chemistry*. W. B. Saunders Company, 3 edition, 1999.
- [17] E. Verpoorte. Microfluidic chips for clinical and forensic analysis. *Electrophoresis*, 23:677–712, 2002.
- [18] W. Thormann, I. S. Lurie, B. McCord, U. Marti, B. Cenni, and N. Malik. Advances of capillary electrophoresis in clinical and forensic analysis(1999-2000). *Electrophoresis*, 22:4216–4243, 2001.
- [19] G. J. M. Bruin. Recent developments in electrokinetically driven analysis on micro-fabricated devices. *Electrophoresis*, 21:3931–3951, 2000.
- [20] D. C. Duffy, H. L. Gillis, J. Lin, N. F. Sheppard Jr., and G. J. Kellogg. Microfabricated centrifugal microfluidic systems: characterization and Multiple Enzymatic Assays. *Analytical Chemistry*, 71:4669–4678, 1999.
- [21] A. M. Leach, A. R. Wheeler, and R. N. Zare. Flow Injection Analysis in a Microfluidic Format. *Analytical Chemistry*, 75(4):967–972, 2003.
- [22] I. Moser, G. Jobst, P. Svasek, M. Varaharam, and G. Urban. Rapid liver enzyme assay with miniaturized liquid handling system comprising thin film biosensor array. *Sensors and Actuators B*, 44:377–380, 1997.
- [23] K. Hayashi, R. kurita, T. Horiuchi, and O. Niwa. Selective detection of l-glutamate using a microfluidic device integrated with a enzyme-modified pre-reactor and an electrochemical detector. *Biosensors and Bioelectronics*, pages 1–7, 2003.
- [24] H. Nakamura, Y. Murakami, K. Yokoyama, E. Tamiya, and I. Karube. A Compactly Integrated Flow Cell with a Chemiluminescent FIA System for Determining Lactate Concentration in Serum. *Analytical Chemistry*, 73(2):373–378, 2001.
- [25] S. Bohm, W. Olthius, and P. Bergveld. A micromachined double lumen microdialysis probe connector with incorporated sensor for on-line sampling. *Sensors and Actuators B*, 63:201–208, 2000.
- [26] E. Dempsey, D. Diamond, M. R. Smyth, G. Urban, G. Jobst, I. Moser, E. Verpoorte, A. Manz, H. M. Widmer, K. Rabenstein, and R. Freaney. Design and development

of a miniaturized total chemical analysis system for on-line lactate and glucose monitoring in biological samples. *Analytica Chimica Acta*, 346:341–349, 1997.

- [27] J. V. Zoval and M. J. Madou. Centrifuge-based fluidic platforms. *Proceedings of IEEE*, 92(1):140–153, 2004.
- [28] <http://www.gyros.com>.
- [29] <http://www.tecan.com>.
- [30] <http://www.micronics.net>.
- [31] <http://www.biosite.com>.
- [32] <http://www.istat.com>.
- [33] M. G. Pollack, A. D. Shendorov, and R. B. Fair. Electrowetting-based actuation of droplets for integrated microfluidics. *Lab on a Chip*, 2, 2002.
- [34] J. A. Schwartz, J. V. Vykoukal, and P. R. C. Gascoyne. Droplet-based chemistry on a programmable micro-chip. *Lab on a chip*, 4:11–17, 2004.
- [35] Michael G. Pollack. *Electrowetting-based microactuation of droplets for digital microfluidics*. PhD thesis, Duke University, Durham, NC, USA, 2001.
- [36] Hong Ren. *Electrowetting-based droplet formation*. PhD thesis, Duke University, Durham, NC, USA, 2004.
- [37] H. Ren, V. Srinivasan, and R. B. Fair. Design and testing of an interpolating mixing architecture for electrowetting-based droplet-on-chip chemical dilution. In *Transducers Conference 2003*, 2003.
- [38] Philip Y. Paik. Rapid droplet mixers for digital microfluidic systems. Master's thesis, Duke University, 2003.
- [39] P. Y. Paik, V. K. Pamula, M. G. Pollack, and R. B. Fair. Electrowetting-based droplet mixers for microfluidic systems. *Lab on a chip*, 3(1):28–33, 2003.
- [40] P. Y. Paik, V. K. Pamula, and R. B. Fair. Rapid droplet mixers for digital microfluidic systems. *Lab on a chip*, 3:253–259, 2003.

- [41] V. Srinivasan, V.K. Pamula, P. Paik, and R.B. Fair. Protein stamping for maldi mass spectrometry using an electrowetting-based microfluidic platform. In *SPIE Optics East, Lab-on-a-Chip: Platforms, Devices, and Applications*, 2004.
- [42] V. K. Pamula, V. Srinivasan, H. Chakrapani, R. B. Fair, and E. J. Toone. A droplet-based lab-on-a-chip for colorimetric detection of nitroaromatic explosives. In *Proceedings of IEEE MEMS 2005 Conference*, 2005.
- [43] V. Srinivasan, V. K. Pamula, K. Divakar Rao, M. G. Pollack, J. A. Izatt, and R. B. Fair. 3-d imaging of moving droplets for microfluidics using optical coherence tomography. In *Proceedings of MicroTAS 2003*, 2003.
- [44] S-K. Cho, H. Moon, and C-J. Kim. Creating, transporting, cutting, and merging liquid droplets by electrowetting-based actuation for digital microfluidic circuits. *Journal of Microelectromechanical Systems*, 12(1):70–80, 2003.
- [45] J. Ding, K. Chakrabarty, and R. B. Fair. Scheduling of microfluidic operations for reconfigurable two-dimensional electrowetting arrays. *IEEE Transactions on Computer-aided design of Integrated Circuits and Systems*, 20:1463–1468, 2001.
- [46] J-Y. Yoon and R. L. Garrell. Preventing biomolecular adsorption in electrowetting-based biofluidic chips. *Analytical Chemistry*, 75:5097–5102, 2003.
- [47] World Health Organization. Technical report on diabetes, 2002.
- [48] R. Kurita, K. Hayashi, X. Fan, K. Yamamoto, T. Kato, and O. Niwa. Microfluidic device integrated with pre-reactor and dual enzyme-modified microelectrodes for monitoring in vivo glucose and lactate. *Sensors and Actuators B*, 63:70:1–8, 2002.
- [49] J. Wang. On-chip enzymatic assays. *Electrophoresis*, 23:713–718, 2002.
- [50] T. Laurell and J. Drott. Silicon wafer integrated enzyme reactors. *Biosensors and Bioelectronics*, 10:289–299, 1995.
- [51] J. Wang, M. P. Chatrathi, and A. Ibanez. Glucose biochip: dual analyte response in connection to two pre-column enzymatic reactions. *Analyst*, 126:1203–1206, 2001.
- [52] Y. Lv, Z. Zhang, and F. Chen. Chemiluminscence microfluidic system sensor on a chip for determination of glucose in human serum with immobilized reagents. *Talanta*, 59:571–576, 2003.
- [53] P. Trinder. Determination of glucose in blood using glucose oxidase with and alternative oxygen acceptor. *Annals in Clinical Biochemistry*, 6:24–27, 1969.

- [54] P. Fossati, L. Prencipe, and G. Berti. Enzymic Creatininte Assay: A New Colorimetric Method Based on Hydrogen Peroxide Measurement. *Clinical Chemistry*, 29(8):1494–1496, 1983.
- [55] M. J. Madou and R. Cubicciotti. Scaling issues in chemical and biological sensors. *Proceedings of the IEEE*, 91(6):830–838, 2003.
- [56] J. Wang. Electrochemical detection for microscale analytical systems: a review. *Talanta*, 56:223–231, 2002.
- [57] A. J. de Mello and N. Beard. Dealing with real samples: sample pre-treatment in microfluidic systems. *Lab on a chip*, 3:11N–19N, 2003.
- [58] R. Aebersold and M. Mann. Mass spectrometry-based proteomics. *Nature*, 422:198–207, 2003.
- [59] S. Ekstrom, P. Onnerfjord, J. Nilsson, M. Bengtsson, T. Laurell, and G. M.-Varga. Integrated microanalytical technology enabling rapid and automated protein identification. *Analytical Chemistry*, 72:286–293, 2000.
- [60] M. Brivio, R. H. Fokkens, W. Verboom, D. N. Reinhoudt, N. R. Tas, M. Goedbloed, and A. van den Berg. Integrated microfluidic system enabling (bio)chemical reactions with on-line maldi-tof mass spectrometry. *Analytical Chemistry*, 74:3972–3976, 2002.
- [61] M. Gustafsson, D. Hirschberg, C. Palmberg, H. Jornvall, and T. Bergman. Integrated sample preparation and maldi mass spectrometry on a microfluidic compact disk. *Analytical Chemistry*, 76:345–350, 2004.
- [62] A. R. Wheeler, H. Moon, C-J. Kim, J. A. Loo, and R. L. Garrell. Electrowetting-based microfluidics for analysis of peptides and proteins by matrix-assisted laser desorption/ionization mass spectrometry. *Analytical Chemistry*, 76:4833–4838, 2004.
- [63] V. Srinivasan, V. K. Pamula, and R. B. Fair. An integrated digital microfluidic lab-on-a-chip for clinical diagnostics on human physiological fluids. *Lab on a chip*, 4:310–315, 2004.
- [64] U-C. Yi and C-J. Kim. Soft printing of droplets digitized by electrowetting. In *Transducers 2003*, pages 1804–1808, 2003.
- [65] J. Yinon and S. Zitrin. *Modern methods and applications in the analysis of explosives*. John Wiley and Sons, 1993.

- [66] US EPA. 2,4,6-trinitrotoluene health advisory. Technical report, U.S. Environmental Protection Agency, 1989.
- [67] J. Yiron. *Toxicity and metabolism of explosives*. CRC Press, 1990.
- [68] U.S. Environmental Protection Agency. *SW-846 Method 8330*.
- [69] L. C. Shriver-Lake, P. T. Charles, and A. W. Kusterbeck. Non aerosol detection of explosives with a continuous flow immunosensor. *Analytical Bioanalytical Chemistry*, 377:550–555.
- [70] <http://www.sdix.com>.
- [71] T. F. Jenkins and M. E. Walsh. Development of field screening methods for tnt, 2,4-dnt and rdx in soil. *Talanta*, 39:419–428, 1992.
- [72] R. T. Medary. Inexpensive rapid field screening test for 2,4,6-trinitrotoluene in soil. *Analytica Chimica Acta*, 258:341–346, 1992.
- [73] H. Craig, G. Ferguson, A. Markos, A. Kesterbeck, L. Shriver-Lake, T. Jenkins, and P. Thorne. Field demonstration of on-site analytical methods for tnt and rdx in ground water. Technical report, US EPA, 1996.
- [74] A. B. Crockett, H. D. Craig, T. F. Jenkins, and W. E. Sisk. Field sampling and selecting on-site analytical methods for explosives in soil. Technical report, US EPA, 1996.
- [75] F. Terrier. Rate and equilibrium studies in jackson- meisenheimer complexes. *Chemical Reviews*, 82:77–152, 1982.
- [76] C. Quilliet and B. Berge. Electrowetting: a recent outbreak. *Current Opinion in Colloid and Interface Science*, 6:34–39, 2001.
- [77] H. Moon, S. K. Cho, R. L. Garrell, and C-J. Kim. Low voltage electrowetting-on-dielectric. *Journal of Applied Physics*, 92:4080–4087, 2002.
- [78] A. M. Rollins, M. D. Kulkarni, S. Yazdanfar, R. Ung-arunyawee, and J. A. Izatt. In-vivo video rate optical coherence tomography. *Optics Express*, 3:219–229, 1998.
- [79] S. A. Boppart. Optical coherence tomography of living and fabricated microfluidic systems. In *LEOS 2001*, pages 190–191, 2001.

## **Biography**

Full Name: Vijay Srinivasan

Place of Birth: Chennai, Tamil Nadu, India

Date of Birth: November 26, 1977

Schools attended:

- Indian Institute of Technology Madras, Chennai, India, B.Tech., May 1998
- Duke University, Durham, NC, M.S., December 2000
- Duke University, Durham, NC, Ph.D., May 2005.

Publications:

1. A. Dewey, V. Srinivasan, and E. Icoz, "Towards a visual modeling approach to designing microelectromechanical system transducers," *Journal of Micromechanics and Microengineering*, vol.9, no.4, pp.332-340, 1999.
2. A. Dewey, V. Srinivasan, and E. Icoz, "Visual modeling and design of microelectromechanical system transducers," *Microelectronics Journal*, vol.32, no.4, pp.373-381, 2001
3. Vijay Srinivasan, Vamsee K. Pamula, Michael G. Pollack, and Richard B. Fair, "A digital microfluidic biosensor for multianalyte detection", Proc. IEEE Micro Electro Mechanical Systems Conference, pp. 327-330, 2003.
4. Hong Ren, Vijay Srinivasan, and Richard B. Fair, "Design and testing of an interpolating mixing architecture for electrowetting-based droplet-on-chip chemical dilution", *Transducers 2003*, pp. 619-622, 2003.
5. Hong Ren, Vijay Srinivasan, Michael G. Pollack, and Richard B. Fair, "Automated electrowetting-based droplet dispensing with good reproducibility," Proc. Micro Total Analysis Systems, pp. 993-996, 2003.
6. Vijay Srinivasan, Vamsee K. Pamula, K. Divakar Rao, Michael G. Pollack, Joseph A. Izatt, and Richard B. Fair, "3-D imaging of moving droplets for microfluidics using optical coherence tomography," Proc. Micro Total Analysis Systems, pp. 1303-1306, 2003.
7. Vijay Srinivasan, Vamsee K. Pamula, Michael G. Pollack, and Richard B. Fair, "Clinical diagnostics on human whole blood, plasma, serum, urine, saliva, sweat, and tears on a digital microfluidic platform," Proc. Micro Total Analysis Systems, pp. 1287-1290, 2003.

8. R. B. Fair, V. Srinivasan, H. Ren, P. Paik, V.K. Pamula, M.G. Pollack, "Electrowetting-based On-Chip Sample Processing for Integrated Microfluidics," IEEE Inter. Electron Devices Meeting (IEDM), pp. 32.5.1-32.5.4, 2003.
9. Vijay Srinivasan, Vamsee K. Pamula, Richard B. Fair, "A Droplet-based microfluidic lab-on-a-chip for glucose detection," Analytica Chimica Acta, vol.507, pp.145-150, 2004.
10. Vijay Srinivasan, Vamsee K. Pamula, Richard B. Fair, "An integrated digital microfluidic lab-on-a-chip for clinical diagnostics on human physiological fluids," Lab on a Chip, vol.4, pp.310-315, 2004.
11. Vijay Srinivasan, Vamsee K. Pamula, Phil Paik, and Richard B. Fair, "Protein stamping for MALDI mass spectrometry using an electrowetting-based microfluidic platform," Proc. SPIE Lab-on-a-chip platforms, devices, and applications, 2005.
12. R. B. Fair, V. Srinivasan, V. K. Pamula, A. Khylstov, K. N. Weaver, "Integrated chemical/biochemical sample collection, pre-concentration, and analysis on a digital microfluidic lab-on-a-chip platform," Proc. SPIE Lab-on-a-chip platforms, devices, and applications, 2005.